BENDIX RLD REPORT NO. 2542
COPY NO. 62

Final Summary Report

MASS SPECTROMETER FOR LUNAR ANALYSIS STUDY

30 November 1963

PERIOD COVERED: 1 JUNE 1963 THROUGH 31 AUGUST 1963

Prepared for

National Aeronautics and Space Administration
George C. Marshall Space Flight Center
Huntsville, Alabama 35812

Under Contract No. NAS 8-5370

Prepared by:

The Bendix Corporation
Research Laboratories Division
Southfield, Michigan 48076

Bendix RLD Report No. 2542

Final Summary Report

MASS SPECTROMETER FOR LUNAR ANALYSIS STUDY

30 November 1963

A SURVEY OF THE STATE-OF-THE-ART OF MASS SPECTROMETRY APPLIED TO COMPOSITIONAL ANALYSIS OF THE LUNAR ATMOSPHERE AND CRUST IS DOCUMENTED ALONG WITH A RECOMMENDED PROGRAM FOR THE DEVELOPMENT OF HARDWARE TO ACCOMPLISH SUCH A MISSION.

PERIOD COVERED: 1 JUNE 1963 THROUGH 31 AUGUST 1963

Prepared for

National Aeronautics and Space Administration
George C. Marshall Space Flight Center
Huntsville, Alabama 35812

Under Contract No. NAS 8-5370

Prepared by:

The Bendix Corporation
Research Laboratories Division
Southfield, Michigan 48076

Authors: G. J. O'Halloran
L. D. Ferguson
F. W. Poblenz
L. Walker

REPORTABLE ITEMS

Reportable items were not generated on this program nor were there any subcontracts awarded under this program in which a "Report of New Technology" clause either was or should have been contained.

TABLE OF CONTENTS

LIST OF ILLUSTRATIONS

LIST OF TABLES

SECTION 1

INTRODUCTION

This Final Summary Report concerning the investigation of a mass spectrometer to analyze the lunar atmosphere has been prepared for the National Aeronautics and Space Administration, George C. Marshall Space Flight Center, Huntsville, Alabama, to provide a complete summary of The Bendix Corporation, Research Laboratories Division effort under Contract NAS8-5370 and to define a recommended follow-on program. This report has been prepared in accordance with Part I, Article III, Paragraphs B, C, and D as amended.

1.1 GENERAL DISCUSSION

An important goal of the over-all U.S. Space Program is the acquisition and compilation of acutely needed information concerning the chemical composition of the lunar atmosphere and crust. It is expected that such data will contribute to a much better understanding of the origin and history of the earth-lunar system and will possibly lead to the revelation of important scientific information about the long term exposure of chemical species at low pressures over a range of temperatures while exposed, at least at times, to intense nuclear radiation. New information concerning the lunar crust is expected to directly aid in planning the operational phases of on-going programs which are concerned with placing men and machines on the moon and the safe return of at least the former to the earth.

It is very likely that a few direct measurements of the chemical and physical properties of the materials which constitute the lunar crust-atmosphere system will significantly help resolve the scientific controversy in these areas.

1.2 SUMMARY OF PROGRAM

The Research Laboratories Division has participated in several programs concerned with measuring the chemical composition of the earth atmosphere, the lunar atmosphere, and the lunar crust by means of mass spectrometry. Each of these programs concerned direct sampling equipment which performed the analysis at or very

near the position from which the sample was extracted, and each program has led to hardware which has been successfully flown in the intended type of vehicle or has led to considerable advancement in the state-of-the-art of Time-of-Flight Mass Spectrometry. The investigation of a mass spectrometer to analyze the lunar atmosphere provided Bendix with the opportunity of extending this information and experience, compiling this comprehensive review, and evaluating the newer techniques which are applicable to this type of measurement problem. In addition, the program provided the opportunity to accomplish a small but important amount of experimental activity concerning mass spectrometer source and detector characteristics.

1.2.1 Program Effort

The over-all goal of the investigation is associated with the development of a miniaturized Time-of-Flight Mass Spectrometer with the capability to determine the composition of the lunar atmosphere and crust. The work included both analytical and experimental activity.

The specific goals of the effort included the evaluation of available detectors and ion sources for use with Time-of-Flight instruments, and the preparation of the final report. In order to provide the requisite background information which was used to define a recommended approach to develop a flyable lunar mass spectrometer, the Research Laboratories Division significantly increased the amount of available funding by contributing from its own budget. This made possible the compilation of the information in this Final Summary Report which is general in nature.

1.2.2 Program Activity

The program began with a definition of the physical and radiation environments to which the resulting hardware would be exposed. In addition, two types of sample models were assumed in order to provide a definition of the measurement problem (the system input). These models are discussed in detail in the subsequent text. In general, they consist of (1) the expected identity and partial pressures of the components of the lunar atmosphere, and (2) the expected identity and concentrations of the lunar crust material itself.

After these models were compiled, available Time-of-Flight Mass Spectrometer techniques were investigated to define the

most feasible approach to completing the development of this instrument for the lunar composition analysis.

Source experiments completed showed that the 800 amu resolution goal could be reached, while detector evaluation indicated that adequately low water vapor levels could be achieved.

Attempts to evaluate the "contamination," if any, resulting from the mission itself; e.g., rocket exhaust or instrument outgassing, were not completed due to the enormity of the task. The original idea was to categorize, for each type of model, those components which occur due to the landing phase of the mission, and those that are due to system outgassing. It appears that the proposed instrumentation can be constructed in such a way that it will not significantly contaminate the expected sample.

Representative performance parameters were determined for the selected instrumentation system and the mass spectra were computed and plotted in order to provide a concrete representation of the components expected.

The program activity concluded with the preparation and submission of this Final Summary Report and a presentation at the George C. Marshall Space Flight Center, Huntsville, Alabama.

1.3 SUMMARY OF REPORT

Section 2 is devoted to a general discussion regarding the desirability of a lunar compositional analysis. The operational and environmental constraints at launch, voyage, approach, and landing are discussed in Section 3, which concludes with an analysis of the measurements that are to be made and a compilation of the lunar atmosphere and soil models. Compositional analyses techniques are discussed in Section 4, including a parametric analysis of sensor systems and a comprehensive discussion of Time-of-Flight Mass Spectrometry, which has been suggested for fulfilling the lunar analysis instrumentation requirement. Section 5 includes a summary of the experimental activity accomplished during the program.

SECTION 2

GENERAL DISCUSSION OF THE NEEDS FOR LUNAR COMPOSITIONAL ANALYSES

This section presents a concise listing of some of the reasons for analyzing the lunar crust-atmosphere system.

2.1 OPERATIONAL INFORMATION REQUIREMENTS

In order to effectively plan future space flights to the moon, it is necessary that additional information be obtained about the moon's surface atmosphere. The "best guesses" currently available give little confidence concerning even the major topographic features. It is expected that any directly measured information will be of great value in correlating other directly taken data concerning soil grain size, ability to support large loads, and the like. In addition, information is needed concerning the availability of water in any of its forms and the availability of oxygen-bearing material for operational needs.

2.2 RESEARCH AND ASTROPHYSICAL REQUIREMENTS

Compositional lunar information should provide extremely useful information concerning the time and mechanism of both its origin and the earth's. The lunar planet is a logical source for such information, since it is the most readily accessible astronomical object. In general one of the big motivations for analyzing the composition of the lunar atmosphere/crust is simply man's basic desire to learn more about his environment. Appendix A presents presently available lunar characteristics.

SECTION 3

GENERAL DISCUSSION OF THE LUNAR ANALYSES PROBLEMS

This section discusses the inputs to the lunar composition measurement instrument; it provides a definition of the expected signal and the anticipated noise.

3.1 GENERAL

The lunar instrumentation considered in this report is intended to be conveyed to, and operated in, the near vicinity of the lunar crust. The discussion of this measurement problem has been divided, for convenience, into two general areas. First, the expected environmental characteristics to which the equipment will probably be exposed are discussed and quantitatively estimated. Second, the samples to be analyzed are discussed so that the probable quantitative composition of the sample can be ascertained. This will provide the designer with all the aspects of the problem, enabling him to compute the characteristics of the expected signal, the probable noise, and to judge whether the system design will withstand the expected environments.

3.2 ENVIRONMENTAL CONSTRAINTS FOR LAUNCH, VOYAGE, APPROACH, AND LUNAR LANDING

The environmental criteria must take into consideration all conditions that will be encountered in the life span of the system. For example, a lunar instrumentation vehicle must be launched, carried through the earth atmosphere, follow a space trajectory, enter the destination atmosphere, traverse a de-orbit trajectory, and set down. In addition, both before and after flight, the system and its parts must be transported, stored and serviced. Each of these phases imposes a different environment on the system. A discussion of these environmental considerations and design problems is presented in the following subsections.

3.2.1 Mechanical Stresses

Both the natural environment and the environment generated by the space vehicle itself will subject the analyzer to many stresses

and strains, which can arise as a result of excessive expansion or contraction due to temperature changes, fatigue due to severe shock, extreme vibration and acceleration, and radiation induced changes in materials.

3.2.1.1 Vibration

The lunar analyzer proposed by Bendix consists of a sample inlet system, an analyzer, a detector, and an output system. The designs of the analyzer, detector, and output system would be similar to those of an existing satellite Time-of-Flight Mass Spectrometer system which has successfully withstood the following vibration tests:

6-30 cps	-	0.50-inch double amplitude displacement (5 minute sweeps up and down the frequency range).
30-2000 cps	-	15 G acceleration - 5 minute sweeps up and down.
2000-3000 cps	-	10 G acceleration - 5 minute sweeps up and down.

3.2.1.2 Shock

Shock denotes a rapid change of load or a change in the direction of the force vector on a system with an accompanying large change in acceleration. A system, even though undergoing large values of acceleration, is not normally considered to be undergoing shock unless the derivative of the acceleration with respect to time is large; shock is generally caused by the sudden physical contact of one system with another.

It is anticipated that the maximum shock resulting from a lunar landing will not exceed a force of 20 G's for 11 milliseconds. This shock presents no particular difficulty, since similar Bendix equipment has been subjected to environmental tests of ±40 G's for 3 milliseconds along 3 mutually perpendicular axes with no adverse effects.

3.2.1.3 Acceleration

The anticipated maximum value for acceleration is 20 G's along each of 3 mutually perpendicular axes; this, also, is not considered to be a problem, since similar Bendix equipment has been subjected to 10 G's along the launch axis and ±5 G's in the 2 perpendicular axes with no adverse effects.

3.2.2 Temperature

The anticipated temperature range (218°K to 338°K) during launch, voyage, and landing should not present an especially critical problem; and since it is not advantageous nor desirable to operate the analyzer at these times, this consideration is minimized even further.

The more important and more severe temperature environment occurs during the post lunar landing period, where lunar surface temperature variations of 120°K to 400°K are encountered. Therefore, careful consideration would be given to these temperature variations during the development of the analyzer.

3.2.3 Noise

The noise problem is also minimized since the analyzer is not expected to operate during flight. However, should the analyzer be required to operate during flight special components would have to be developed, especially if the analyzer was required to operate during the time the maximum anticipated acoustic noise level (136 db over the range of 37 to 9600 cps) occurs.

3.2.4 Humidity

The analyzer should be capable of operating over a relative humidity range of 0 to 100 percent without any problem. Equipment similar to the lunar analysis system has already been tested in humid environments of equivalent severity with no adverse effects.

3.2.5 Sterilization by Radiation

It is presently believed that lunar mission sterilization is not essential.[1] However, cleanliness procedures will be required to assure that no more than 0.01 gram of living tissue is deposited on the moon per flight.

However, should sterilization be required, radiation is one of the more likely types to be used, so that all internal parts are reached. A radiation dose of 10^6 rad from some suitable gamma source was originally proposed for sterilizing the spacecraft; however, some sources indicate that on the basis of an expontial kill,[2] a dose of 1.2×10^7 rad would be required to reduce the original viable organism count by a factor of 10^{13}.

The results of using from 10^6 to 1.2×10^7 rad of radiation could be devastating to both the spacecraft components and the payload. At these radiation levels, damage can occur in many types of plastics, elastomers, lubricants, semiconductors, optical glasses, and even solid propellants if they are utilized. It is probable that many components and systems would have to be replaced or redesigned if a spacecraft required sterilization by radiation.

3.2.5.1 Cislunar Space Radiation

During the trip from earth to the moon there are two important sources of radiation that the lunar vehicle can encounter: The first source is the Van Allen Belt and the second source is the radiation which results from a solar flare. Since the actual mission time to the lunar surface is short (less than 1 week), the probability of encountering a solar flare is small; however, this possibility is discussed in more detail in subsection 3.3.3.1.

The Van Allen Belt, through which the vehicle must pass, consists of protons and electrons which are trapped in the earth's magnetic field at distances of about 400 kilometers out to about 88,000 kilometers from the earth. The heart of the proton belt occurs about 4,400 kilometers out from the earth; the density is about 3×10^4 protons/cm^2-sec, and the protons have energies above 40 Mev. The electron belt peaks between 9,200 and 21,600 kilometers out from the earth, depending on the electron energy of concern.

3.2.6 Fungus

The specification requirements for fungus do not appear to present any difficulties, since the proposed system can be produced without exposed, fungus supporting material.

3.2.7 Pressure

The analyzer will be subjected to a very extensive range of pressures. Prior to launch, a nominal atmospheric pressure of 760 mm Hg will be experienced. If an un-pressurized compartment is used to house the analyzer, a pressure of 10^{-2} mm Hg will be experienced at an altitude of 40 miles and a pressure of 10^{-9} mm Hg will be experienced at an altitude of 380 miles. These extreme vacuum conditions, of the voyage and the lunar surface itself, necessitate using materials

with minimum outgassing characteristics. Table 1 presents a list of materials and their vacuum outgassing characteristics. Although it is not necessary nor desirable to operate the analyzer during the period prior to lunar descent, it is necessary to prevent the outgassing of materials used in the analyzer from interfering with its operation after the lunar landing.

3.3 OPERATIONAL AND ENVIRONMENTAL CONSTRAINTS AFTER LUNAR LANDING

Prior to discussing the environmental constraints which will affect the analyzer after the lunar landing, it is necessary to assume that the proper pre-launch preparations were carried out, that the lunar analysis spacecraft achieved the correct lunar trajectory, and that the spacecraft was brought to a safe landing upon the lunar surface. This implies that the vehicle's structural strength will be capable of withstanding the shock of landing and that the moon's surface at the point of landing has sufficient bearing strength to hold the vehicle. The various hypotheses on the nature of the lunar surface make this second implication subject to question. However, regardless of whether the surfaces of the maria were formed by fluidization of volcanic ash or whether the surface layer is the result of 4.5 billion years accretion of micrometeorites, there definitely appears to be a dust layer whose thickness has been estimated as a uniform few millimeters to ten feet in spots.

The fairy castle theory and the "free radical" approach both postulate that there are fairly strong bonds holding the dust particles together in a three dimensional lace or honeycomb type structure. However, the force of a vehicle landing would probably shear some of these bonds leaving fresh surfaces with unsatisfied bonds. Some of these particles, with unsatisfied bonds, could cold-weld on the surface of the vehicle, since the spacecraft would have an almost atomically clean surface as a result of its trip through the vacuum of space. The assumption of a safe landing would have to include, therefore, provisions for controlling lunar dust, so that it would not cling to optical or other sensitive instrument surfaces.

It must also be assumed that the vehicle's power supply does not modify the environment. This implies that shielding be used if nuclear power sources are employed and that no interferences will be caused by the jets of hydrogen or other gases used to assist in the landing.

Table 1 - Outgassing Data for Elastomers, Plastics, Ceramics, and Metals

A_m = area of sample (cm^2);
S_a = pumping speed for air at 25°C (1/sec);
K_1 = air equivalent outgassing rate after 1 hr of pumping (Torr-l-sec^{-1}-cm^{-2});
K_4 = outgassing rate after 4 hr of pumping;
a_1 = absolute value of slope of log-log graph of outgassing rate vs. time after 1 hr of pumping;
a_4 = absolute value of slope of log-log graph after 4 hr;
t_m = time at which a begins to increase rapidly above a_1 for given sample (hr);
ω_m^2 = square of sample thickness, ω_m (mm).

MATERIAL	A_m	S_a	10^7K_1	a_1	10^7K_4	a_4	t_m	ω_m^2
A. ELASTOMERS								
1. Natural gum rubber (32 Durometer)	75	0.5	12	0.5	6.0	0.5	12	9
Natural gum rubber (32 Durometer)	1	0.5	13	0.5	6.5	0.5	10	9
2. Natural white rubber J.1260 total outgassing	100	0.35	11.5	0.40	6.6	0.42	5	2.6
3. Natural white rubber J.1260 non-condensable in liquid air	100	0.35	2	0.5	0.2	1.6	-	2.6
4. Natural crepe rubber (vulcanized with S 20 min)	22.2	0.7	73	0.7	31	0.65	-	*
5. Natural crepe rubber (vulcanized with Te 20 min)	22.2	0.7	61	0.5	28	0.60	-	*
6. Neoprene F-905	65	0.3	50	0.49	25	0.55	>30	16
7. Neoprene 60° Shore	-	1	80	0.45	43	0.49	>7	-
8. Neoprene	65	3.5	300	0.4	180	0.4	15	-
9. Neoprene (24 hr at 95 per cent humidity)	7.6	0.32	1400	0.75	480	0.4	-	-
10. Neoprene (outgassed + 24 hr dry N_2)	7.6	0.32	120	0.5	-	-	-	-
11. Neoprene GNA (V-4-2) (1/2 hr 50 per cent rel. humidity)	30	2	-	-	30	-	-	-
12. Neoprene (bell jar gasket, 50 Durometer)	68	0.4	30	0.5	14.5	0.5	-	8
13. Neoprene 1157 (sulfur free)	65	1.5	54	0.45	30	0.45	20	10
14. Red vacuum hose (24 hr at 95 per cent humidity)	141	0.32	88	0.6	30	0.8	3	*
15. Red vacuum hose (outgassed + 24 hr dry N_2)	141	0.32	11	0.5	-	-	-	*
16. Perbunan	65	3.5	35	0.3	22	0.5	5	-
17. Perbunan PD 651 (vulcanized 30 min)	22.2	0.7	56	0.4	31	0.5	4	*
18. Perbunan DR-39 (low acrylonitrile)	22.2	0.7	94	0.65	41	0.56	20	*
19. Perbunan (Bayer)	12	0.1	20	0.5	10	0.5	-	-
20. Perbunan (Bayer) (tempered)	12	0.39	4	0.59	1.2	1.1	-	-
21. Butyl GRI (V-3) (1/2 hr 50 per cent relative humidity)	30	2	-	-	20	-	-	-
22. Butyl (DR-41) (40% C black; vulcanized 12 min)	22.2	0.7	15	0.68	4	0.64	-	*
23. Butyl (BU. 12000)	100	0.35	20	0.64	6	0.42	-	26
24. Butyl (BU. 12000) (non-condensable liquid air)	100	0.35	1	0.42	0.55	0.51	-	26
25. Convaseal	65	3.5	14	0.2	9	0.39	-	-
26. Convaseal (extruded 3/8 in. square)	39	0.4	10	0.5	4.9	0.6	50	91*
27. Convaseal	100	0.4	5.0	0.46	2.6	0.4	30	10
28. Polyisocyanate rubber D-43	22.2	0.7	280	0.45	127	0.37	10	*
29. Nygon	65	3.5	130	0.5	65	0.6	5	-
30. Hycar H-50 (ASTM spec. SB-510)	6.5	1.5	120	0.42	70	0.45	>50	10
31. Hycar H-50 (ASTM spec. SB-510)	65	1.5	140	0.48	74	0.5	>96	10
32. Silicone rubber (Wacker R 60)	12	0.39	70	1.07	17	1.1	-	-
33. Silicone rubber (Wacker R 80)	12	0.39	180	1.0	44	1.2	-	-
34. Silicone rubber (24 hr 95 per cent humidity)	100	0.32	230	0.65	46	1.3	-	-
35. Silicone rubber (outgassed + 24 hr dry N_2)	100	0.32	13	0.5	-	-	-	-
36. Silastic	-	1	25	0.55	6	1.8	-	-
37. Silicone rubber	22.2	0.7	94	0.75	31	0.8	20	-
38. Silastic X-6145-C	65	1.5	25	1.0	5.6	1.07	>90	10
39. Silastic 8-164 (red, 62 Durometer)	65	1.3	12	0.9	3.7	0.9	70	10
40. Silastic 80 (white, cured 24 hr at 480° F, 74 Durometer)	65	1.3	28	1.0	6.0	1.0	>50	10
41. Silastic 50 (white, 55 Durometer)	65	1.3	30	1.0	6.4	1.0	>50	10
42. Silastic 67-163 (red, 61 Durometer)	65	1.3	19	0.93	5.4	1.0	>50	10
B. PLASTICS								
1. Teflon, Dupont	12	0.23	4	0.7	1.6	0.7	-	-
2. Teflon, high temperature (24 hr at 95 per cent humidity)	27	0.32	42	0.93	6	-	-	-
3. Teflon, high temperature (outgassed - 24 hr dry N_2)	27	0.32	0.1	2	-	-	-	-
4. Teflon, Ceroc (24 hr at 95 per cent humidity)	42	0.32	35	0.46	19	-	-	-
5. Teflon, Dupont	65	1.5	5	0.68	1.2	1.2	3	2.6
6. PTFE	-	1	3	0.45	1.5	0.56	-	-
7. Kel-F (Oak Ridge National Laboratories)	65	1.5	0.4	0.57	0.17	0.53	-	10
8. Kel-F 270	47	0.4	-	-	0.16	0.55	-	0.6
9. Araldite D	650	3.5	80	0.8	22	0.78	-	-
10. Araldite D	30	0.7	19	0.3	12.5	0.5	-	-
11. Araldite B	30	0.7	18	0.4	9.2	0.5	-	-
12. Araldite F	30	0.7	15	0.5	7.3	0.5	-	-
13. Araldite, Type F (cured 15 hr 266° F)	62	0.4	5.5	1.3	0.9	1.3	10	0.3
14. Epoxy resin 200 (24 hr 95 per cent humidity)	50	0.32	110	0.6	-	-	-	-
15. Epoxy resin 200 (outgassed + 24 hr dry N_2)	50	0.32	0.2	1.6	-	-	-	-
16. Eppon, Shell Oil Co.	41	0.4	40	1.2	8.5	1.2	50	40
17. Plexiglas (Alsthom)	30	0.7	31	0.4	18	0.4	-	-
18. Plexiglas M222 (Rohm and Haas)	12	0.10	19	0.43	10	0.57	-	-

P-1194

Table 1 - (Cont'd)

MATERIAL	A_m	S_a	$10^7 K_1$	a_1	$10^7 K_1$	a_4	t_m	ω_m^2
B. PLASTICS (Continued)								
19. Plexiglas (24 hr at 95 per cent humidity)	62	0.32	115	0.65	40	0.75	-	-
20. Plexiglas (outgassed + 24 hr dry N_2)	62	0.32	10	0.5	-	-	-	-
21. Mylar (24 hr at 95 per cent humidity)	289	0.32	0.1	4.3	-	-	-	-
22. Mylar V-200 (24 hr at 95 per cent humidity)	370	0.32	23	0.75	4	-	-	-
23. Mylar V-200 (outgassed + 24 hr dry N_2)	370	0.32	1.3	1.33	-	-	-	-
24. High temperature Thermalon (24 hr at 95 per cent humidity)	82	0.32	13	2.3	0.1	-	-	-
25. Polyvinylchloride (34 hr - 95 per cent humidity)	70	0.32	8.5	1.0	0.2	-	-	-
26. Polyvinylchloride (outgassed + 24 hr dry N_2)	70	0.32	0.08	3.2	-	-	-	-
27. Polyethylene (BASE)	12	0.10	2.3	0.5	1.15	0.5	-	-
28. Polyethylene (Dynamit-AG)	12	0.23	2.6	0.5	1.3	0.5	-	-
29. Polyamid (Bayer)	12	0.12	46	0.5	23	0.5	-	-
30. Ultramid (BASF)	12	0.1	17	0.5	8.5	0.5	-	-
31. Polyvinylcarbazol (BASF)	12	0.23	16	0.5	8	0.5	-	-
32. Polystyrol (BASF)	12	0.14	6	0.5	3	0.5	-	-
33. Polystyrol (Dynamit-AG)	12	0.14	15	0.5	7.5	0.5	-	-
34. Polyurethane (Bayer)	12	0.85	5	0.5	2.5	0.5	-	-
35. Textolite 11564 (24 hr at 95 per cent humidity)	61	0.32	55	0.7	18	1.1	-	-
36. Textolite 11564 (outgassed + 24 hr dry N_2)	61	0.32	0.1	3.3	-	-	-	-
37. Nylon	-	1	120	0.5	60	0.5	-	-
38. Peramfil (General Electric Co.)	57	0.4	400	1.8	40	1.2	50	23
39. Polyester (Zenith Plastic Co., fiber glass laminate)	52	0.4	23	0.84	7	0.84	50	16
40. Polyester (Plastone, fiber glass laminate)	59	0.4	25	0.84	8	0.81	50	40
41. Polyester (Perault)	30	0.4	34	0.72	13.5	0.67	40	40
42. Polyester, Norsodyne	430	0.7	16	0.36	10	0.36	100	-
43. Celluloid	12	0.39	86	0.5	43	0.5	-	-
44. Polythene	80	0.4	200	1.6	20	1.6	-	-
45. Methylmethacrylate	174	0.7	42	0.9	14	0.57	-	-
46. Epicote	82	0.7	25	0.5	12.5	0.5	-	-
C. CERAMICS								
1. Porcelain, glazed	30	0.7	6.5	0.5	3.0	0.5	-	-
2. Steatite	30	0.7	0.9	1	0.24	1	-	-
D. METALS								
1. Stainless steel	-	1	-	-	0.049	1.6	0.014	-
2. Stainless steel	65	3.5	1.75	1.1	0.44	0.84	0.21	0.75
3. Stainless steel	-	0.7	0.9	0.75	0.3	0.75	0.2	0.75
4. Mild steel	65	3.5	5.4	1	1.4	1	0.5	1
5. Mild steel (slightly rusty)	-	1	6.0	3.1	0.28	1.5	0.13	1
6. Steel, rusty	65	3.5	44	1.4	5.5	1.4	1.6	1.3
7. Iron	12	-	4	1	1	1	-	-
8. Nickel plated mild steel (polished, vapor degreased)	-	1	5	2	0.036	1.4	0.01	-
9. Nickel plated steel	65	3.5	2.8	2	-	-	-	-
10. Chrome plated mild steel (polished, vapor degreased)	-	1	0.1	1	0.023	0.93	0.009	-
11. Aluminum, anodized	65	3.5	-	-	3.6	0.8	1.1	2.3
12. Aluminum, bright rolled (cleaned in Stergene)	65	3.5	-	-	0.22	1	0.075	1
13. Aluminum	12	-	15	1	3.7	-	-	-
14. Duraluminum	-	0.7	1.7	0.75	0.6	0.75	0.35	0.75
15. Aluminum spray coated mild steel	65	0.4	0.6	0.75	0.2	0.75	0.1	0.75
16. Aluminum spray coated mild steel (rusted)	65	0.4	1.8	0.65	0.8	0.75	0.4	0.75
17. Copper (24 hr at 95 per cent humidity)	100	0.32	0.2	2	-	-	-	-
18. Copper	12	-	23	1	-	-	-	-
19. Brass (24 hr at 95 per cent humidity)	43	0.32	0.15	2.5	-	-	-	-
20. Brass, cast	650	3.5	10	1	2.5	1	1.1	0.75
21. Brass, wave-guide section	50	0.3	4	2	0.3	1.4	0.1	1.2
22. Nickel	12	-	6	1	1.5	1	-	-
23. Nickel	12	-	10	1	2.5	1	-	-
24. Molybdenum	12	-	7	1	1.7	1	-	-
25. Tantalum	12	-	9	1	-	-	-	-
26. Zirconium	12	-	13	1	-	-	-	-
27. Tungsten	12	-	2	1	-	-	-	-
28. Silver	12	-	6	1	-	-	-	-

* Sample not in form of flat sheet (O-ring, tube, etc.)
(From Dayton, B. B. "Vacuum Chamber, Outgassing and Speed Relations", Vacuum Technology, 1959)

P-1194

It is also assumed that there will be no outgassing of vehicle or instrument surfaces. Wire insulation, lubricants, bearings, retainer rings, and similar material could outgas, evaporate, or decompose thereby contaminating the lunar atmosphere or lunar surface. Such contamination could give highly misleading analyzer readings. This problem was encountered by workers at the Smithsonian Institution's Astrophysical Observatory when they analyzed atmospheric samples collected by high altitude aircraft and balloons.[3] It was certain that a large number of the particles were not of natural origin, making it necessary for them to report inconclusive results. However it is possible, by careful material selection and design, to avoid outgassing problems without losing other essential properties.

A laser sample inlet system would be used to vaporize soil samples so the vapors could be introduced into the lunar analyzer for subsequent analysis. It would operate without special cooling equipment and lase at a wavelength in the 5000-6000 Å range. Because of the wide variation in temperature between the lunar night and day, especially near the equator where the temperature vary from 120°K to 400°K, respectively, it might be more practical to do the sampling during the lunar night.

It is conceivable that by scheduling the analysis at night, two advantages could be obtained: One, there would be less temperature adjustment or corrections necessary for the associated circuitry; and two, the power required to operate the other instruments during the day would not be as great. The disadvantage is that a popular source of power, the solar cell, cannot be capitalized upon unless a battery-charging system would be employed.

Obviously, all the possible environmental parameters can not be anticipated; however, the more prominent of these are discussed in the remainder of this subsection.

3.3.1 Mechanical Constraints

After the lunar landing the environmental parameters which could induce mechanical stress or strain would be no more severe than that normally experienced in the laboratory, except those caused by the extreme temperature variations (120°K to 400°K). The resulting expansion and contraction caused by such temperature variations will require the use of metals with similar properties. However, this is not a particularly difficult design problem, since Bendix has accomplished several very extensive material surveys.

3.3.2 Temperature

Lunar temperatures, as measured by vacuum thermopiles, are characterized by extremes, reaching 270°F (405°K) at the subsolar point on a full moon and then dropping to about 175°F (353°K) at the quarter phase at the same point. In the limb area (edge of the moon) at full moon, temperature readings of 67°F (293°K) have been made. When the sun rays are on the moon's horizon, temperatures fall to about -75°F (214°K), while nighttime temperatures are believed to plunge as low as -240°F (122°K). Due to the moon's slow rotation, the daily rate of temperature change is likewise slow; although, during an eclipse by the earth a temperature drop from +160°F (344°K) to -110°F (194°K) in an hour has been observed. It is believed that, the large thermal mass of the analysis vehicle, analyzer compartment, and the power dissipated by electronics will serve to maintain a constant temperature during a particular analysis period.

The temperature range of 120°K to 400°K should not present a problem in designing the analyzer, although care will have to be exercised in the choice of the vacuum sealing and gasket materials in order to make certain that leaks do not develop in the analyzer thereby allowing gases from the vehicle to interfere with the analysis.

Appendix B presents data concerning various radio observations of the moon's temperature.

3.3.3 Radiation

The spacecraft and lunar analyzer will encounter both galactic and solar radiation while on the lunar surface and during the journey to the moon. This subsection describes the sources of radiation, the interaction of this radiation with matter in order to assess the lunar analysis device for possible damaging effects, and makes recommendations to radiation harden the system where required.

3.3.3.1 Ionizing Radiation

There are three probable sources of radiation at the lunar surface: That due to solar radiation; galactic cosmic radiation, sources outside the solar system; and natural radioactivity, possibly produced by the first two radiation sources. Whereas the solar radiation varies in intensity and energy with solar activity, the galactic radiation, originating outside the solar system, is believed to have a constant intensity. The galactic cosmic radiation is a flux of high energy

atomic nuclei completely stripped of their planetary electrons and moving with velocities near or in the relativistic range. The galactic radiation consists of nuclei of those elements which are most prominent in nature. The principal constituents of this flux are hydrogen nuclei or protons. The relative abundance of galactic cosmic particles is 85.9 percent protons, 12.7 percent helium nuclei (alpha particles), and 1.4 percent particles with mass greater than helium.[4] The proton flux intensity is about 3 particles/cm^2-sec with energies greater than 10^9 ev.

The outward flux of plasma from the sun's corona is referred to as the solar wind and is composed of protons and heavier particles. During quiescent solar periods the particle density is about 10 particles/cm^3, the velocities of the particles vary from 2 to 7 x 10^7 cm/sec (0.21 to 2.5 kev), and the flux intensity is about 3 x 10^8 particles/cm^2-sec.[5] During disturbed solar conditions the flux can increase to 1.0 x 10^{10} particles/cm^2-sec with velocities up to 1.5 x 10^8 cm/sec (10 kev).[6]

If a magnetic field is present, such as in the earth's case, the solar wind does not reach the surface. There is presently no evidence for existence of a magnetic field on the moon. Table 2 shows solar radiation energy and wavelength distribution.

Shortly after a solar flare, usually less than an hour, energetic protons appear at the moon's surface. The duration of bombardment lasts anywhere from several hours to a day or more. A

Table 2 - Solar Radiation

Spectra of Solar Radiation	Wavelengths Bands of Solar Radiation, Å	Solar Energy Over Wavelength Bands Noted % Total	Distribution Over Wavelength Bands, Pyrons	Distribution Milliwatts/cm^2
Vacuum ultra-violet	< 2000	0.2	0.004	0.28
Ultraviolet	2,000-3,800	7.8	0.156	10.92
Visible	3,800-4,200	5.0	0.100	7.00
	4,200-7,000	36.0	0.720	50.00
Infrared	7,000-10,000	22.0	0.440	30.80
	10,000-20,000	23.0	0.460	32.20
	20,000-30,000	4.0	0.080	5.60
	730,000	2.0	0.040	2.80

P-1868

Some authorities claim 3800-4000 is still in ultraviolet. (Chem. Rubber Handbook).

large flare can produce about 1 x 10^{11} protons/cm^2 with energies greater than 1 Mev[7] (Figure 1). The radiation damage produced by solar flare protons is a function of the proton energy spectrum, the flux intensity, and the flare duration.

During the period from 1966 to 1972 (the predicted period of high solar flare activity) these solar flares will be of particular importance to the lunar mission. Figure 2 shows the frequency of solar flare events at the earth's polar cap.

Radiation at the lunar surface can be the result of a combination of the following: galactic, cosmic, and solar radiation induced neutron scattering from the surface material; the decay of short-lived unstable isotopes produced by the same cosmic and solar radiation; and the decay of the radioactive materials originally present in the surface material.

Estimates of the surface radiation indicate a possible neutron flux of 0.02 neutron/cm^2-sec and a gamma component of 0.6 gamma/cm^2-sec (2.7 x 10^{-8} ergs/gm(c)-sec).[8]

The lunar radiation environment is summarized in Table 3.

Table 3 - Summary of Lunar Radiation Environment
(Ambient and Distributed)

Radiation	Description
Galactic Cosmic Particles	Particle abundance and type is: protons 85.9 percent; alphas 12.7 percent; various heavier nuclei 1.4 percent. Flux intensity = 3 particles/cm^2 -sec (E>1,000 Mev). Integrated flux = 1 x 10^8 particles/cm^2 -year.
Solar Wind	Composed of low energy protons and heavier particles. Quiet sun: Flux intensity = 3 x 10^8 particles/cm^2-sec (E $\leq$ 2.5 kev). Integrated flux = 1 x 10^{10} particles/cm^2-year Active sun: Flux intensity may increase to: 1 x 10^{10} particles/cm^2-sec with energies up to 10 kev.
Solar Flare	Quiet sun: No significant flares between 1962 and 1965 Active sun: Years of probable flare activity from 1966 through 1974 with a possible maximum activity in 1968. During a large flare the integrated proton flux (Figure 1) could reach: 1 x 10^{11} p/cm^2 (E > 1 Mev). Flare duration might be 40 to 60 hours.
Lunar Surface Radio-activity	Estimated neutron flux = .02 neutrons/cm^2 -sec Integrated flux = 6.3 x 10^5 neutrons/cm^2 -year Probable gamma flux due to isotope decay =0.6 gamma/cm^2-sec = 2.7 x 10^{-8} ergs/gm(c)-sec, integrated gamma flux =0.85 ergs/ gm(c)-year.

P-1868

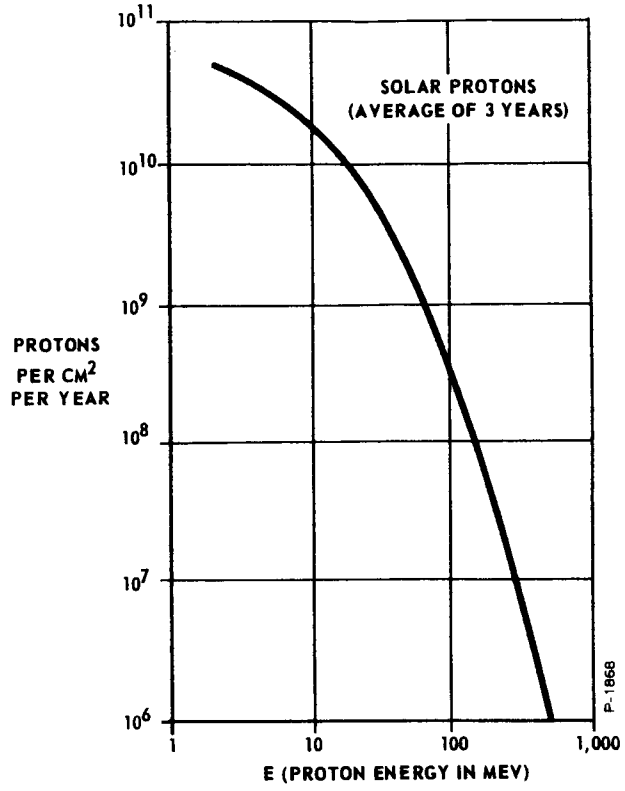

Figure 1 - Solar Flare Proton Density at Moon's Surface

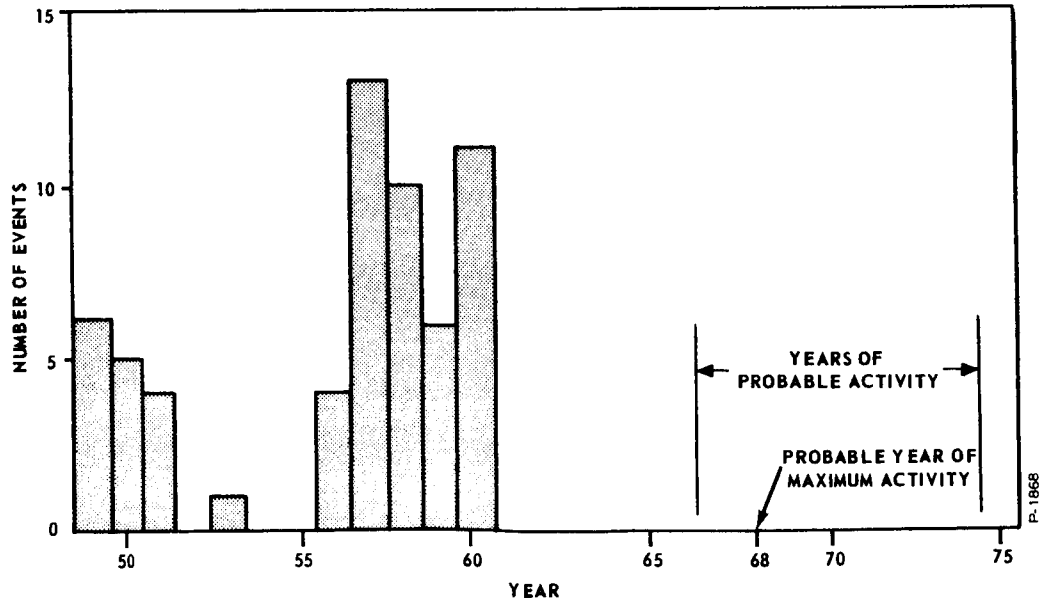

Figure 2 - Frequency of Solar Flare Impingement on the Polar Cap

3.3.3.1.1 Interaction of Radiation with Matter

There are two primary mechanisms by which electrons with energies up to 1 or 2 Mev can interact with matter. One method is by direct interaction -- in such cases these electrons excite the orbital electrons of an atom to the point where they leave the parent atom. The loss of energy and hence, the penetration of these electrons into matter is regulated by this interaction. A second method occurs when these electrons are accelerated by the electric field of a nucleus of an atom. During this process a photon is emitted which has energies up to that of the electron. These photons are referred to as bremsstrahlung and can cause radiation damage similar to that caused by gamma rays.

Protons originating in solar flares or the Van Allen Belt are likely to have high energies. The primary manner in which these protons lose their energy is through collisions with the electrons of atoms. The collisions of protons in matter are similar to the collisions of photons with electrons; the proton penetration in matter is a function of the number of collisions. High energy protons are quite penetrating compared with electrons of the same energy; i.e., it is more difficult to shield out these high energy protons. However, the production of bremsstrahlung is unimportant for the high energy protons under consideration.

Thus far, all of the interactions of protons and electrons which cause them to lose energy, results in ionization of the material. Another important consideration is the Rutherford scattering of protons with the atomic nuclei. This process, generally, does not affect atomic displacements in metals and semiconductors. Interestingly, the number of displacements produced decreases with increasing proton energy, but rises with increasing electron energy.

The interaction of low energy protons and heavier nuclei ($10 \text{ ev} < E < 1 \text{ Mev}$) with matter is a process called sputtering; in this process, the surface atoms in a solid or liquid are knocked-off by impinging atoms or ions. Sputtering due to the solar wind should be less than 3 Å of surface loss per year of exposure.[9] One problem with sputtering is not so much the damage to the surface, but the re-deposition of the knocked-off material on another surface.

3.3.3.1.2 Radiation Effects on Electronic Components

The effects of space and lunar radiation on electronic components such as resistors, coils, capacitors, and magnetic materials do not present any serious design problems, as indicated by Table 4. Table 5 shows that most materials (including some electronic components) are orders of magnitude less sensitive to ionizing radiation than most semiconductor devices. Table 6 shows that only semiconductor devices are sensitive to atomic displacements likely to be produced during a large solar flare. It therefore seems reasonable to assume that the maximum radiation level at which a circuit will operate reliably is determined by the sensitivity of the semiconductor devices employed.

Transistors and other semiconductor devices can be damaged by space radiation in one or more of the following ways: ionization effects, surface effects, or crystal lattice damage.

Ionization effects in transistors are radiation dose rate dependent and the effects disappear when the radiation

Table 4 - Summary of Space and Lunar Radiation Exposures and Damaging Effects

Radiation	Exposure Dose	Damaging Effects
Van Allen Belt	Less than 10 rads for a 3 day trip to the moon	None
Galactic Cosmic Particles	From 5 to 12 rads/year*	None
Solar Wind	Sputtering is main damage mechanism	May remove up to 3Å from exposed surfaces.
Lunar Surface Radioactivity	6.3×10^{5} neutron/cm^2 -year 8.5×10^{-3} rads/year of gammas	Both doses too low for concern
Solar Flare	Up to 1×10^{11} protons/cm^2 -year Ionization = 10^{3} to 10^{4} rads through 1 gm/cm Atomic displacements = 10^{-12} to 10^{-11}	Solar flares can produce permanent and/or temporary damage in certain types of semiconductors, in particular, transistors.

P-1968

*"The Radiation Hazard of Space," Space/Aeronautics, pp 72-77, May, 1963.

Table 5 - Ionizing Radiation Doses to Produce Threshold Damage in Materials and Components

Component or Material	Dose - ergs/gm(C)**
Photographic film	10^{-1} - 10^{1}
Transistors (sensitive to surface effects)	10^{4} - 10^{6}
Optical glass (unprotected)	10^{6} - 10^{7}
Teflon (in air)	10^{6} - 10^{7}
Teflon (in vacuum)	10^{8} - 10^{9}
Semiconductor devices including (transistors, diodes, unijunctions, SCR's, photosensitive devices)	10^{8} - 10^{10}
Vacuum tubes	10^{8} - 10^{9}
Elastomers	10^{8} - 10^{10}
Generally approved Plastics (except teflon)	10^{8} - 10^{11}
Hydraulic fluids	10^{8} - 10^{11}
Capacitors	10^{8} - 10^{11}
Glass (nonbrowning)	10^{10}
Resistors	10^{10}
Magnetic materials	10^{11}

*Threshold Damage - a change of 10 to 15 percent in a device parameter or material characteristic.

** 1 rad = 100 ergs/gm(C)

P-1868

Table 6 - Radiation Damage Due to Atomic Displacements in Materials and Components

Component or Material	Fraction of Atoms Displaced
Optical glass	10^{-11} to 10^{-7}
Semiconductor (devices)	10^{-12} to 10^{-10}
Minority carrier effects	10^{-12} to 10^{-10}
Majority carrier effects	10^{-9} to 10^{-6}

P-1868

is removed. The effects are manifested primarily as increases in collector leakage current. For power transistors, increases in the collector current of a few microamperes are typical, while for high frequency or switching types of transistors the increase in the collector current should be in the nano-ampere range.

Crystal lattice damage is dependent upon the total radiation dose received by the transistor (usually doses greater than 1×10^6 rad or 10^{10} to 10^{12} proton/cm^2). This type of damage is caused by the interaction of energetic radiation with the atoms of the lattice and is manifested primarily as a decrease in transistor gain. It is a permanent type of damage, in that it remains after the radiation is removed.

Radiation can cause permanent or semi-permanent surface damage to transistors. The types of transistors manufactured today are usually quite sensitive to surface conditions; i.e., their electrical characteristics can be appreciably affected by surface changes. Much less is known about the origins of surface changes than about the origins of bulk property changes.

Recent reports[10] of radiation studies reveal that surface effects can manifest themselves in transistors at total radiation doses as low as 10^4 ergs/gm (C), typically between 10^4 to 10^6 ergs/gm (C). It has been shown that for one type of transistor the collector current increased from 1 to 2 orders of magnitude when exposed to a gamma dose rate of 1 rad/hour for 100 to 1000 hours. In addition to collector current changes, ionizing radiation has been found to cause changes in gain characteristics and increases in noise.

The Bendix Research Laboratories Division and other companies have performed studies on transistors to determine the effects of radiation dose, dose rate, bias, transistor environment, surface protection, and the phenomena of damage recovery. It has been observed that the greatest changes in a parameter generally occur when reverse bias and radiation are applied simultaneously to gas encapsulated silicon transistors with unprotected surfaces.

This whole problem of low level radiation damage is new; however, Bendix has a program to determine what types of devices are insensitive to these surface effects or at least exhibit a minimum of sensitivity when exposed to ionizing radiation. Insurance that there is no problem in the electronic systems can be

provided by performing radiation tests on all of the transistors before they are incorporated in the circuits. The following approach would be taken with regard to transistor selection:

(a) Mesa and epitaxial constructions appear to be most resistant to radiation effects.

(b) High alpha cutoff frequency transistor types are more resistant to radiation damage than are lower cutoff frequency units of the same material and construction.

(c) Surface passivated transistors and evacuated cans appear to lend themselves to minimizing surface radiation effects.

In order to understand what effects radiation can cause in a photomultiplier tube, it is necessary to understand how such devices operate.

The electron multiplier phototube utilizes the phenomenon of secondary emission to amplify signals composed of free electrons. Basically, photons impinge on a cathode liberating photoelectrons which in turn are beamed toward an anode (referred to as a dynode) by means of an electrostatic field. The secondary electrons from this dynode are multiplied by successive dynodes through the process of secondary electron emission.

The Bendix magnetic multiplier differs from the conventional tubes in that it utilizes a continuous surface of high resistance semiconductor material instead of a series of individual dynodes. This unique multiplier arrangement affords a number of advantages not available in conventional multiplier tubes. The two main advantages are very low dark currents and almost no photo emission.

A literature survey has revealed a paucity of radiation test data on conventional photomultipliers. Generally, the tests have looked at the dark current of tubes as a function of neutron and gamma dose rates. Figure 3 is a plot of all available data as a function of the gamma dose rates during testing. There appears to be a great discrepancy in the data on identical tubes tested by different experimenters. However, the objective in presenting the data of Figure 3 is to show that at least one form of ionizing radiation, gamma rays can cause difficulty in effecient tube operation, depending on the tube

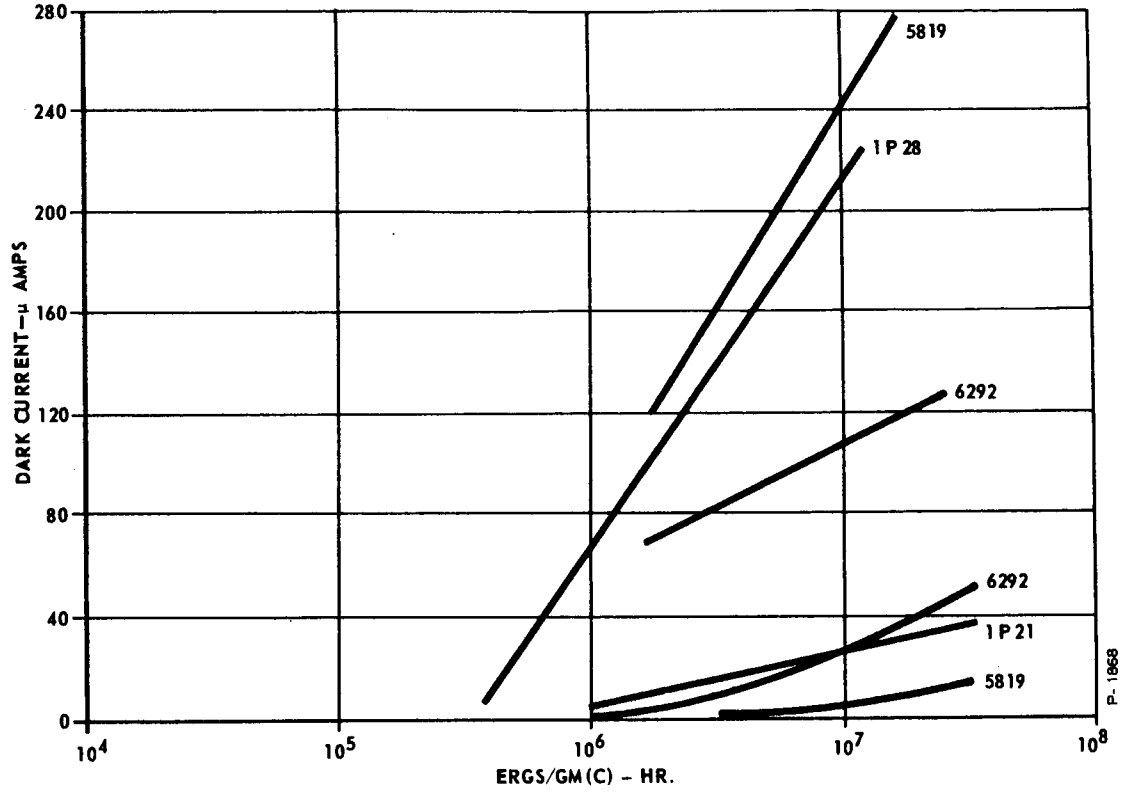

Figure 3 - Photomultiplier Tube Dark Current as a Function of Gamma Dose Rate

application. Many experimenters claim that at low gamma dose rates the dark current increase is directly proportional to the dose rate. Therefore, if sufficient test data were available, and if the radiation environment in which the tube will operate has been defined, it should be possible to predict the effects of ionizing radiation on tube performance.

The Bendix magnetic electron multiplier could be very sensitive to ionizing radiation because of the low dark current; however, the exact degree of sensitivity can only be determined by performing a radiation test on the tube.

Within the framework of the assumptions made, radiation damage appears to be a minor problem. By judicious selection of transistors, it should be possible to eliminate problems likely to occur in the analyzer electronics system. However, the Bendix magnetic multiplier should be tested in a suitable radiation environment to determine its acceptability for this mission.

3.3.3.2 Electromagnetic Radiation

The intensity of solar radiation, as established by rocket exploration of the upper atmospheres, is about 2.00 gram-calories/cm^2/min. (140 milliwatts/cm^2). This solar constant is defined as the rate at which energy is received from the sun upon a unit surface perpendicular to the sun's rays, above the earth's atmosphere, at its mean distance from the sun.

It can be seen that this is a fair approximation of the average energy received by that part of the moon's surface facing the sun. This energy has a spectrum as shown in Table 2.

The solar radiation above 3,000 Å can cause excitation in materials but should not be damaging to these materials. Materials are affected by the solar radiation on shorter wavelengths, only when this radiation is absorbed in the material. This absorption results when the incident photons produce ionization. Photon energies of 12 to 25 ev are thought to be the threshold for producing ionization in materials. This corresponds to a wavelength on the order of 1000 to 500 Å. Because of their short penetration into materials, when strong absorption of these photons occur, the radiation damage is confined to surfaces or surface coatings.

Ultraviolet radiation in air is known to darken glass and have deleterious effects on polymeric materials. In a vacuum, however, the absence of oxygen prevents some of the reactions from occurring.

Wahl and co-workers at Cornell Aeronautical Laboratory tested various glasses and laminates in a vacuum of $6 \pm 3 \times 10^{-6}$ Torr using a mercury lamp as an ultraviolet source. The lamp gave 2 pyrons of energy over the range of wavelengths from 2500 to 7000 Å, twice the intensity of the sun.

They found no change in the fused silica glass and aluminum-silica glass after 100 hours exposure to the mercury lamp, either in appearance or transmission of light as measured in the spectrophotometer. This is equivalent to 200 hours in space, (8-1/3 earth days), almost half the span of the daylight hours of a lunar day.

However, laminated glass did turn yellow and the transmittance of Plexiglass and Selectron went down substantially, almost to the point of opacity in the case of Plexiglass-55.

3.3.4 Pressure

The anticipated low values 10^{-8} to 10^{-13} mm Hg of lunar atmosphere (as determined in subsection 3.4.1) are not expected to present operating problems since the inherent ultimate sensitivity of the lunar analysis system to be proposed is in the 10^{-13} to 10^{-14} mm Hg range. However, extreme care will have to be exercised in the design of the analyzer to insure the ultimate in vacuum cleanliness, not only in the interior of the analyzer but also on the exterior and electronics section.

A very serious problem could arise from the interference caused by the outgassing of the analyzer compartment, outgassing of the exterior of the analyzer vehicle, outgassing due to the heating of the lunar surface by the landing rockets of the analyzer vehicle, or from the exhaust products of the vehicle itself.

Without regard to radiation, the effect of vacuum conditions at lunar temperatures on some metals and most polymers (plastics and elastomers) is evaporation and/or decomposition. Cadmium and zinc have high vapor pressures and should be avoided where sublimation or possible condensation on other and cooler surfaces would create problems.

The polymers find use as wire insulation, which might well be unprotected and open to space and lunar vacuum. Among the types of failures which can be found when the wrong insulation is used are evaporation of the entire coating, leaving bare spots of wire to short circuit; evaporation of some component of the coating, especially addition agents like ultraviolet absorbers or low molecular weight portions of the polymer itself which leads to decomposition or brittleness or other changes of physical properties; and condensation of the vaporized material on sensitive optical surfaces.

It can be seen that, before using such materials out in space, it is necessary to determine how much weight is lost in vacuum and, hopefully, the nature of the gases evolved. Another measure of outgassing is the pressure which can be achieved in a given vacuum chamber where a sample is placed in it. An empty chamber might, for instance, reach 3×10^{-7} Torr in 10 hours, and approach an ultimate pressure of 2×10^{-7} Torr. When a sample of material with a high vapor pressure is put in, the pump might not be sufficient to pull out all the gas which comes off, as well as the air that leaks into the system; consequently, 3×10^{-7} Torr is never achieved.

Table 7 shows the insulation weight changes after 100 hours in vacuum at 100°C and room temperature. Table 8 shows the nature of the outgassing products evolved from Teflon TFE and FEP. It is clear from the absence of fluorine that the products are adsorbed gas from the air, rather than breakdown products. Other data suggests that the irradiated modified polyolefin continues to outgas long after the time estimated for absorbed gas. Here it is apparent that there is either a decomposition or selective evaporation of the polyolefin. PVC (poly vinyl chloride) and silicon rubber seem to stabilize somewhat, leading to the conclusion that most of the volatile material would come off during the first few hours in space and there would be little change afterward. The Teflon curves are more or less parallel to the empty chamber curve, as one might expect from the mass spectrometer results, which show no material breakdown.

Table 7 - Insulation Weight Changes after 100 Hours in Vacuum

Insulation Sample	% Weight Change		Final Pressure Torr	
	100°C	R.T.	100°C	R.T.
"Teflon" TFE	0.04	0.01	3.2×10^{-7}	3.0×10^{-7}
"Teflon" FEP	0.08	0.04	2.2×10^{-7}	2.2×10^{-7}
Irradiated Modified Polyolefin	--	2.2	--	2.4×10^{-6}
Silicone Rubber	--	5.2	--	2.8×10^{-7}
"Teflon" FEP - "Pyre M.L."* (SUROK)	0.15	--	4×10^{-7}	4.0×10^{-7}
PVC	--	3.6	--	7.0×10^{-7}

P-2065

*DuPont trademark.

Table 8 - Outgassing Products Evolved at 100°C and 10^{-7} Torr

Time (hours)	Reference Amplitude							
	"Teflon"-TFE-Fluorocarbon				"Teflon"-FEP-Fluorocarbon			
	H_2O	N_2	O_2	CO_2	H_2O	N_2	O_2	CO_2
1	6.5	5.0	1.0	2.0	6.5	5.0	0.5	3.0
25	1.5	1.2	0.8	1.0	2.8	0.8	0.4	0.4
50	1.0	1.0	0.8	0.8	2.7	0.8	0.3	0.4
100	0.7	0.8	0.8	0.8	1.0	0.5	0.3	0.3

P-2065

It is for reasons such as these that Teflon and Pyre-ML covered Teflon are being used in space vehicles. The Pyre-ML covered version was developed about a year ago after it had been noted that the polyimides (of which Pyre-ML is one) had remarkable advantages for wire coating, being resistant to high and cryogenic temperatures, nuclear radiation (2000 megarads) and vacuum. It can be seen that its volatility is slightly higher than Teflon, but far lower than other insulations. Teflon and Pyre-ML are DuPont trademarks and the combined coating is known as Surok and marketed by Suprenant Division of International Telephone and Telegraph. One advantage of the combined coating is that it adheres well to any potting material and is somewhat tougher than most wire coatings, as judged by chisel pentration tests.

Some of the expected interference components due to outgassing of the vehicle or from the lunar surface are described in subsection 3.4.1. Special consideration would be given to this problem.

3.4 DISCUSSION OF MEASUREMENTS THAT ARE TO BE MADE

A very thorough investigation of current scientific literature dealing with "The Lunar Atmosphere and Soil Environment" has resulted in a definition of the most likely constituents -- successful analyzers should be capable of measuring at least the components of these models.

Table 9 - Likely Lunar Atmosphere Components

	Gas or Vapor	M (amu)	Pressure	
			Atmospheres	mmHg
L_1	Argon	39.94	5×10^{-16}	4×10^{-13}
L_2	Carbon Dioxide	44.01	1×10^{-11}	9×10^{-9}
L_3	Sulphur Dioxide	64.06	2×10^{-11}	1×10^{-8}
L_4	Water	18.02	5×10^{-12}	4×10^{-9}
L_5	Krypton	83.7	5×10^{-5}	3×10^{-2}*
L_6	Xenon	131.3	6×10^{-6}	5×10^{-3}*

*The relatively high values for krypton and xenon arise from a rather large assumed value of crustal effusion flux.

The following subsections discuss several lunar environmental models and show the criteria by which the lunar atmospheric gases listed in Table 9 were chosen.

3.4.1 Lunar Atmosphere

Based on theoretical models, upper limits have been obtained for the lunar atmosphere. In France, Dollfus[11] made polarimetric observations which indicated that the density of the lunar atmosphere was only about 10^{-9} that of the terrestrial atmosphere. A detailed investigation by J. N. Lipskij[12] indicated a density of 10^{-4}; however, this analysis has been effectively questioned by E. J. Opik,[13] who concludes that the absence of observable optical effects near the moon's cusps indicate that the upper limit is about one millionth (and probably less) that of the terrestrial atmosphere.

Observations by Elsmore[14] indicate that a pressure of about 10^{-13} atmospheres can be deduced as an upper limit. His observations were based on the refraction of a radio star's signal as it passes by the lunar disk.

It appears that the moon's thin atmosphere results because of its low gravitational field (1.62 m/sec^2) and elevated daytime temperatures (400°K). The kinetic theory of gases show that molecules are continually in movement at velocities dependent on the molecular weight of the gas and on the temperatures. Some gas molecules that might have formed an ancient lunar atmosphere have, probably, long since dissipated into space due to the fact that the velocity of escape from the moon is so low and the daytime temperatures are so high. That the moon has only a thin atmosphere has been indicated by many direct and indirect experiments.

Nevertheless, there is evidence to suggest a very thin lunar atmosphere, probably fed by gases seeping out of the crust, particularly around semi-dead volcanoes and cracks in the surface. These gases would accumulate locally in pockets and depressions but tend to dissipate; consequently, the atmosphere could only be sustained by continuous replenishment.

Radio-astronomical observations have indicated that the moon has some sort of atmosphere composed of rare, and relatively heavy gases like krypton, xenon, and perhaps argon. Singer[15] concludes that neither krypton nor xenon can be retained by the moon since electric

forces created by the ionizing effects of solar ultraviolet radiation would tend to eject these gases into space over periods of hundreds of years. Thus, for a krypton-xenon atmosphere to persist, continuous replenishment would be required. However, it is presumed that argon is continually being produced on the surface from the radioactive decay of potassium-40, but that it also will leak into space rather rapidly.

There might be some residual gases caused by volcanic activity. Some observers have reported sighting an occasional mist in certain areas of the moon, probably a result of outgassing. Other evidence suggests there could be a very diffuse ionosphere, but just what causes it is not known. However, the very existence of an ionosphere implies an atmosphere that is ionized. The most plausible theory is that the solar wind interacts with the atmosphere to produce an ion layer with a density of about 300 to 500 protons/cm^3.

Even an extremely tenuous atmosphere would destroy most of the meteors that presumably bombard the moon. If the lunar atmosphere at the surface was, for example, 10^{-5} as dense as the earth's atmosphere at the surface and since the earth's gravitational attraction is much greater than the moon's, their densities would be about the same at an altitude of about 40 miles. Such an atmosphere would be able to destroy most meteorites before they reached the surface. However, the latest evidence indicates a much less dense lunar atmosphere. If it were 10^{-13} that of the earth, equal densities would occur at some 175 miles. How useful this atmosphere would be as a meteoritic shield is very speculative.

Lunar temperatures, as measured by vacuum thermopiles, are characterized by extremes reaching 270°F (405°K) at the subsolar point on a full moon and dropping to about 175°F (353°K) at the quarter phase at the same point. In the limb area (edge of the moon) at full moon, temperatures of about 67°F (293°K) occur. When the sun is on the moon's horizon, temperatures fall to about -75°F (214°K), while nighttime temperatures are believed to plunge as low as -240°F (122°K). Due to the moon's slow rotation, the daily rate of temperature change is slow; however, during an eclipse by the earth a temperature drop from +160°F (344°K) to -110°F (194°K) in an hour has been observed. Other measurements indicate that the temperature of the disk of the new moon is about -200°F (144°K) and that in deep layers the temperature averages about -38°F (234°K). It is likely that heat flows into, and out of, the moon very slowly, which suggests that the crust (as

opposed to the surface layers) is a very good insulator. From this fact, it is assumed that the temperature on the moon is different in the sense we know it on earth, because of the absence of an atmosphere to permit equilibrium to be reached. The moon not only receives solar radiant energy, but also solar corpuscular radiation, high energy protons (principally cosmic radiation), and micro-meteorite bombardments, all of which play an important part in determining the environment.

In the absence of direct measurements, our information on the lunar atmosphere must be obtained by other methods. The problem resolves to one of finding possible atmosphere sources and comparing the strength of these sources with the mechanisms of dissipation. If the sources are weaker than the rate of dissipation, an atmosphere cannot build up. The following subsections discuss two possible sources of a lunar atmosphere.

3.4.1.1 Atmosphere from Internal Sources

Particles of a gas or vapor behave in a manner defined by Maxwell-Boltzmann statistics. If the particle density is great enough (Maxwell-Boltzmann statistics requires a large statistical sample) some particles can acquire, by particularly energetic or weak collisions, velocities considerably higher or lower than the average velocity. If a particle acquires a velocity higher than the velocity of escape and is appropriately directed, that particle can be lost from the lunar environment. The number of such particularly fast particles of mass M bears a constant ratio to the total number of all gas molecules, and is predictable statistically for each temperature. It is possible to estimate theoretically the number of molecules or atoms of any gas that escape from the lunar atmosphere in a given time. An analysis by Jeans reveals that if the mean molecular velocity of thermal agitation is one third that of escape velocity, one-half of the corresponding atmosphere will be dispersed in a few weeks. If this velocity ratio is 1/4, then the half-life of an atmosphere would be 50,000 years, and for the ratio 1/5, the atmospheric half-life would be 10^9 years.

3.4.1.1.1 Jeans' Criterion for a Stable Lunar Atmosphere

Jeans'[16] simple isothermal gravitational criterion for determining what gas or vapor of mass number M can form a stable atmosphere for astronomical periods (greater than 10^9 years -- the moon's age) is

$$v\ (\text{average}) \leqq 0.2\ v\ (\text{escape}) = 0.476\ \text{km/sec} \qquad (1)$$

where

v (average), the average molecular velocity of the gas, is

$$\sqrt{\frac{8\,k\,T_c}{\pi\,m}} \qquad (2)$$

and

v (escape), the lunar escape velocity, is

$$\left[\frac{2\,GM}{R}\right]^{1/2} = 2.38\ \text{km/sec.}$$

All gases with v (average) satisfying the above expression are considered stable atmospheric components. The following table, Table 10, list various gases or vapors and their respective average molecular velocities for T = 400°K. It is seen that all gases with mass numbers greater than oxygen (32.00) are considered stable lunar gases.

3.4.1.1.2 Spitzer's Determination of the Lifetime of a Lunar Atmosphere

A more detailed analysis for determining the atmosphere near the moon is attributed to Dr. Spitzer.[17] This analysis supersedes Jean's treatment, but Jean's results for an isothermal atmosphere are still considered representative. In Dr. Spitzer's analysis the atmospheric lifetime, t_1, is considered to be the time required for an isothermal atmosphere to deplete to a density value 1/e of n_o, the density at t = 0.

A number of atoms at any height in the atmosphere are assumed to be moving in an upward direction with a velocity equal to, or greater than, the escape velocity. These are atoms whose total energy is positive. In an isothermal atmosphere the number of atoms per unit volume of momentum space depends on the total energy; thus, the density in the six-dimensional phase space (coordinates x, y, z, v_x, v_y, v_z) of the positive energy atoms will remain constant with height. At low altitudes none of these atoms can escape,

Table 10 - Average Molecular Velocities of Possible Lunar Atmospheric Gases or Vapors

Gas or Vapor	Mass amu	10^{23} m gm	$10^{10}\rho_o$ gm/cm^3	v_m -- km/sec				
				0°C	25°C	156°K	342°K	400°K
H_2	2.016	0.3347	0.8878	1.693	1.770	1.28	1.90	2.06
He	4.003	0.6646	1.7631	1.201	1.256	0.905	1.340	1.45
CH_4	16.04	2.663	7.063	0.6005	0.6273	0.450*	0.670	0.725
NH_3	17.03	2.827	7.498	0.5829	0.6089	0.440	0.650	0.70
H_2O	18.02	2.992	7.936	0.5665	0.5919	0.426	0.630	0.682
Ne	20.18	3.351	8.886	0.5355	0.5596	0.404	0.595	0.644
CO	28.01	4.651	12.34	0.4543*	0.4746	0.341	0.508	0.550
N_2	28.02	4.652	12.34	0.4542	0.4745	0.3422	0.508	0.550
Air	28.98	4.811	12.77	0.4468	0.4668	0.336	0.500	0.540
O_2	32.00	5.315	14.09	0.4252	0.4441	0.322	0.475*	0.514
Ar	39.94	6.631	17.59	0.3805	0.3976	0.286	0.425	0.460*
CO_2	44.01	7.308	19.38	0.3624	0.3787	0.274	0.408	0.442
CH_3Cl	50.49	8.383	22.23	0.3385	0.3356	0.259	0.376	0.416
SO_2	64.06	10.64	28.21	0.300	0.3039	0.226	0.336	0.364
Cl_2	70.91	11.77	31.23	0.2856	0.2984	0.205	0.318	0.344
Kr	83.7	13.90	36.85	0.2629	0.2747	0.199	0.293	0.317
C_7H_{16}	100.2	16.63	44.12	0.2403	0.2510	0.181	0.268	0.290
Xe	131.3	21.80	57.82	0.2099	0.2193	0.164	0.234	0.242
CCl_4	153.8	25.54	67.72	0.1939	0.2026	0.146	0.216	0.234
Hg	200.6	33.31	(88.33)$^\gamma$	0.1698	0.1774	0.128	0.19	0.206

P-1868

$^\gamma$The vapor pressure of Mercury at 0°C is 1.85×10^{-4} mm Hg thus the value in parentheses has no physical significance - actual density = 21.79×10^{-10}.

*Indicates gases with that molecular weights or greater will satisfy Jeans' criteria and could be a lunar atmosphere component.

since the probability of collision is too high. At a sufficiently great height, however, the mean free path in the atmosphere becomes very great, and the particles with sufficient energy can escape. The computation of the total outward flux of these positive energy atoms gives the total number of atoms leaving the moon per second, a quantity denoted by L.

The standard gas kinetic manipulations using Boltzmann's velocity distribution function are used to derive the number of molecules per second, L, leaving the lunar atmosphere. The model chosen is that of an isothermal layer of various gases at a temperature of 400°K. The loss of gas molecules is assumed to take place from a critical height, R_c, measured from the moon's center. If the escape velocity, $v_{esc.}$, at R_c is less than the velocity of a given molecule, then it can escape from the gravitational field of the moon. Thus, the density of an atmosphere surrounding a celestial body like the moon can be expressed as

$$n(h) = n_o e^{-(h/H)} \tag{3}$$

where

$$H = \frac{kt}{Mm_o g} \quad (1 + h/R_o)$$

R_o = radius of the moon

M = mean molecular weight (amu)

m_o = mass of unit atomic weight

g = acceleration of gravity

k = Boltzmann constant -- 1.38×10^{-16} erg-deg^{-1} K-mole^{-1}

and

h = height above the surface of moon.

The critical height, R_c, is that distance from the moon's center at which the collision frequency is low enough so that essentially no collisions occur.

If the flux of lunar atmospheric particles is assumed to pass through a spherical surface of radius R_c (the critical height), then the number of particles per second passing through this surface can be represented by the normal kinetic theory expression

$$dN\left(\frac{\text{mol}}{\text{cm}^2\ \text{sec}}\right) = \frac{n_c}{4}\bar{v} \cdot \tag{4}$$

Thus, L can be defined as

$$L = \frac{1}{4} \cdot \overbrace{4\pi R_c^2}^{\text{Area}} \overbrace{n_c}^{\text{Density}} \int_{v_{esc.}}^{v_\infty} v\,P(v)\,dv \tag{5}$$

where the integral is evaluated from the escape velocity, $v_{esc.}$, to the maximum v_∞ so that only molecules with escape velocity or greater are counted. Then,

$$L = 4\pi R_c^2 \cdot \frac{n_c}{4} \cdot 4\pi\left[\frac{m}{2\pi k T_c}\right]^{3/2} e^{\frac{GM'm}{R_c k T_c}}$$

$$\int_{v_{esc}}^{v_\infty} v^3 e^{-\left(\frac{m v^2}{2 k T_c} + \frac{GM'm}{R_c k T_c}\right)} \cdot dv \tag{6}$$

$$L = 4\pi^2 R_c^2 \cdot n_c\left[\frac{m}{2\pi k T_c}\right]^{3/2} \cdot e^{\frac{GM'm}{R_c k T_c}} \cdot 2\left(\frac{k T_c}{m}\right)^2 \cdot$$

$$\cdot \int_{\beta_{esc.}}^{\infty} \left[\beta - \frac{GM'm}{R_c k T_c}\right] e^{-\beta}\,d\beta \tag{7}$$

After substituting

$$\beta = \frac{1}{2}\frac{m v^2}{k T_c} + \frac{GM'm}{R_c k T_c},\quad d\beta = \frac{m v}{k T_c}\,dv,\ \text{and}\ v dv = \left(\frac{k T_c}{m}\right) d\beta; \tag{8}$$

$$v^2 = \left[\beta - \frac{GM'm}{R_c k T_c}\right] \cdot \left(\frac{2kT_c}{m}\right) \tag{9}$$

and

$$e^Y = \exp\left[\frac{GM'm}{R_c k T_c}\right] = e^{\left(\frac{3v_\infty^2}{2c^2}\right)} \tag{10}$$

Thus, L can be determined by integration:

$$L = \frac{8\pi R_c^2}{\sqrt{3\pi}} \cdot \frac{n_c}{2\sqrt{2}}\left[\frac{3kT_c}{m}\right]^{\frac{1}{2}} e^Y\left[\int_{\beta_{esc.}}^{\infty} \beta e^{-\beta} d\beta - \frac{GM'm}{R_c k T_c}\int_{\beta_{esc.}}^{\beta} e^{-\beta}\, d\beta\right] \tag{11}$$

$$L = \frac{4\pi R_c^2}{\sqrt{6\pi}} \cdot n_c \cdot C\left[-e^{-\beta}\left((\beta+1) - \frac{GM'm}{R_c k T_c}\right) e^Y\right]_{\frac{1}{2}\frac{m v_{esc}^2}{kT_c} + \frac{GM'm}{R_c kT_c}}^{\infty} \tag{12}$$

$$L = \frac{4\pi R_c^2}{\sqrt{6\pi}} \cdot n_c \cdot C\left[-\left(1+\beta - \frac{GM'm}{R_c kT_c}\right) e^{-\beta}\right] e^Y \Bigg|_{2\left(\frac{GM'm}{R_c kT_c}\right)}^{\infty} \tag{13}$$

$$L = \frac{4\pi R_c^2}{\sqrt{6\pi}} \cdot n_c \cdot C\, e^{-Y} \frac{GM'm}{R_c kT_c}\left[1 + \frac{R_c kT_c}{GM'm}\right] \tag{14}$$

$$L = \frac{4\pi R_c^2}{\sqrt{6\pi}} \cdot n_c \cdot C\, e^{-Y} \frac{GM'm}{R_c kT_c}\left[1 + \frac{R_c kT_c}{GM'm}\right] \tag{15}$$

where

$$C = \sqrt{\frac{3kT_c}{m}} \tag{16}$$

This represents the number of particles per second of mass m lost from the lunar atmosphere at a temperature T.

In the preceding derivation, the Maxwell-Boltzman velocity distribution function representing the fraction of molecules of mass m in the lunar atmosphere having a velocity between v and v + dv at a critical height, R_c, with a gravitational potential energy of $GM'm/R_c$ is

$$P(v) = 4\pi \left[\frac{m}{2\pi k T_c}\right]^{\frac{3}{2}} \cdot e^{\frac{GM'm}{R_c kT_c}} v^2 e^{-\left[\frac{1}{2}\frac{mv^2}{kT_c} + \frac{GM'm}{R_c kT_c}\right]} . \tag{17}$$

This can be shown to be correctly normalized by setting the integral

$$\int_0^\infty P(v)\, dv \tag{18}$$

equal to one, as follows:

$$4\pi \left[\frac{m}{2\pi k T_c}\right]^{\frac{3}{2}} e^{\frac{GM'm}{R_c kT_c}} \int_0^\infty v^2 e^{-\left(\frac{m v^2}{2kT_c} + \frac{GM'm}{R_c kT_c}\right)} dv = 1 \tag{19}$$

$$4\pi \left[\frac{m}{2\pi k T_c}\right]^{\frac{3}{2}} e^{\frac{GM'm}{R_c kT_c}} e^{\frac{-GM'm}{R_c kT_c}} \int_0^\infty v^2 e^{\frac{-mv^2}{2kT_c}} dv = 1 \tag{20}$$

$$4\pi\left[\frac{m}{2\pi k T_c}\right]^{\frac{3}{2}} \sqrt{\frac{\pi}{4}} \left[\frac{2kT_c}{m}\right]^{\frac{3}{2}} = 1 \qquad (21)$$

Thus, the expression for L can also be written as

$$L = 4\pi R_o^2 C n_o Y e^{-Y}\left[\frac{R_c}{R_o}\left(1 + \frac{R_c}{Y R_o}\right)\right] . \qquad (22)$$

More elaborate investigations, based on a study of detailed collisional processes, have been made by Milne[18] and Jones[19] which include an atmosphere in adiabatic equilibrium. However, as shown by Spitzer[17], conduction will establish an isothermal temperature distribution for some distance below the critical level; hence Milne's generalization would appear to have little interest. However, for an isothermal atmosphere the extensive analysis of collisions carried out by Jones leads to a formula similar to Equation (22), except that the bracketed term $R_c/R_o\left[1 + (R_c/R_o\right]$ is replaced by R_o/R_c.

If the distribution of the atoms in the atmosphere is that of an isothermal gas with a Boltzmann distribution of velocities and there are no collisions, Jeans' equations should give the number of particles per second escaping. In view of the many variables in atmospheric densities and temperatures, the difference between the two sets of results is of little consequence. Thus, normal computations of L take the form

$$L = \frac{4\pi R_o^2}{\sqrt{6\pi}} C n_o e^{-Y} . \text{ (See Appendix C)} \qquad (23)$$

If the total number of particles, N_T, in an isothermal atmosphere is divided by L the result is t_1, the time during which the density in the atmosphere would fall by 1/e, if the atmosphere was, in fact, isothermal. This quantity is given by

$$t_1 = \frac{\sqrt{6\pi}}{3 g_e} C \frac{e^Y}{Y} . \qquad (24)$$

Table 11 - Lifetimes of Various Gases

Gas or Vapor	M (amu)	$\bar{v}_{400°K}$ x 10^{-5} cm/sec	$C_{400°K}$ x 10^{-5} cm/sec	y	e^y	$t_{400°K}$ year
H_2	2.016	2.05	2.22	1.70	0.7393 5.487	20.6×10^{-4}
He	4.003	1.45	1.57	3.42	1.4874 30.22	4.17×10^{-4}
CH_4	16.04	0.725	0.787	13.6	5.9146 8.215×10^5	1.37×10^0
NH_3	17.03	0.70	0.761	14.4	6.2626 1.831×10^6	2.76
H_2O	18.02	0.684	0.741	15.3	6.6540 4.508×10^6	6.3
Ne	20.18	0.645	0.702	17.1	7.437 2.735×10^7	32.3
CO	28.01	0.548	0.595	23.8	10.3506 2.242×10^{10}	1.62×10^4
Air	28.98	0.540	0.585	25.4	11.0465 1.113×10^{11}	6.0×10^4
O_2	32.00	0.519	0.557	27.2	11.8293 6.75×10^{11}	4.0×10^5
Ar	39.94	0.460	0.499	33.9	14.7431 5.542×10^{14}	2.36×10^8
CO_2	44.01	0.446	0.475	37.4	16.2653 1.842×10^{16}	6.75×10^9
CH_3Cl	50.49	0.418	0.444	42.8	18.6137 4.109×10^{18}	1.23×10^{12}
SO_2	64.06	0.372	0.393	54.4	23.5856 3.852×10^{23}	8.05×10^{16}
Cl_2	70.91	0.345	0.374	60.2	26.1809 1.517×10^{22}	2.73×10^{19}
Kr	83.7	0.318	0.345	71.0	30.8779 7.549×10^{30}	1.06×10^{24}
C_7H_{16}	100.2	0.290	0.313	85.0	36.9665 9.258×10^{36}	9.85×10^{29}
Xe	131.3	0.253	0.275	111.5	48.4914 3.10×10^{48}	2.21×10^{41}
CCl_4	153.8	0.234	0.252	130.8	66.8849 7.672×10^{66}	4.31×10^{59}
Hg	200.6	0.205	0.222	169.5	73.7156 5.195×10^{73}	1.96×10^{66}

P-1868

Thus, it is observed that the atmospheric lifetime, t_1, is independent of the density, n_o, and all collision cross sections; hence, it can be used for all components of a lunar atmosphere. Jeans considers t_1 to be the time required for the density of the atmosphere to fall to zero if L is constant. The difference between the numerical results found by Jones and those given by Jeans is entirely the result of Jeans' misinterpretation of t_1. If the correct interpretation is taken, the time given by Jeans for different values of Y are in good agreement with those computed by Jones. In order to show the relative lifetimes of arbitrary gases or vapors the expression for t_1 (Equation 24) was evaluated for the gases; the results are tabulated in Table 11. If 10^9 years is considered as the moon's age, then argon has the smallest mass number, of the gases considered, which has a lifetime comparable to the moon's age and hence is the lightest component which using this model can be considered as a possible lunar gas. Table 12 lists the gases or vapors chosen which have lifetimes commensurate with the age of the moon.

Table 12 - Possible Gases or Vapors Having Lifetimes Comparable to the Age of the Moon

Gas or Vapor	Symbol
Argon	Ar
Carbon Dioxide	CO_2
Methyl Chloride	CH_3Cl
Sulphur Dioxide	SO_2
Chlorine	Cl_2
Krypton	Kr
Heptane	C_7H_{16}
Xenon	Xe
Carbon Tetrachloride	CCl_4

P-1868

3.4.1.1.3 Determination of the Partial Pressure of Lunar Atmosphere Constituents

The composition and density of the lunar atmosphere are determined by the competition between the processes of gas accumulation and the escape of these gases into space. According to E. H. Vestine,[20] the probable sources of surface gases are:

(a) Radioactive decay of potassium producing argon with a source strength, J, of $5 \times 10^{+5}$ cm^{-2} sec^{-1}.

(b) Residual volcanic activity producing gases like sulphur dioxide, carbon dioxide and water vapor. The estimated source strength, of these gases based on terrestrial data, is 10^{10} cm^{-2} sec^{-1}.

As Jeans' model of the lunar atmosphere shows, the reduced gravitational potential of the moon indicates that gases will escape much more rapidly from the lunar surface than from the earth's atmosphere. The rate of escape also depends on the maximum temperature which determines the number of atoms or molecules in the high energy tail of the thermal distribution.

If an isothermal atmosphere and a Maxwellian distribution of particle velocities is assumed, then a calculation based on the balance between these two processes leads to the following equation which defines the equilibrium density of molecules at the lunar surface:

$$n_o = J\sqrt{\frac{\pi m}{2kT_c}} \left[1 + \frac{m M'G}{kT_c R_c}\right]^{-1} \exp \frac{m M'G}{kT_c R_c} \qquad (25)$$

where

J = the number of molecules ejected from the lunar surface per cm^2 per sec.

T = lunar atmospheric temperature

m = mass of an atmospheric particle

M = mass of the moon

and

R_o = radius of the moon $\approx R_c$.

Substituting the above values of J and T into the above equation, gives an equilibrium density, n_o, of about 5×10^{14} molecules/cm^3 or a pressure of 10^{-5} atmospheres for argon.

A similar calculation for the volcanic gases sulphur dioxide, carbon dioxide, and water vapor, yields values of pressure greater than 1 atmosphere for sulphur dioxide and carbon dioxide and greater than 4×10^{-9} atmospheres for water vapor. However, these values will be lowered substantially when allowance is made

for the effects of photodissociation or chemical reactions with the crust and for the fact that the age of the moon (4.5×10^9 years) does not allow enough time for the sulphur dioxide and carbon dioxide concentration to build up to equilibrium. Table 13 summarizes the assumed effusion rates from the lunar surface and the resultant density and partial pressure values for some possible lunar gases. The effusion rates, J, for argon, carbon dioxide, sulphur dioxide, and water vapor are given by E. H. Vestine who explains the surprisingly high values for the partial pressures of carbon dioxide, krypton, and xenon by the fact that the moon's age is insufficient for the assumed equilibrium to be established. More important, however, is the questionable accuracy of the effusion rates used and the possible inadequacy of the model for the higher mass numbers.

3.4.1.2 Atmosphere from External Interplanetary Sources

A question as to what is happening to the sulphur dioxide continually being generated by meteoritic impact and possibly feeble volcanic action arises. It is true these processes would release water vapor which combines with the sulphur dioxide to form sulphuric acid; but, since no sulphuric acid vapor is known to exist, the sulphur dioxide would not be affected. If the low upper limit of 3×10^{-8} atmosphere, set by Lyot and Dollfus[21] in their investigation with the coronograph, is to be considered valid, then the absence of the theoretical value of the atmosphere remains unexplainable. The limit was determined from the threshold intensity observable near the marks of the quarter-moon, expressed in terms of scattering power. The negative results of photographic plates make it possible to set a very low limit of 10^{-9} atmospheres for sulphur dioxide, one of the very few gases that could be retained by the moon.

Dr. Herzberg[22] suggested the possibility that the cold half of the moon might have a very low vapor pressure, causing a virtual depletion on the bright side. According to the International Critical Tables, the pressure of sulphur dioxide at T = -110°C (end of a total lunar eclipse) is 130 μ; however, Lyot and Dollfus' experiments show that a 3 μ limit is reached at T = 140°C. Since the coldest spot on the moon is much colder, it is indeed conceivable that the low calculated vapor pressure is due to the conceivable escape of the sulphur dioxide molecules toward the cold hemisphere. In addition,

Table 13 - Modified Jeans' Lunar Atmosphere Model

	Properties	Argon Ar	Sulphur Dioxide SO_2	Carbon Dioxide CO_2	Water H_2O	Krypton Kr	Xenon Xe
Jeans' Gravitational Isothermal Atmosphere Model	Crust Effusion Rate J - molecules/sec-cm^2	5×10^5	10^{10}	10^{10}	10^{10}	2×10^{16}	1.8×10^{15}
	Atmospheric Surface Density-mol/cm^3	4×10^{14}	4×10^{27}	2×10^{20}	8×10^{10}	2×10^{41}	4×10^{57}
	Atmospheric Pressure (at.) (mmHg)	1.6×10^{-5} 1.2×10^{-2}	$2.2 \times 10^{+8}$ 1.6×10^{11}	1×10^{1} 9.1×10^{3}	11×10^{-9} 3×10^{-6}	5×10^{21} 5×10^{24}	2.2×10^{38} 1.6×10^{41}

P-1868

photochemical decomposition could possibly destroy the gas on the luminous side of the moon.

Just as internal sources are present which can account for a lunar atmosphere, the sun and other celestial bodies could offer a source of a lunar atmosphere.

3.4.1.2.1 Effect of the "Solar Proton Wind" on the Extent of the Lunar Atmosphere

The preceding estimates of the lunar atmosphere are greatly reduced by the effects of the solar wind. It appears, in fact, that the solar wind could blow away all but a very small fraction of the lunar atmosphere. Consider a solar wind consisting of protons with the conventional density of 10^3 cm^{-3} and a velocity of 10^8 cm/sec or energies of 10 kilovolts (Bierman)[23]. In an elastic collision with an atom, 1 Kev of kinetic energy is transferred; this is sufficient energy for the escape of the atom. If it is assumed that every atom struck by a solar proton escapes, the rate of ejection of particles is readily calculated. The rate of ejection, R_P, of particles/cm^3 can be defined as

$$R_P = n_o n_p v_p \sigma \tag{26}$$

where

n_p = density of protons

v_p = velocity of protons

and

σ = proton-particle cross section.

If the equilibrium particle density, n_o, is now estimated at the lunar surface, by equating the rate of ejection of particles from a vertical column 1 cm^2 in cross-sectional area, as calculated by R_P above, to the rate of injection of particles, J, into the column at the surface

$$n_o = \frac{J}{n_p v_p \sigma h} \tag{27}$$

where

$$h = \frac{k T R_o^2}{m M' G} = \frac{R_o}{Y} . \qquad (28)$$

Then if $\sigma = 10^{-16}$ cm^2,

$n_o = 10^4$ cm^{-3} and $P_o = 5 \times 10^{-16}$ atmospheres of argon

$n_o = 3 \times 10^8$ cm^{-3} and $P_o = 2 \times 10^{-11}$ atmospheres of sulphur dioxide

$n_o = 2 \times 10^8$ cm^{-3} and $P_o = 1 \times 10^{-11}$ atmospheres of carbon dioxide

$n_o = 9 \times 10^7$ cm^{-3} and $P_o = 5 \times 10^{-12}$ atmospheres of water vapor.

These results, however, are dependent on the assumption that the moon's magnetic field is too weak to shield the atmosphere effectively from the solar wind. If an upper limit of 100 gammas (10^{-3} oersteds)[24, 25] for the seleno-magnetic field is assumed, it is found that the magnetic pressure of such a field of this intensity will have no shielding effect. A summary of the partial pressure of possible lunar gases in Table 14 shows that the values of argon and the volcanic gases lie to either side of an experimental estimate of 10^{-13} atmospheres which has been derived from measurements of the lunar ionosphere by Elsmore and Whitfield.[26]

3.4.1.2.2 The Moon's Hydrogen Atmosphere

Gold[27] has suggested that the high velocity protons from the solar wind, would be absorbed by the lunar surface and subsequently emitted by the surface as a gas of neutral hydrogen at the temperature of the point of emission. Since the thermal velocity of the emitted gas will be considerably smaller than the incident solar wind velocity, the density will be correspondingly greater in accordance with the equation of continuity; and, in fact, great enough to produce a substantial lunar atmosphere of cool atomic hydrogen. J. R. Herring and A. L. Licht[28] take into account the variation in the moon's surface temperature and the variation in the component of solar proton flux normal to the moon's surface.

Table 14 - Herring and Licht's Lunar Atmosphere Model

	Properties	Argon Ar	Sulphur Dioxide SO_2	Carbon Dioxide CO_2	Water H_2O	Krypton Kr	Xenon Xe
Herring & Licht's Atmosphere Model with "Solar Wind" Influence	Crust Effusion Rate molecules/sec-cm^2	5×10^5	10^{10}	10^{10}	10^{10}	2×10^{16}	1.8×10^{15}
	Atmospheric Surface Density - mol/cm^3	1×10^4	3×10^8	2×10^8	9×10^7	8×10^{14}	1×10^{14}
	Atmospheric Pressure (at.) (mmHg)	5×10^{-16} 4×10^{-13}	1.6×10^{-11} 1.2×10^{-8}	1×10^{-11} 8×10^{-9}	5×10^{-12} 4×10^{-9}	4×10^{-5} 3×10^{-2}	5×10^{-6} 4×10^{-3}

P-1868

The surface temperature determined by Pettit and Nicholson[29] is used to obtain a curve representing N(p)/J, the number of protons/cm^3 on the moon's surface divided by the flux of solar protons as a function of θ, the angle between the subsolar (position of the sun) point, S, and the normal to the moon's surface at the point P. For a solar wind flux, J = 10^{10} p/cm^2/sec; N_s = 0.39 x 10^5 p/km^3; and, for the dark side of the moon, N_d = 0.085 x 10^5 p/km^3; therefore, N_s/N_d = 4.

3.4.1.2.3 Lunar Ionosphere

The dominant ionization process is the charge-exchange between solar protons and hydrogen atoms. The cross section for this process is about 10^{-15} cm^2 as compared with 10^{-18} cm^2 for photo-ionization. The ionization density due to charge-exchange is computed under the assumption that every ionized particle escapes from the moon's atmosphere. The possibility that some newly ionized protons could be knocked into gravitationally bound orbits that do not intersect the lunar surface is neglected. The estimation of density of such protons is not possible without a more detailed analysis of the velocity distribution in the hydrogen atmosphere. Thus, the ionization density computed is regarded as a lower limit. The results of the computation give the following value for the ion density:

$$N_p = 1.7 \times 10^3 \left[\frac{R}{r} - \left(\frac{R}{r}\right)^2\right]$$

Thus, if r = 2R, N_P = 400 particles/cm^3, and if r = 10 R, N_P = 170 particles/cm^3. The latter value is just detectable over the assumed interplanetary density of 100 p/cm^3. This result is in good agreement with the results Krassovsky[25] reported for Lunik III in which the interplanetary ion density was found to start increasing above the ambient value at a distance of 10 R from the center of the moon.

3.4.1.2.4 Atmosphere Generated by Outgassing from the Analyzer Vehicle

The vehicle transporting the lunar analyzer to the moon can induce undesirable quantities of contaminating gases; such as the retrograde rocket exhaust gases, outgassing from the vehicle's exterior or interior surfaces, and outgassing from the

the lunar surface due to the lunar surface being heated by the retrograde rockets during landing.

An idea of the magnitude of the pressure which could exist in the vicinity of the lunar vehicle due to outgassing can be realized by considering the expansion of a gas from a point source into a hemispherical shell which has a radial distance equal to the distance a particle can travel in one second. Assuming the gas diffusing into the shell is carbon dioxide, and that it diffuses without colliding with background gases (pressure is less than 10^{-8} Torr -- free molecular flow), a simplified expression can be derived for the relationship between the average pressure existing in the shell and the magnitude of the leak rate. Thus, assuming the average velocity of the leaking gas is 3.5×10^4 cm/sec, results in a pressure of

$$P(\text{mm Hg}) \approx 3 \times 10^{-4} J \text{ (lb/sec)} \qquad (31)$$

where J is the exhaust or leak rate in lb/sec. It is seen that for a level of carbon dioxide partial pressure to exceed that of the assumed ambient lunar atmosphere level of 10^{-8} mm Hg, then $J = 0.33 \times 10^{-4}$ lb/sec. Due to the extremely tenuous background atmosphere the diffusion constants for all gases are high and the gases leave the area according to their average molecular velocities.

3.4.2 Lunar Soil

The character of the lunar surface layer has been the subject of confusion and dissension. The confusion and much of the dissension appear to stem primarily from the common tendency to generalize from a single line of evidence to a grossly oversimplified model. Not only does a model of the lunar surface layer have to allow for a wide variation in the character of the layer from place to place on the moon, but is must also be consistent with all of the available evidence bearing on the nature of this layer. J. W. Salisbury and V. G. Smalley, Air Force Cambridge Research Laboratories, Bedford, Massachusetts, have compiled what is believed to be a most informative article, "The Lunar Surface Layer," concerning the lunar surface.

In this article, all available evidence was reviewed and, after a comparison with theoretical predictions, conclusions were made concerning the most probable character of the lunar surface

layer. They recognize that there is insufficient evidence to arrive at firm conclusions, but believe that a likely model is much to be preferred to some of the extreme models currently in use. The following subsections contain a large portion of the above article.

3.4.2.1 Measurements of the Nature of the Lunar Surface Layer

All evidence for the physical nature of the lunar surface layer is indirect, depending upon inferences drawn from such directly measurable properties as the character of infrared emission, radio emission, radar reflection, light polarization, and light reflection. The major problem in evaluating the interpretations of these measurements is to distinguish between what was actually measured, what was assumed, and the conclusions drawn. When this is done, many conflicts can be eliminated.

The following methods have been used to arrive at a conclusion concerning the nature of the lunar surface outlined in Table 15.

Table 15 - The Nature of the Lunar Surface Layer

Above Surface	Lunar Atmosphere $\sim 10^{-13}$ Atmospheres
0.5 cm to 5 cm	Quartz SiO_2 Olivine $(Mg, Fe)_2 \cdot SiO_4$ Pyroxene $(Ca, Mg, Fe) \cdot SiO_3$
5 cm to 5 m	Rubble and Debris Lava Meteoritic Material
5 m ↓	Granite Igneous Rock Core

P-1868

3.4.2.1.1 Infrared Measurements

Infrared measurements have long been used to determine the nature of the lunar surface layer. Pettit[30] suggested that the rapid drop in surface temperature during an eclipse indicated that the surface was covered with a layer about 2.6 cm (1 inch) thick of porous material, something like pumice. More recently, Jaeger and Harper[31] have suggested that the temperature curves are more compatible with a two layer model consisting of 2 mm (0.08 inch) of dust over a relatively deep layer of pumice or gravel. Even more recently, Tyler and Copeland[32] developed a model assuming a homogeneous surface material with temperature-dependent thermal properties.

Two problems are apparent: First, what is actually being measured (making the highly questionable assumption that the moon is a black body with an emissivity of 1) is the thermal inertial constant, $(K\rho c)^{-1/2}$. Thus, in order to talk about the thermal conductivity, K, of the surface materials, all authors have had to make assumptions regarding the density, ρ, and the specific heat, c. Second, and most important, little is known about the heat transfer behavior of fine powders, pumice or gravel, in an ultrahigh vacuum. As a result, all that can be said with any degree of certainty is that the lunar surface material has an unusually high thermal constant, which with reasonable assumptions regarding extremes of density and specific heat, indicates a very low thermal conductivity.

3.4.2.1.2 Radio Emission

Radio emission for the moon has also been used as a measure of its temperature. Because radio waves can penetrate silicate materials to a certain extent, depending upon the wavelength and the nature of the silicate, such temperatures are representive of subsurface temperatures. Here again disagreement has arisen over the meaning of these measurements. Gibson[33] has evolved a complex three-layer model of typical lunar surface materials on the basis of emission at 8.6 mm (0.34 inch) wavelength. He suggests that the topmost layer is about 0.5 cm (0.2 inch) in depth and composed of a material resembling ordinary sand; that the intermediate layer is several centimeters or more in depth and is most notably characterized by a high electric conductivity; and that the lowermost stratum of indefinite depth is more like rock. Kislyakov,[34] on the other hand, finds that his analysis of emission at 4 mm (0.16 inch) is in agreement with a mono-layer model.

Not only does the same critical problem of the unknown thermal behavior of rock powders in a lunar environment arise, but there are also significant effects of composition and porosity on the apparent subsurface temperature. Thus, although it is known with some degree of certainty that the lunar surface materials have a thermal conductivity which is very low at the surface, and which appears to rise with depth, it is difficult to agree on a detailed model.

3.4.2.1.3 Radar Reflections

Radar reflections from the moon provide a third source of information about the nature of the surface materials. Evans,[35] for example, concludes from his measurement of the reflection coefficient that the surface is covered by a thin layer of fine dust. Cudaback,[36] on the other hand, suggests, on the basis of the same evidence, that the surface is covered with fine rock filaments like cotton candy. The reflection coefficient depends on the dielectric constant, which is a function of the composition, surface roughness, and density. By assuming reasonable limits on composition and roughness, the conclusion is reached that the density of the surface layer is very low. Whether or not this low density is indicative of a loose, fine powder, rock filaments, or highly vesiculated lava remains to be seen.

Radar reflections can also be interpreted in terms of surface roughness, by considering the reflection as a function of the radar signals wavelength. Thus, signal fading of radar reflections on meter (3.2 feet) and 10 cm (4 inch) wavelengths indicates that the surface is smooth and undulating, with an average gradient of 1 in 10.[35] Observations made at 3.6 cm (1.5 inch) indicate, on the other hand, that the surface is rougher than at meter wavelengths, with a mean surface gradient of 1 in 3. In addition, 14 percent of the surface is sufficiently rough to be a diffuse reflector at 3.6 cm.

3.4.2.1.4 Polarization

Dollfus[37] described a technique for determining the nature of the lunar surface by measuring the reflected polarized light. The technique considers that a fraction of the light is reflected by the surface, I_s, and given a polarization P_s, and the remainder, I_i, enters the substance, where it is diffused and partially absorbed. A small fraction T of I_i subsequently emerges from the

substance, refracted with a polarization P_i. The total polarization, P, of the combined emergent flux, in the simple case of linear polarization, is

$$P = \frac{P_s I_s + P_i T I_i}{I_s + T I_i} . \qquad (32)$$

In short, the polarization of a substance is a function of its structure, transparency, and index of refraction. This polarization changes with changing angles of incidence and observation to give a polarization curve, which can be used in some cases to identify the substance. The studies of Dollfus indicate that only opaque powders having no P_i factor in their total polarization will give a polarization curve similar to that produced by the lunar surface materials. Further, the lunar polarization curve appears best matched by the surface geometry of very fine opaque powders which have combined or agglomerated into larger grains. The natural terrestrial substance having such properties is fine volcanic ash. This is not to say that the moon is covered with volcanic ash, but only that it is covered with a material having similar polarization properties.

3.4.2.1.5 Photometric Measurements

Photometric measurements provide a fifth source of information concerning the nature of lunar surface materials. The photometric curve is the variation of intensity of reflected sunlight as a function of angle of incidence and observation; it is a measure of surface geometry. According to Fessenkov,[38] the lunar photometric curve can be at least partly explained by a model of which two thirds of the surface would consist of deep holes with vertical walls and sharp edges. The lunar photometric curve is not consistent with a surface covered with agglomerated volcanic ash. Laboratory experiments reveal that the naturally occurring substance whose reflectivity most closely approximates the photometric curve is the spongy lichen Cladonia rangiferina. This is not to say, of course, that the moon is covered with lichens, but it is apparently covered with a highly porous substance having a very complex surface of considerable relief compared to the wavelength of light.

3.4.2.1.6 Albedo and Color

Additionally, albedo and color provide indirect information as to the nature of the lunar surface. When albedo or reflectivity is plotted against color, a color-brightness field is defined for lunar rocks against which the color-brightness fields of terrestrial rocks can be compared. It is immediately apparent that lunar rocks are very dark (low reflectivity) and have almost no color. Sytinskaya[39] pointed out some time ago that the small region in the color-brightness diagram occupied by lunar materials is, for the most part, not occupied by any terrestrial materials. This indicates that lunar surface materials are either of an unknown sort or, more likely, that the lunar environment has affected the color and brightness of known materials in a manner that has no terrestrial counterpart.

Table 16 summarizes the conclusions concerning the lunar surface based on the preceding measurements.

Table 16 - Summary of Conclusions Concerning the Nature of the Lunar Surface

Measurement	Conclusion
Infrared emission	Low thermal conductivity.
Radio emission	Low thermal conductivity.
Radar reflection	Low density. Surface gradient 1 in 10 on a meter and 10 cm scale, 1 in 3 on a 3.6 cm scale.
Polarization	Agglomerated powder composed of opaque grains.
Photometry	Highly porous, complex and irregular surface. Relief many times the wavelength of light.
Albedo and color	Non-terrestrial reflectivity.

P-1868

3.4.2.2 Processes Acting to Create a Lunar Surface Layer

Having examined the conclusions that have been drawn from indirect measurements concerning the nature of lunar surface materials, the next logical step is to examine the predicted

nature of these materials as a function of the processes known to be active on the lunar surface. Six mechanisms are generally called upon to produce a fragmented layer of lunar surface material or "soil." They are: meteoroid impact, micrometeoroid infall, radiation, internal seismic shock, volcanism, and thermal fracture.

3.4.2.2.1 Meteoroid Impact

Meteoroid impact is a potent mechanism for pulverization, as has been abundantly demonstrated by terrestrial meteorite craters and laboratory hyper-velocity impact experiments. Most of the energy in meteorite impact is expended in the form of shock waves, which were to pulverize the target material and to eject a portion of this beccia to form a crater. At velocities attainable in the laboratory (4.27 to 6.1 km/sec or 2.6 to 3.6 mi/sec), Moore and Gault[40] found that the mass ejecta was roughly 10^2 times the mass of the projectile. Bjork's[41] calculations of the mass of the projectile that produced Meteor Crater, Arizona indicate the following ejecta: mass ratios of approximately 10^3 at a meteorite velocity of 11 km/sec (6.6 mi/sec), and $10^{3.4}$ at a velocity of 72 km/sec (43 mi/sec). It would seem, therefore, that 10^3 is an appropriate ejecta mass ratio to assume for lunar meteoroid impacts on a solid surface at the median velocity of 15-20 km/sec (9-12 mi/sec) suggested for lunar meteoroids by Whipple,[42] or at higher velocities associated with comets or cometary debris. At these velocities, Gault estimates (private communication) that a very small percentage of the ejecta, amounting to 3 to 5 times the projectile mass, will escape from the moon, and a similar small percentage will be vaporized or melted. The very large proportion of pulverized material ejected on impact and still remaining on the moon indicates that meteoroid impact is an extremely effective mechanism for the production of a fragmented lunar surface layer.

3.4.2.2.2 Micrometeoroid Infall

Micrometeoroid infall alone, ignoring pulverization, is considered sufficient by many scientists to blanket the moon with a fine-grained surface layer. The tons per year of fine material floating down through the terrestrial atmosphere have been measured and the results translated into a layer of material that would be produced on the lunar surface. Not only is the origin of much of this infall in doubt, the high velocities, of even submicron particles, which

would result in a pulverizing impact are also in doubt. Simple infall, as opposed to impact pulverization, would thus be eliminated as a soil-producing mechanism.

3.4.2.2.3 Radiation

Radiation has frequently been suggested as a soil-forming mechanism. Gold[43] proposed that X-rays and ultraviolet radiation act in such a way as to break down rock grains into particles of minute size, but there is no experimental evidence to verify this. Particulate radiation has also been suggested as a pulverizing agent, but this is true of only certain minerals, and then only when the source of radiation is internal (Fairbairn and Hurley[44]). The work of Wehner[45] indicates that particulate bombardment can produce atomic sputtering rather than comminution, and that most of the sputtered atoms should escape into space. Regardless of the end product, it appears from a study of space erosion of meteorites that neither particulate nor electromagnetic radiation is significant as an erosive agent. Fisher,[46] for example, has calculated an upper limit of 1.1×10^{-8} cm/yr (0.44×10^{-8} in/yr) for the rate of erosion of an iron meteorite in space. Thus, it would appear that radiation is not a significant soil-producing mechanism.

3.4.2.2.4 Seismic Shock

Seismic shock produced by internal lunar disturbances has been suggested by Gilvarry[47] as an erosion and soil-producing mechanism. Although it seems clear that seismic shocks, if present, would tend to reduce steep slopes to the angle of repose, the amount of pulverization over the entire lunar surface would not be large because crustal movement and brecciation would be localized along linear fracture zones. In addition, it appears from the geometry of the lunar crustal fracture surrounding the circular maria that much of the lunar seismic activity could have been related to meteoroid impact.

3.4.2.2.5 Volcanism

Volcanism has been suggested by Green[48] to have produced a surface layer composed of volcanic ash and other volcanic ejecta. Although most theories on the origin of lunar surface features accept volcanism relatively early in lunar history; e.g., during the formation of the maria, there is no evidence

of widespread volcanism today. As Alter[49] has pointed out, even Kozyrev's observation of a gas cloud in Alphonsus was not, as unfortunate translations would indicate, an observation of a volcanic eruption in the generally accepted sense. Kozyrev estimated that the density of gases at the vortex of the crater was 7.6×10^{-7} mm mercury (10^{-9} atmospheres), which is indicative of gas leakage from the interior rather than an erupting volcano. It appears, therefore, that volcanism is not a major lunar soil-producing mechanism at the present time. It should be understood, however, that volcanism could have been the major soil-producing mechanism during the lunar past. Unfortunately, the past significiance of volcanism cannot be determined from currently available data, and volcanism as a process is ignored in this treatment of the lunar surface layer.

3.4.2.2.6 Thermal Fracture

Thermal fracture is commonly assumed to be an effective pulverization mechanism due to the rapid and extreme changes in lunar surface temperature permitted by the lack of a detectable atmosphere. Ryan[50] has presented good experimental evidence, however, to show that such temperature changes will not produce appreciable thermal fracture. Under terrestrial conditions a much more limited temperature range results in rock breakage only because of the presence of water, which undergoes a relatively large volume change at 0°C (32°F). One may postulate the presence of water in some primeval lunar atmosphere (Gilvarry[51]), which would make possible effective thermal fracture on the moon at that time. It appears, however, that this mechanism is not currently operative in lunar soil production, and probably has not been for approximately 4×10^9 years.

3.4.2.3 Predicted Nature of the Lunar Surface Layer

The previous discussion of the six mechanisms commonly called upon to produce a lunar surface layer clearly demonstrates that the pulverizing effect of meteoroid impacts is by far the most important of these mechanisms. Ancient surface material will probably contain an unknown amount of volcanic ash in addition to meteoroid impact ejecta, and may possibly have been affected by thermal fracture and internal seismic shock. The present discussion of lunar surface material will, however, be guided principally by the mechanics of meteoroid impact.

3.4.2.3.1 Depth

Depth of the lunar surface layer is one problem upon which none of the indirect evidence can be brought to bear, but which is amenable to theoretical treatment. Photographs show that the lunar surface has been struck many times by large meteoroids in its long history, and each of these impacts will have ejected a large amount of debris onto the lunar surface. Depth of the rubble layer ejected from photographically visible meteorite craters on the maria is not difficult to estimate from their volume. Fortunately, relatively large craters produce by far the greater portion of ejecta due to the third power relationship of radius and volume, and the craters visible on photographs are the most important in debris layer production. Thus, the first conclusion that can be reached from theoretical consideration of the processes operating on the lunar surface is that the surface layer is composed primarily of rubble, not dust. A tabulation of visible craters indicates that, assuming 26 percent pore space, they would produce an even layer of rubble on the maria about 12.5 m (41.5 feet) thick. Because 95 percent of this material is concentrated in or near crater rims, intercrater areas should be covered by an average thickness of about 63 cm (2 feet) of debris of primary crater origin. Secondary craters, formed by blocks ejected from primary craters will add to this debris layer. Although the vast majority of secondary craters are small because of the relatively low velocity of the ejected blocks which made them, their very high frequency suggests a significant addition of debris. For example, Copernicus, a crater 90 km (56 miles) in diameter, has more than 1000 1.5-3 km (1-2 miles) secondary craters around it, and there must be tens of thousands of still smaller secondary craters in the vicinity. Unfortunately, the exact frequency of secondary craters is not known at this time, and the amount of debris added by them to the surface cannot be computed. Nevertheless, the important generalization can still be made concerning the depth of rubble on the maria that it is thin in intercrater areas, probably averaging no more than a few feet (less than 1 m) in depth. This debris layer will thicken abruptly as craters are approached. On the basis of primary crater frequency alone, it is possible to predict that rubble depths of 15 m (50 feet) associated with the rims of 100 m (320 feet) craters are common; i.e., within a radius of 4 km (2 1/2 miles) of the average mare landing site.

The depth of rubble on the highlands is as variable as that on the maria, but the minimum depth is much

greater. This greater thickness is due to both the greater crater density on the highlands and, in the important central portion, to the presence of one very large crater, the Imbrian basin.

In the southern highlands the volume of debris ejected from primary craters would produce an even layer of rubble approximately 275 m (870 feet) thick. Concentration of most of this material in or near crater rims would mean an average thickness of about 14 m (45 feet) for intercrater areas. Addition of material from secondary impacts would increase this depth a certain amount. As the rubble layer deepens, however, it progressively armors the surface against destruction by the smaller secondary impacts. Thus, the addition of debris from this source will not be as great in the highlands as it is in the maria, and an average intercrater depth of rubble of no more than 28 m (90 feet) appears reasonable. On the basis of primary crater frequency alone, it is almost certain that rubble depths of 83 m (275 feet) associated with the rims of 1.6 km (1 mile) craters are common, and that the rubble layer will be composed of discontinuous layers of debris overlapping one another in a complex fashion.

This rubble layer is much deeper in the immediate vicinity of large craters, and should deepen rapidly as the southern shore of Mare Imbrium is approached, due to the large addition of debris from the impact that formed the original Imbrian basin and the Apennine Mountains. Rubble depths greater than 1000 m (3200 feet) are to be expected near and in the Apennine Mountains.

3.4.2.3.2 Roughness

Roughness of this rubble surface on a meter (3.3 feet) scale will depend upon the number of craters formed in it, the size of blocks ejected from these craters, and the rapidity with which depressions are filled up or obliterated. Crater frequency on a scale so far below the resolution of photographs is difficult to predict. McGillem and Miller[52] attempted to extrapolate the frequency of large primary craters visible on photographs down to the frequency of smaller craters in the 1-10 m (3.2-32 feet) diameter range, but this technique provides only a bare minimum number because of the certain presence of great numbers of small secondary craters produced by ejected debris. It appears that the only valid generalizations that can be made concerning crater frequency are that it is greater in the highlands than in the maria, and that frequency rises more and more

rapidly as crater diameters diminish below 1 km (3200 feet) due to the larger and larger numbers of secondary craters.

The size of blocks ejected from craters is more predictable than crater frequency, and probably more important for vehicle mobility on the lunar surface because of the large number of blocks ejected from each crater. Of major interest is the maximum block size. Calculations have shown that the maximum block size to be expected in the vicinity of a 1 km (0.6 mile) crater is about 16 m (51 feet), and of a 100 m (320 feet) crater is about 4.5 m (14.5 feet), when they are formed on a solid surface. In view of the expected great numbers of secondary craters, it seems that a block size of 4.5 m should be frequent on the maria. A block size of 22 m (70 feet) associated with 1.6 km (1 mile) craters would be equally frequent in the highlands if ejected blocks were not fragmented on impact. Assuming that fragmentation of such large blocks must be the rule rather than the exception, block sizes as great as 10 m (33 feet) should be frequent in the highlands. The frequency of smaller block sizes should rise rapidly as their diameters decrease.

In view of this predicted high frequency of smaller blocks, particularly in the highlands, the radar data on surface roughness seems a bit surprising at first sight. Five factors tend, however, to reduce the relief of the rubble layer mantling the lunar surface. First, when large and small blocks are thrown very far from their parent crater, the force of their impact tends to fragment them, as was noted above. Second, seismic shock associated with the impact of large meteoroids will tend to level steep debris slopes. Third, volcanism during the lunar past probably filled or partially filled ancient depressions with volcanic ash. Fourth, the walls of depressions tend to trap debris ejected from micrometeoroid craters within the depression, thus ensuring that such debris builds up faster in a depression than it does on level ground. Fifth, meteoroidal debris could be subjected to electrostatic transport which, allied with the force of gravity, will lead to preferential deposition in depressions. Of these factors, only the later two are considered of primary importance during the geologically recent past.

3.4.2.3.3 Entrapment of Meteoroidal Debris

Entrapment of meteoroidal debris by the walls of a depression results from the geometry of debris production. An estimate of its effectiveness can be obtained from an

analysis of entrapment of meteoroidal material in an ideal trench one meter (3.3 feet) wide and one meter deep. This trench is assumed to be infinitely long, so that debris thrown up or down the trench is equivalent to the amount returned. Thus, the problem can be considered in two dimensions. Any point on the wall of the trench is able to accept incoming meteoroids over an angle α. Debris ejected from an impact is trapped by the opposite wall through an angle β. As a result, the trench gradually fills with fine debris, and the depth, i, decreases. At the same time, the eroded wall recedes some distance.

Assuming that the density of the wall rock is 3.25 g/cm^3, that the density of the fine debris is 0.5 g/cm^3, that the ratio of the mass of the ejecta to that of the projectile is $\eta = 10^3$, and that the 2π steradian flux of meteorites $\phi = (1.4)\,10^{-14}$ g/cm^2/sec, calculation of the filling rate can be made as follows:

First, the vertical walls are divided into 10 sections, and the midpoint of each section is considered to have α and β angles typical of the whole section. Then, looking at a small slab of wall, 10 cm high and 1 cm wide, and Δ_i cm thick, the volume of this slab = $V_i = 10\,\Delta_i$ cm^3 and the frontal area = $A_i = 10$ cm^2. With the assumed density of 3.25 g/cm^3, the weight of the slab = $W_i = 10\,A_i\,(3.25)$ grams. After a period of time, the weight of material removed from the slab is

$$W_i = \phi\, t\, A_i\, \eta\, \frac{\alpha i}{180}\,. \tag{33}$$

Therefore,

$$32.5\,\Delta_i = \phi\, t\, A_i\, \frac{\alpha i}{180}$$

and

$$\Delta_i = \alpha_i\, t \left(\frac{\phi\, \eta\, A_i}{180\,(32.5)}\right) \quad (t \text{ in seconds})$$

or

$$\Delta_i = \alpha_i\, t\,(7.54)\,10^{-4} \text{ cm} \quad (t \text{ in } 10^3 \text{ years})$$

Assuming a time interval of 50,000 years, the walls will have receded; the fraction of the debris eroded from the walls which is retained within the trench is $(\Delta_i \beta_i)/180 = F_i = 15.31$ cm. The volume of debris

(doubled to account for both walls) is (15.31) (2) (10) (3.25/15) = 1990 cm^3. Then total depth of dust after 50,000 years is 19.2 cm. Recomputing angles of α and β for the new positions of the walls, and allowing for the change in depth of the trench, the computation just described can be repeated again and again to provide a picture of the progressive evolution of the trench.

Actually, the trench would fill slightly faster than has been computed here because of the addition of debris from secondary impacts on the opposite wall of the trench, as well as the addition of a slightly greater amount of debris thrown into the trench than is thrown out of it from impacts in the dust at its bottom. Considering, however, the four orders of magnitude uncertainty of current knowledge of the lunar meteoroid flux, the present calculation appears sufficiently detailed. It indicates that a trench will fill quite rapidly if the maximum meteoroid flux is assumed, as it was in this case (Dubin and McCracken[53]). The flux can be as much as four orders of magnitude lower, however, in which case the trench would take most of lunar history to fill.

Having explored the evolution of a trench, it is important to examine the fate of the adjacent level ground. Here an entirely different chain of events takes place. As soon as the dust layer is built up to a depth greater than the depth of penetration of the high-frequency meteoroids, pulverization sharply decreases and existing fine debris is both redistributed and ejected into space by meteoroid impact. Because several times the mass of impacting projectile is lost to the moon (Whipple,[54] Gault,[55] et al), a steady-state thin equilibrium layer of dust is achieved on level ground. Thus, lunar relief is continually diminished.

3.4.2.3.4 Electrostatic Transport

Electrostatic transport of meteoroidal debris has been studied by several authors, most recently by Grannis,[56] Gold,[57] and Singer and Walker.[58] The electrostatic charge build-up on the soil particles can cause "hopping" of particles, which once airborne, follow the gravitational field and tend to collect in low areas. This process can contribute to a layer of fine dust existing in depressions in the lunar surface. In any event, one or more (and probably all) of the five factors discussed above tend to reduce the local relief of the lunar surface on a meter scale. As a result, the rubble is mantled by a layer of fine debris or dust, which is probably no more than a few

centimeters thick over near level ground, but which can be meters deep in steep-walled depressions.

3.4.2.3.5 Dust Behavior

Dust behavior becomes a very important factor if it is locally deep. Experiments within our lunar simulation chamber have demonstrated that fine silicate powders adhere to one another in an ultrahigh vacuum (Salisbury et al).[59] Gross adhesion in these experiments was estimated to be approximately 750 dynes/cm^2 (0.01 psi), although the stress at contact points between grains can be as great as 3×10^8 dynes/cm^2 (4.4×10^3 psi). Greater adhesion between particles is expected on the lunar surface, where radiation cleaning should provide ultraclean surfaces, but the strength demonstrated so far within the chamber is sufficient to eliminate significant design problems for vehicles or space suits.

3.4.2.3.6 Agreement

Agreement with evidence for the nature of the lunar surface materials of the model developed above is excellent. The dust layer would have the low density, low thermal conductivity, and low relief demanded by infrared, radio and radar measurements. It should also have a complex surface produced by the "fairy castle" arrangement noted by Hapke[60] as typical for very fine powders. If Hapke's prediction of the effect of radiation damage on iron-rich minerals is correct, the dust should also have the opacity and low albedo of lunar surface materials.

3.4.2.4 Summary - Lunar Soil Model

To fit the thermal conductivity, albedo, and back scattering measurements, the top surface layer must have a construction which is best likened to fairy castle packing. Experiments have shown that powders (particle size 15 microns) fit this complex fairy castling structure and also exhibit a low bulk density (from 1/6 to 1/10 that of the parent material). It would appear that the lowered gravitational field of the moon would allow the same process to exist for particles as large as 50 microns. This fairy castling structure is very open or porous with spaces of various sizes and shapes. In fact, Hapke insists that the cavities or spaces must be interconnected to account for the strong back scattering of light.

This surface layer varies in thickness from a minimum of several millimeters to as much as a meter, depending where upon the moon's surface it is measured. This layer has a high chondritic silicate content with small amounts of iron and magnesium and possible smaller amounts of calcium. It is possibly composed of pumice or volcanic ash. The fairy castling is brought about by impacting of meteorites, and, in general, the moon has a positive accretion rate resulting from this bombardment.

Below this surface layer lies an intervening layer of rubble caused by secondary impacting which resulted from crater formation. The depth of this layer also varies over the surface of the moon. From radio (radar, microwave) measurements, it is deduced that the size of the pieces of rubble cannot be much larger than a meter. Such measurements, which can penetrate to a depth of several meters indicates a smooth and undulating surface. However, visual observations, surrounding craters created by meteor impacting, indicate that surface roughness must necessarily come about by debris from the impact. It is believed that the depth of such rubble varies from fractions of meters in the plains to many meters near craters. The composition would necessarily be that of the primordial moon surface, possibly lava.

The bulk material of the moon appears below this layer. This composition must necessarily fit the nonvolatile components of cosmic abundance and might be chiefly composed of granite and igneous material. It is believed that the core is solid because of the moon's weak magnetic field as reported by Russian measurements.

With respect to the rigidity of the surface of the moon and the question of this surface supporting a probing mass, most authors agree that the fairy castling structure has fairly good structural properties. Some authors have found from experiment that the minimum gross adhesion for fine silicate powders is 750 dynes/centimeter^2 or 0.01 psi. They expect this to be greater on the surface of the moon because of ultraclean material brought about by radiation effects. Their conclusions indicate that the surface has enough structural rigidity to support vehicles and space men. However, it would appear that safety dictates a course whereby surface conditions that are presently proposed be verified.

The origin of craters on the moon is still speculative. At present, there is not enough evidence to support either

of the two existing ideas on crater formation; i.e., either via volcanic means or by meteoric impact. It might be possible to examine material taken from craters to determine their content and possibly decide by which method craters were formed. To examine samples for such purpose requires knowledge of the main ingredients which would differentiate lava and meteors. Meteors are divided into three categories: irons, stony irons, and stones. The first two categories contain elements of nickel and iron in amounts far greater than that from lava -- nickel content in iron meteorites ranges from 6 to 20 percent. Such meteorites comprise 35 percent of those examined. Stony irons comprise only 4 percent and are composed of silicate materials and an equal amount of nickel-iron. It seems that a determination of the nickel content of a sample would indicate whether the sample is from one of the above categories.

The stony meteorites do not lend themselves to such analysis; such meteorites are broken into two groups -- chondrites and achondrites, with the former far more numerous than the latter. The chondrites are distinguished by their crystalline structure (contain spherical aggregates of olivine and/or pyroxene). Thus, it might be extremely difficult to differentiate the stony meteorites from lava. However, it could be established that samples of given crater areas fell in either of the first two categories, then certainly the theory on meteor impact would find strong support.

The earth's crust is principally composed of 8 elements with oxygen by far the most dominant element. By weight, it comprises 46.5 percent; by volume, 92 percent. In contrast, the next most abundant element is silicon which comprises 27.7 percent by weight and only 0.8 percent by volume.

In terms of cosmic abundance, the earth's crust is deficient in hydrogen, helium, carbon, nitrogen, and neon. Such deficiency is explainable in either of the current theories on the formation of the earth. Oxygen is less in the earth's crust than that given by cosmic abundance; but not to the same extent as the other gases. Obviously, this is because of the many stable compounds it forms with other elements. The next set of elements, iron, silicon, magnesium, sulphur, nickel, aluminum, and calcium are found in the crust of the earth in the same proportions as they are for cosmic abundance. This leads us to believe that the elements in the moon's surface should follow cosmic abundance and probably resemble the earth's crust very closely.

3.4.2.4.1 Possible Measurement of Carbon on Lunar Surface

It has been noted that a small percentage of meteorites found on the earth contain a high percentage of carbon. Such meteorites are of the chondrule type. This has led to speculation that carbon is contained on the moon's surface. In fact, one idea is presented which states that 7 to 11 percent carbon content in the moon would account for the moon's low density (3.34 gm/cm^3 compared to earth's 5.5 gm/cm^3). Although it is known that carbon reduces iron and silicon oxides and eventually the density would increase, carbon might account for the black mountainous areas west of Copernicus and possibly the carbon content might be larger than would be expected using cosmic abundance as a guide.

SECTION 4

COMPOSITIONAL ANALYSES TECHNIQUES

Suitable instrumentation for the mission discussed in this report is not currently available. Moreover, there is considerable difference of opinion concerning the type of equipment which would prove most useful. This section discusses the physical and chemical characteristics of the lunar atmosphere and soil models, compares the operating capabilities of available analytical techniques, and summarizes the performance to be expected of instrumentation based on the most promising technique. The discussion is facilitated by first specifying the physical and chemical properties of the components of the lunar atmosphere and soil models. This provides a straightforward method to look for outstanding or characteristic properties to use in the selection of an analytical technique.

4.1 GENERAL

Since equipment is not available on an off-the shelf basis, the selection of an analytical technique was guided by the condition that a development program of two-years duration must realistically lead to the required hardware with the added condition that a feasibility demonstration, in the laboratory, must be made within about nine months.

The details of the selected analysis technique and a discussion of the performance of the hardware based on it are included. The computed output for the equipment is derived in order to detail what is expected. In this way, the systems evaluation team has available a critique on the system input/output characteristics to aid in evaluating the system and its interfaces with the remainder of the mission hardware.

4.2 COMPILED CHARACTERISTICS OF ANTICIPATED SAMPLES

Physical characteristics of the components of the lunar atmosphere model are included in Table 17. Appendix D summarizes the physical characteristics of several of the gaseous components discussed in Section 3 which did not survive the culling used in defining the lunar atmosphere model.

Table 17 - Physical Properties of the Lunar Atmosphere Components

Property	Argon Ar	Carbon Dioxide CO_2	Water Vapor H_2O	Sulphur Dioxide SO_2	Xenon Xe	Krypton Kr
Atomic Number	18	N. A.	N.A.	N.A.	54	36
Molecular Mass (amu)	39.94	44.01	18	64.06	131.3	83.7
Critical Pressure (atm.)	49.7	73.0	217.7	80.1	58.2	56.
Critical Temperature (°C)	-122.	31.1	374.0	157.2	16.6	- 63.
Critical Density (g/cc)	0.531	0.460	0.4	0.52	1.155	0.78
Density g/ℓ 0°C 760 mm Hg	1.784	1.977	0.958 100°C	2.821	5.851	3.708
Viscosity - μ - poise T°C	221.7 20	145.7 15	125.5 100°C	tc	223.5 16.5	245. 15
Specific Heat Cap. cal/gm	0.1253	0.1989	0.4820	N.A.	N.A.	N.A.
C_v - cal/gm	0.075	0.152	0.364	N.A.	N.A.	N.A.
$\gamma = C_p/C_v$	1.668	1.304	1.324	1.29	1.66	1.68
	15	15	100°C	15	19	19
Thermal Conductivity BTU/hr/sq. ft/°F/ft	1.58	0.0085 32°F	--	0.005 32°F	N.A.	N.A.
Velocity of Sound m/sec 0°C, P = 1 atm.	319	259.3	401	213	N.A.	N.A.
Magnetic Susceptibility) emu x 10^{-6} at temperature T	- 0.45 20°C	- 0.4 20°C	--	- 0.285 (liq.)	N.A.	N.A.
Dielectric Constant P = 1 atm.	1.000546	1.000985	+0.00785 140°C	1.00993	N.A.	N.A.
Index of Refraction	1.000281	1.195 (liq.) 1.000451 15°C	1.000254	1.41 (liq.) 1.00069	N.A.	N.A.
Boiling Temperature at P = 1 atm. °C	-185.7	- 78.5 (subl.)	100.0	- 10	-107.1	-152.9
Melting Temperature °C, P = 1 atm.	-189.2	- 56.6 (5.2 atm.)	0.00	- 72.7	-112	-156.6
Appearance Potential	A+ 15.76 A++ 43.4	C+ 26.6 CO_2 13.8 CO+ 20.5 O 19.6	$H^+ + OH$ 19.6	N.A.	Xe^+ 12.127	Kr^+ 13.997

Table 18 - Physical Properties of Lunar Soil Model Component

Property	Iron Fe	Nickel Ni	Aluminum Al	Magnesium Mg	Calcium Ca	Silicon Si	Oxygen O	Quartz SiO_2	Olivine $(Mg, Fe)_2 SiO_4$	Pyroxene $(Ca, Mg, Fe) SiO_3$
Atomic Number	26	28	13	12	20	14	16	N.A.	N.A.	N.A.
Molecular Mass	55.847	58.71	26.9815	24.312	40.08	28.086	15.9994	80.08	248.40	293.253
Density g/ml.	7.86	8.9	2.70	1.74	1.55	2.33	1.14	2.6	3.3	
Specific Heat C_v Cal/gm/°C	0.11	0.105	0.215	0.25	0.149	0.162	0.247			
Thermal Conductivity cal/cm^2/cm/°C/sec	0.18	0.22	0.50	0.38	0.30	0.20	6×10^{-5}	0.03 ∥ axis 0.016 ⊥ axis	1.5×10^{-5}	
Velocity of Sound m/sec @ °C	5130. 20	4973.	5104.	4602.			317.2 0			
Boiling Temperature °C, P = 1 atm.	3000.	2730.	2450.	1107.	1440.	2680	-183.			
Melting Temperature °C, P = 1 atm.	1536.	1453.	660.	650.	838.	1410.	-218.8	-218.8	1710	

P-1868

The physical properties of the lunar soil components are called out in Table 18.

4.3 SUMMARY OF SENSING TECHNIQUES

The sensing techniques which might be applicable for measuring one or more of the components of the lunar models are discussed below. Restrictions due to size, weight, reliability, etc., are not imposed until the parametric analysis.

4.3.1 Mass Spectrometry

Mass spectrometry refers to a broad range of techniques in which the sample is analyzed by taking or generating molecular or atomic species of the sample, ionizing them, and then measuring the charge-to-mass ratio of the discrete sample ions.

The mass spectrometry techniques which show promise in the lunar application are discussed in the following subsections.

4.3.1.1 Time-of-Flight Mass Spectrometry

The gas to be analyzed in the Time-of-Flight Mass Spectrometer is allowed to enter the source of the instrument through an appropriate leak opening. The low pressure, 10^{-4} to 10^{-6}, mm Hg, gas is ionized by a pulsed electron beam. The resulting group of positive ions is ejected from the source region by another electrical pulse which is applied to accelerating grids. These grids are arranged such that all ions which leave the source have the same energy. Consequently, the ions have a velocity distribution which depends upon their mass. In this way, the ions separate into bunches such that each bunch contains ions of only one mass, and the separation becomes larger as the entire group proceeds toward the cathode of the electron multiplier. The collision of the ions on the cathode of the multiplier produces a packet of secondary electrons such that there is a one-to-one quantitative correspondence between the number of electrons and the number of arriving positive ions.

The magnetic electron multiplier is of the crossed electric and magnetic field design, and the resulting electron packets cycloid down the dynode strips in such a way that a current gain of about 10^6 is achieved by the time the packets enter the gating section of the multiplier. It takes about 2 microseconds for the first

packet of electrons, which corresponds to the sample constituent of lowest mass, to travel from the ion source to the entrance of the gating section. The last packet, corresponding to the heaviest sample constituent, takes about fifteen microseconds. In this way, the gating section of the multiplier is supplied with a series of electron packets which are spread out in time over a 13 microsecond interval. This whole process of mass separation is repeated at a rate between 10 and 100 kilocycles per second so that a new group of molecules is being ionized and separated by mass every hundred microseconds or less.

The gating section of the magnetic electron multiplier can be fitted with 10 or more pairs of gate-anode assemblies. These gate-anode pairs have a configuration such that an electronic pulse applied to the gate will cause the electron packets which are then passing the assembly to be gated onto the corresponding anode. The electrical capacity of these gate-anode assemblies is sufficiently low such that extremely short (50 milli-microseconds) pulses can be applied to any gate, thereby allowing each anode to collect the electron current due to a particular mass in the sample. In this way, the partial pressure of as many gases can be continuously monitored as there are gate-anode assemblies in the gating section. Complete mass spectra, at the repetition rate of the instrument, can be obtained by continuously biasing the gate electrode. Such an output signal will necessitate rather sophisticated data storage or telemetering equipment. However, if the gating pulse is applied a little later in each operating cycle, the entire mass spectrum can be covered at a rapid rate. This uses only one output channel leaving the remainder to continuously and simultaneously monitor the more important masses.

4.3.1.2 Coincidence Time-of-Flight Mass Spectrometry

Since so many measurements need to be taken for which there exists no instrument with the desired capabilities, it is of interest to consider new designs that may be superior. One such design has been under preliminary consideration in the Space Physics Laboratory of the Aerospace Corporation, Segundo, California. A schematic drawing of the instrument is shown in Figure 4. The spectrometer separates masses on a Time-of-Flight basis but analyzes only one particle at a time. A feedback arrangement automatically adjusts the ionization current to the single-particle-per-pulse level. Flight time is precisely measured by appropriately scaled pulses from a 100 megacycle oscillator.

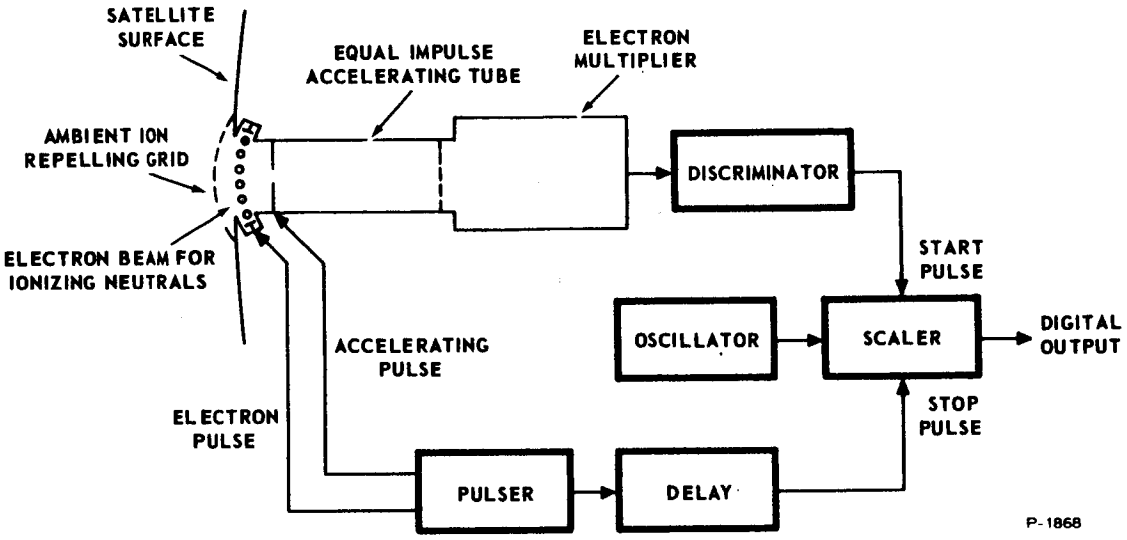

Figure 4 - Coincidence Mass Spectrometer

A sensitivity of 10^{-12} Torr is obtained by using an electron multiplier. Note, however, that the multiplier is used only as a sensitive fast timer and is not used for determining the amplitude of the pulse. Thus, problems of possible multiplier gain changes and nonlinear response to different masses are largely eliminated.

Since each count is recorded individually, the total intensity or amplitude of any mass peak during any interval can be obtained precisely by summing the counts, this, however, can be accomplished on the ground. In addition the output is digital in form and therefore requires no analog-to-digital conversion for computer reduction of the data.

Spectra are obtained very rapidly, since the pulse repetition rate is greater than 10^5 per second. It is not necessary to take time to integrate currents. A good, complete spectrum is obtained every second.

A resolution of 1 amu in 60 should be obtained using a 10-cm flight tube. Thus, the resolution actually obtained, even with non-optimum performance, should be very good. Another claimed feature of this spectrometer is its "constant-momentum" ion acceleration (as contrasted to the "constant-energy" acceleration of most spectrometers), which means that the times of arrival are directly proportional to the mass rather than being proportional to the square

root of the mass. It follows that the masses are separated by greater times, leading to greater resolution. The resolution is not limited by slit width or mechanical alignment.

In contrast to other spectrometers, which accelerate many particles at once, there should be no loss of accuracy due to space charge effects or to interference effects usually present when trying to determine a 5 percent abundent component in the presence of the other 95 percent.

Since there is only one collector with no sweeping or gating for different masses, the mass range is continuous for masses 1 through 50, or higher, if desired. This means that unexpected neutrals can also be detected.

Naturally occurring ions would normally be repelled from the ion source by a grid. However, the spectrometer could also be used to determine the ion composition by shutting down the grid and the ion source.

The best techniques of ion source construction could be incorporated in this spectrometer. Simplicity of operation should lead to simplicity of construction.

While the design described in the previous subsection looks very promising, there are several basic problem areas which must be investigated further before actual construction of an instrument should be attempted.

The problems concerned with single-particle counting of positive ions in this energy and mass range have received little previous study. The secondary emission of electrons due to positive ions is a statistical process and is low in magnitude, so that 16- or 20-stage multipliers appear necessary to obtain pulses suitably above noise, and spurious pulses caused by penetrating cosmic rays must be eliminated.

With pressures varying over a considerably range, the problem of instrumental outgassing, which plagues all mass spectrometers, is magnified. Materials and techniques must be developed so that measurements at 10^{-12} Torr will not be swamped by outgassing of components absorbed at 10^{-7} Torr. Ionization current control over this range is a problem, although with some sacrifice in statistics at the extremes of pressure, it appears that a feedback range of 10^2 or 10^3 would be adequate.

For precision timing and high duty cycle the electronics must be fairly fast. In particular, development would be necessary in the area of the oscillator and scaler.

4.3.1.3 Magnetic Deflection Mass Spectrometry

In Magnetic Deflection Mass Spectrometry a magnetic field is employed to differentially displace the ions according to the mass-to-charge ratio. The equation relating this separation to the H-field, the curvature R, and the accelerating potential V is

$$m/e = KH^2 R^2/V \ . \qquad (34)$$

By varying H or V, the beam of ions can be swept so as to hit a collector. Outputs from this collector correspond directly with the number density of the ions which were originally formed in the source region.

The double-focusing spectrometer detects the ions by means of collectors at various fixed positions, so that only the masses for which collectors are available can be observed. Information is obtained for one mass at a time, and output from the collectors is recorded sequentially. Therefore, the rate of observation is limited, and a continuous spectrum as a function of position cannot be obtained. The use of electron multipliers to increase the collection sensitivity is difficult because of the strong field of the primary magnet and because a separate multiplier is required for each mass.

The low mass range, low resolution, and very low duty cycle of the instrument are thought to be sufficient for initial exploratory flights. However, actual performance figures are as yet unknown.

4.3.1.4 Radio Frequency Mass Spectrometry

The Bennett Radio-Frequency Mass Spectrometer employs velocity selection for determining the selected mass, as opposed to the constant ion energy principle of the Time-of-Flight Spectrometer. The spectrometer tube has parallel plane grids made with knitted wire nets with a large percentage of open area. The grids are arranged in groups of three, and an r-f alternating potential is applied to the middle grid of each group. Stopping potentials are used to turn back all ions except those with the selected mass. The spectrometer had sufficient

resolution for ordinary gas analysis requirements and is simpler, more compact, and more rugged than magnetic beam deflection devices. A modified version of the Bennett Spectrometer has been used for upper atmosphere rocket studies. The rocket-borne spectrometer samples the spectrum between mass numbers 48 and 5 once per second with a resolution of one part in twenty-five. Data can be obtained between pressure limits of 8×10^{-4} mm Hg and 2×10^{-6} mm Hg, corresponding to ambient pressures occurring at earth altitudes between 100 km and 160 km, respectively. The entire instrumentation weighs less than 50 pounds and occupies a total of 1.4 cubic feet.

4.3.1.5 Omegatron Mass Spectrometry

The operation of the omegatron is similar to that of the cyclotron. Electrons emitted from a hot filament are accelerated through a 1/16-inch diameter aperture to form a 4 μ-ampere beam at 90 volts. This beam, which produces ions in an ionization chamber, emerges through a second aperture and is collected by a collector plate, biased positively with respect to the shield to suppress secondary emission. The parallel magnetic H-field has a strong collimating action on the electron beam. The shield box forms a 2-cm cube. The r-f plates, which form the top and bottom of the ionization chamber, are connected to a source of r-f voltage (about 1 or 2 volts). These plates produce an r-f field across the ionization chamber perpendicular to the magnetic field. The ions formed by electrons colliding with the gas molecules within the electron beam spiral around the magnetic lines of force by their own thermal and dissociation emergies. The radii of these spirals are very small, and few ions would normally escape from the electron beam because of their own initial energy. However, upon the application of a weak electric r-f field, the ions are accelerated in Archimedes-like spiral orbits of increasing size, provided that the frequency of the applied r-f voltage is the same as the cyclotron frequency of the ions:

$$f = 1.54\ H/M\ \text{kc sec}^{-1} \qquad (35)$$

A trapping voltage that is positive with respect to the r-f plates is applied to the shield box to produce an electric field which retards the loss of ions in the axial direction of the magnetic field. This gives the r-f field an opportunity to act on the ions over a greater number of cycles. The spiral orbits terminate on a 1/16-inch square ion

collector plate. The ion current to this electrode, detected by a vibrating-reed electrometer, is a measure of the abundance of the gas with a cyclotron frequency equal to applied frequency.

An Omegatron built by Alpert and Buritz has adequate resolution up to mass 40.

4.3.1.6 Quadripole Mass Spectrometry

The Quadripole Mass Spectrometer was first suggested by W. Paul and M. Raether. Most mass spectrometers work by measuring two of the three magnitudes: ion momentum, energy, or velocity. Then, e/m is defined by eliminating the velocity. Consequently, a spatial or temporal separation of ions of different masses generally take place. The momentum is usually measured by ion deflection in a magnetic field, while the energy measurement is usually carried out by the deflection or acceleration of the ions in a static electrical field. The velocity is generally determined from the time required for the ions to traverse a given straight or curved distance. Only those ions can be used which start within a certain short time interval and which satisfy certain phase relations.

In the Quadripole method, the definition of e/m does not require the measurement of any of the quantities just mentioned. Rather, the acceleration of the ions in a time dependent high-frequency electrical field is used to achieve mass separation. The spatial arrangement of the electric field is characterized by the fact that its potential $V(x, y, z, t)$ has to be a purely quadratic function of the x, y, z coordinates. The most general expression of the potential is given by $V(x, y, z, t) = f(t)\ (ax^2 + by^2 - cz^2)$. An electric potential of the form $V = (V_0 + V_1 \cos\omega t)\ (x^2 - y^2)/r^2$ can then be formed by a set of four electrodes which are hyperbolic cylinders placed symmetrically about an axis. The equations of motion of an ion in such a potential field are

$$\frac{d^2x}{dt^2} + \frac{2e}{mr_o^2} \cdot (V_0 + V_1 \cos\omega t)\ x = 0 \qquad (36)$$

$$\frac{d^2y}{dt^2} - \frac{2e}{mr_o^2} \cdot (V_0 + V_1 \cos\omega t)\ y = 0 \qquad (37)$$

and

$$\frac{d^2z}{dt^2} = 0 \ . \qquad (38)$$

These equations lead to differential equations with periodic coefficients, which are characterized by ranges of stable or unstable solutions. Either the ions perform stable gyrations about the center of symmetry and remain bounded until striking the detector or possess an e/m ratio which is not correct for trapping and within a very short time after generation reach the field generating electrodes and are lost (unstable). For fixed values of ω, V_o, V_1, and r_o, there is a finite range of e/m for which stable motion exists -- a range that can be tuned for a particular mass by varying V_o and V_1 (but keeping the ratio V_o/V_1 constant) or ω.

4.3.1.7 Unipole Mass Spectrometry

This technique employs an electric field configuration identical to the Quadripole except that the electric field normally formed by the four hyperbolic cylinders is duplicated by one hyperbolic cylinder and an L-shaped ground plane situated where the asymptotic planes of the hyperbolic cylinders of the Quadripole exist. Thus in effect, the Unipole Mass Spectrometer is one quadrant of the Quadripole Spectrometer and operates with the same basic equations governing the trajectories of the ions being analyzed.

4.3.2 Gas Chromatography

Gas chromatography involves the transport of a sample of gas through a column which contains a solid absorbing agent, the stationary phase. The transport of the constituents of the sample through the column is affected by a gas; the moving phase. Owing to the selective retardation exerted by the stationary phase, the components of the gas sample move through the column at different effective rates. Thus, they tend to segregate into separate zones or bands, which can be detected by any one of the following methods:

- Detection by differences in thermal conductivity
- Detection by mass spectrometry

- Detection by dielectric constant
- Detection by oxidation ($2CO + 0_2 \longrightarrow 2CO_2$)
- Detection by the conductivity of a collecting solution

4.3.3 Pneumatic Refractometry

Pneumatic refractometry utilizes the difference in optical indices of refraction to differentiate between gaseous components. The gas to be analyzed is forced through slits at high velocities into a reference gas. A plane surface is formed between the reference gas and the high velocity gas and a light source is projected normal to this plane surface through the two gases. A photocell then measures the intensity of the image of the transmitted light source. As the index of refraction varies, the size and hence the intensity of the image varies.

By calibrating the output from the photocell, the concentration of a gas differing in index of refraction from the reference gas can be determined.

4.3.4 Interferometry

Interferometry also makes use of the differential optical indices of the various sample components. A thickness, t, of a substance having an index of refraction, n, is introduced into the path of one of two interfering light beams so that the optical path increases due to the decreased velocity of the light through the substance. Thus, the optical path is defined as

$$\Delta = n (x_2 - x_1) = nt \qquad (39)$$

where n is the index of refraction of the substance. Before introduction of the substance, the optical path is practically t. Thus, there is an increase in optical paths of (n - 1) t.

The index of refraction of gases can therefore be measured by introducing the gas into the light path. The gas is allowed to flow into an evacuated tube. The presence of this gas introduces $(n - 1)\, t/\lambda$ extra waves in the path of the beam, and so there will be $\Delta m = (n - 1)\, t/\lambda$ number of fringes by which the fringe system is displaced.

If two similar tubes of equal length are placed in the two parallel beams of an interferometer, and if the gas is slowly admitted to one of the tubes, the index of refraction, n, can be determined by counting the number of fringes, m, crossing the field. This field is viewed through an optical system located at the end of the tubes.

Table 19 gives the index of refraction for gases taken at 0°C and 760 mm pressure.

4.3.5 Paramagnetic Analysis

The most commonly used application of the paramagnetic properties of gases is that associated with the analysis of oxygen. These instruments employ a strong heterogeneous magnetic field in which is suspended a small dumbbell-shaped test body. If oxygen surrounds the spheres of the dumbbell, a displacement takes place in an amount which is related to the paramagnetic properties of the oxygen. The force on the test spheres can be determined knowing both the field and its gradient. This force (in the x-direction) is given by

$$F_x = \mu_o \, (X_m - X_m^1) \, V H_x \frac{\partial H_x}{\partial x} \qquad (40)$$

where

V is the volume of each of the two test bodies

$X_m - X_m^1$ is the difference in susceptibility of the surrounding oxygen atmosphere and the test bodies

H_x is the field strength

A second method utilizes a hot wire bridge made up of fine platinum wire, where a cooling or heating effect is produced in one or more of the bridge arms as a result of the paramagnetic behavior of the oxygen. One of the platinum arms is located in a strong transverse heterogenous magnetic field. This arm experiences a greater cooling effect than the other arm, because the gas in the vicinity of the wire heats and expands and being located in the heterogeneous magnetic field causes a transverse movement.

Table 20 presents the volume susceptibility for a number of gases.

Table 19 - Index of Refraction for Several Gases

Gas	n
0_2	1.000271
NO	1.000297
H_2	1.000132
He	1.000036
N_20	1.000516
CO	1.00034
CO_2	1.000451
A	1.000281
CH_4	1.000444
N_2	1.000297

P-1868

Table 20 - Magnetic Susceptibilities of Some Atmospheric Gases

Gas	Susceptibility (e.m.u.) x 10^{-10}
O_2	1392
NO	612
H_2	- 1.665
He	- 0.76
N_2	- 4.97
CO	- 4.80
CO_2	- 8.80
A	- 7.99
CH_4	- 5.08
C_2H_6	-11.5
C_2H_4	- 5.0

P-1868

4.3.6 Infrared Analysis

Infrared gas analyzers make use of selective optical absorption. The theory of absorption admits of a simple interpretation. If radiation is supposed to pass through the gas in complete quanta, a quantum can be absorbed only if it is either just adequate to move the electron in some other orbit or else to set the electron free altogether. Thus the absorption spectra consists of a series of absorption lines, each line representing absorption at a different frequency. The frequency of absorption is dependent upon the energy levels of the electrons in the atom, and are given by Planck's equation, $h\nu = E_2 - E_1$, where ν is the frequency of absorption.

True absorption represents the actual disappearance of some of the infrared radiation, the energy of which is converted into heat motion of the molecules of the absorbing material. Absorption of radiant energy is given by Bouguer's exponential law, as a function of the thickness of the absorbing medium:

$$I_x = I_o e^{-ax}$$

The absorption coefficient for gases at 760 mm Hg pressure are given in Table 21.

Table 21 - Absorption Coefficients for Some Important Atmospheric Gas Constituents

Gas	λ in μ	α
CO_2	4.20	0.0335
	4.25	0.050
	4.30	0.061
	4.33	0.065
	4.35	0.060
	4.40	0.038
CO	4.7	(maximum)
H_2O	2.55	0.0258
	2.58	0.0644
	2.618	0.0900
	2.65	0.0590
	6	(maximum)

P-1868

The basic analyzer consists of (a) an infrared source, (b) filter cells, (c) sample and comparison cells, (d) rotating shutter, and (d) measuring chamber. The analysis is specific in that only one gas is measured at a time.

The purpose of the filter is to help remove interference caused by components other than the measured one in the gas sample.

The comparison cell contains a similar gaseous mixture -- from which the gas to be detected has been removed -- as is found in the sample cell. The measuring chamber consists of a capacitive manometer and is partially filled with the gas to be detected. Infrared radiation from two sources passes through the filters, and through the comparison cell and sample cell. The difference in absorption between these two cells is detected by the capacitive manometer. A shutter which intercepts the beam from the comparison cell and then from the sample cell provides an a-c electrical output signal from the capacitor. The magnitude of this output signal is a linear function of the concentration of the gas in the sample.

4.3.7 Emission Spectroscopy

Emission spectrographs normally employ the emission line spectra of the material to be analyzed to determine the identity of the sample. The emission of a line-spectrum is a phenomenon which is, approximately, the converse of the phenomenon of photo-electric emission. If the absorption of a quantum of energy of frequency ν results in the ejection of an electron from its orbit with a velocity, v, then the consequence of an electron falling with an initial velocity, v, into an atomic orbit can be expected to be the emission of a quantum of radiation of frequency ν .

Emission spectra of gases are obtained by using a suitable gas discharge tube and a spectrometer or a spectrograph. The spectrograph can be either a prism or a grating instrument. Table 22 gives the spectral range in which useful quantitative analysis of respiratory gases has been performed.

4.3.8 Thermal Conduction Analysis

This type of analysis is based upon the variations in the thermal conductivity of gases. The thermal conductivity, K, is defined by the relation

$$dQ/dt = - K\,dx\,dy\,(dU/dz) \qquad (42)$$

where dQ/dt is the time rate at which heat is conducted in the direction of the temperature gradient, dU/dz, across a parallel slab of area $dx\,dy$. According to the dynamical theory of gases, the thermal conductivity of gases is independent of pressure if the mean free path is small in comparison with the thickness of the conducting layer. Thermal conductivities of gases are given in Table 23. The value of energy, kiloergs, can be converted into calories by multiplying by 0.239×10^{-4}.

The apparatus for measuring the thermal conductivity essentially consists of (a) a conductivity cell, (b) and electrical bridge, and (c) a temperature controller or a thermostatic bath. The conductivity cell consists of a resistive element having either a positive or

Table 22 - Respiratory Gases That Have Been Analyzed by Emission Spectroscopy and the Wavelength Used

Gas	Spectra
N_2	3000° A to 4000° A
CO_2	2883° A to 2896° A
O_2	7753° A, 7626° A

P-1868

Table 23 - Thermal Conductivity of Gases

Gas (0°C)	K (Kiloergs $sec^{-1}\ cm^{-1}\ C^{\circ -1}$)
Argon	1.58
Hydrogen	15.9
Helium	13.9
Nitrogen	2.28
Neon	0.44
Oxygen	2.33
Carbon Monoxide	2.15
Carbon Dioxide	1.37
N_2O	1.44
NO	2.08
NO_2	4.01

P-1868

negative temperature coefficient and of a spherical cell or capillary tubing in which the resistive element is centrally located. This cell forms two arms of a Wheatstone bridge; the remaining two arms consist of two equal or variable resistances.

A constant electrical current is supplied to the bridge by a power source. The bridge is then balanced by introducing a reference gas into both cells and adjusting the value of the two bridge resistors, for a null output. When the sample cell is exposed to a gas having a different thermal conductivity, K, the equilibrium temperature of the resistive element changes. Corresponding to this change in temperature will be a change in resistance, which unbalances the bridge. An infinite impedance device is then used to measure the potential across the unbalanced arms of the bridge, which is a function of the thermal conductivity of the particular gas.

4.3.9 Oxygen Polarography

A polarographic oxygen pressure sensor employs an electrode system which consists of a plantinum cathode, a silver anode, and a gas permeable membrane. The platinum electrode is pressed against the inside of the membrane. The two electrodes are emersed in an electrolyte of potassium chloride. A potential of 0.7 volt is applied across the electrodes, the platinum electrode being negative with respect to the silver electrode. In the absence of reducible gases, the cell polarizes and remains polarized. Oxidizing gases such as oxygen passing through the membrane are reduced at the cathode. Thus, the current flow in the cell due to this reduction (of oxygen) process is proportional to the partial pressure of the oxygen gas outside the membrane.

4.3.10 Dewpoint Hygrometry

A dewpoint hygrometer functions by determining the temperature (dewpoint) of a surface that has upon it a thin coating of dew which is in equilibrium with the water vapor in the contiguous atmosphere. Kinetic equilibrium is closely approximated when the dew thickness is not changing. Automatic dewpoint hygrometers have been produced (by Bendix) in which the dew thickness deposited on a mirror surface forms the critical element in a closed dewpoint sensing servo loop.

4.3.11 Heat of Combustion Analysis

Combustible gas analyzers have been developed which use the heat of combustion of the gases as a means of identification. Basically the analyzer operates on a balanced electrical bridge that has an electrically-heated platinum filament in one arm. Combustible gas, such as CO, flowing over the hot platinum filament burn catalytically at the surface, and thereby raise the filament temperature. The temperature change causes a change in the resistance of the platinum wire. Such a charge can be measured by the potential across the unbalanced bridge. (This principle is similar to that used in a Pirani Pressure gauge that normally operates from 10^{-3} to atmospheric pressure.)

4.3.12 Polarization Gas Analysis

Although polarization gas analyzers employ operating principles which are nearly identical to those which are used in polarography, the operating characteristics of the polarograph and polarization sensors are quite different. The detector elements in a polarization analyzer consist of a galvanic cell with a zinc and a hollow carbon electrode in a special electrolyte designated as "Oxylite." This generates a voltage and current, and the positive carbon electrode is polarized by the products of electrolysis which readily react with oxygen. Polarization inhibits the flow of current, but oxygen applied to the positive pole will depolarize it and restore the current flow.

The Oxygen Indicator utilizes this phenomenon by causing the gas mixture to flow through the interior of the carbon electrode, from where it diffuses through the carbon to the interface with the electrolyte. Here the oxygen combines with the substances causing the polarization. Thus, a depolarizing action is produced which is variable with the oxygen concentration and reflected in the electrical indication of the meter. In the Portable Oxygen Indicator, Type E, the cell characteristics and circuit parameters are chosen to produce electric currents in proportion to the square roots of oxygen concentrations.

4.3.13 pH Gas Analysis

This type of gas analysis measures the H^+ (pH) ion concentration resulting from the dissolution of the gas in a solute. In a CO_2

sensor employing this principle, the electrode structure consists of a glass electrode having a Ag-AgCl internal element and a Ag reference electrode contained in a single assembly within a removable housing. Electrical continuity between the two electrodes is maintained by means of an aqueous electrolyte gel solution. A gas-permeable membrane seals the end of the sensor. After carbon dioxide passes through the membrane, it causes the following reaction in the electrolyte solution:

$$H_2O + CO_2 \rightleftharpoons H_2CO_3 \rightleftharpoons H^+ + HCO_3^-$$

Changes in concentration of dissociated, or free, hydrogen ions (H^+) in the electrolyte solution are detected by the sensor as changes in pH. As the pH of the solution varies, it causes a corresponding variation in potential that is proportional to the log of the concentration of carbon dioxide in the gaseous sample being analyzed. This potential can be indicated directly upon a meter which is calibrated in terms of CO_2 partial pressure.

4.3.14 X-Ray Analysis

An X-ray analyzer contains a method for producing X-rays, a detection system, and a sample chamber. A sample to be analyzed is placed in the sample chamber and bombarded with X-rays. The resultant secondary radiation or attenuated primary radiation is compared to standard spectra. Most X-rays tubes operate in the 40-100kv range and hence require a large power supply. In addition, the tube current must be regulated to provide a constant energy emission from the tube.

4.3.14.1 Fluorescence

In the fluorescence method the sample to be analyzed is bombarded with X-rays and the resulting spatially dispersed secondary X-rays, which occur due to transitions within the sample, are detected, usually by film. Most fluoresence analyses require long film exposure times due to the extremely weak secondary emissions hence limiting the usefulness of such a method.

4.3.14.2 Absorption

In the absorption method the same bombardment procedure is followed except that instead of detecting the secondary

Table 24 - Summary of S

Analyzer / Characteristics	Time-of-Flight Mass Spectrometry	Coincidence Mass Spectrometry	Magnetic Mass Spectrometry	Radio Frequency Mass Spectrometry	Omegatron Mass Spectrometry	Quadrupole Mass Spectrometry	Emission Spectroscopy	Chromatography	Polarography
Gases Analyzed	All in mass range L_1-L_6	All in mass range L_1-L_6	All in mass range L_1-L_6	All in mass range L_1-L_6	All in mass range L_1-L_6	All in mass range L_1-L_6	N_2, O_2, CO, CO_2, L_1-L_6	N_2, O_2, CO, CO_2, H_2O, L_1-L_6	O_2
Type of Analysis	Variable several component, total mass range scan, continuous analysis	Several component continuous analysis	Fixed multi-component continuous analysis	Variable single component continuous analysis	Variable single component continuous analysis	Variable single component continuous analysis	Continuous single component analysis	Non-continuous analysis on N_2, CO_2, O_2, CO readings not simultaneous	Continuous
Sampling Rate	Sample system dependent	Sample system dependent	Sample system dependent	Sample system dependent	Sample system dependent	Sample system dependent	700 ml/min	1-2 ml/min with He carrier at 30 ml/min	Zero if face mask mounted, flow rate if remotely mounted
Response Time	0.05 to 1 sec time constant of sample system	Sample system dependent	Sample system dependent	Sample system dependent	Sample system dependent	Sample system dependent	0.03 sec for 90% F.S.	3 min for N_2 7 min for CO 9 min for CO_2 15-20 min for O_2	90 sec
Accuracy	0.5% of F.S. sample dependent	N.A.	N.A.	N.A.	N.A.	N.A.	±2% for gases whose partial pressure is 0.5 to 80% N_2	Approx. 1 vol. %	±10% or ±30 mm Hg
Linearity	Linear	Sample system dependent	Sample system dependent	Sample system dependent	Sample system dependent	Sample system dependent	+ to 10 vol. % - above 10 vol. % for N_2	Area of peaks give a linear output with respect to vol. % N_2	Max. deviation is 1.5%
Interferences	Contributions to m/e peaks from various mass components	Contributions to m/e peaks from various mass components	Contributions to m/e peaks from various mass components	Contributions to m/e peaks from various mass components	Contributions to m/e peaks from various mass components	Contributions to m/e peaks from various mass components	Emission increases with H_2O vapor, contaminants in tube affect emission	All of N_2 not eliminated as NO interferes with CO	Any reducing gases, SO_2
Stability	0.5% F.S.	N.A.	N.A.	N.A.	N.A.	N.A.	Pressure sensitive calibration changes with contaminants	1% F.S. for life of carrier gas	Temp. dependent
Susceptibility to Shock and Vibration	No problem	No problem	No problem	No problem	No problem	No problem	No problem if optical system is used	No problem	0.3 g's at 5 cps 3-10 g's at 14 to 2000 cps
Weight	<24 lb	10 lb	14 lb	20 lb	≅10 lb	4 lb	25 lb (nitrogen meter)	Weight dependent on detector column, gas supply ~100 lb	1.3 lb
Size	315 cu in.	Small	Small	Small	Small	Small	1200 cu in. (nitrogen meter only)	5000 cu in.	21 cu in.
Power	Instrument 40-watts,	6 watts	3 watts	6 watts	≅10 watts	3 watts	200-300 watts plus pumps (nitrogen meter)	200 watts	2 watts plus pump
Form of Output	Electrometer 0-5 volts	Voltage	Electrometer voltage	Voltage	Voltage	Plate and electrometer	Voltage output from photocell for N_2 meter	Vapor phase analyzed by suitable detector	0.5 volt
Temperature Control	No problem	No problem	No problem	No problem	No problem	No problem	Discharge tube at temperature equilibrium	Column must be temperature controlled such that stationary phase has 0.1 mm Hg vapor pressure	Critical 3% °C
Gravity	Independent	Independent	Independent	Independent	Independent	Independent	Independent	Independent	Independent
Pressure	Low or high pressure device	Low or high pressure device	Low or high pressure device	Low or high pressure device	Low or high pressure device	Low or high pressure device	1.4 to 3.4 mm Hg low pressure device	760 mm Hg	250-1000 mm Hg device
Sensitivity	1 ppm, 10^{-14} mm/Hg sample dependent $>10^6$ dynamic range	10^{-12} mm Hg 10^6 dynamic range	10^{-13} mm Hg 10^6 dynamic range	10^{-10} mm Hg 10^3 dynamic range	10^{-13} mm Hg	10^{-13} mm Hg 10^3 dynamic range	0.01 vol. %	1 ppm	2500 ppm
Humidity	No problem	No problem	No problem	No problem	No problem	No problem	Calibration is affected by H_2O vapor concentration	No problem	Must have 90-100
Life of Analyzer	Indefinite	Indefinite	Indefinite	Indefinite	Indefinite	Indefinite	Discharge tube requires periodic cleaning	Life of carrier gas	7 weeks in 75% relative humidity

ensor Characteristics Studied

Paramagnetic Analysis	Polarization Analysis	Heat-of-Combustion Analysis	Infrared Analysis	Thermal Conduction Analysis	Pneumatic Refractometry	Interferometry	p-H Analysis	Dewpoint Hygrometry	X-Ray Analysis
O_2	O_2	CO	CO_2, CO, H_2O	CO_2, CO, H_2O	O_2, CO_2	O_2, CO_2	CO_2	H_2O	Solids, N_i, M_g, F_e, Al, M_g, C_a, S_i
Continuous	Continuous when using calibrated sample	Semi-continuous	Continuous single component analysis	Continuous single component analysis	Continuous single component analysis	Continuous single component analysis	Continuous single component analysis	Continuous single component analysis	Fixed several component analysis, cannot analyze unexpected sample
40-60 ml/min	150 ml/min	4000 ml/min	480 ml/min	200-500 ml/min	No data available	500 ml/min	Zero if face mask mounted, flow rate if remotely mounted	Zero if face mask mounted dependent on flow rate for remote mounted	1/8 thick, 3-4 sq in. surface analysis
4.5 sec	60 sec	60-120 sec F.S.	0.2 sec 90% F.S.	20 sec	0.2 sec delay time	25 sec latent period 30 sec adjustment period	2 min time constant at 70°F	0.5 sec	3-30 min for analysis
± 1% F.S. on all ranges, min. scale range 0-1% O_2	± 5000 ppm ± 0.5% F.S.	± 25 ppm	0.1% F.S. detection for CO = 400 ppm	± 30 ppm for O_2, CO_2	± 0.1% for CO_2 in air	± 0.05 for O_2 in air ± 0.002 - 0.007 for CO_2	± 1% F.S. ± 0.2 mm Hg	± 2% full scale	1-10% F.S.
Linear up to 60% O_2	Nonlinear readout in √of concentration	Good to 1000 ppm	Linear	Linear for most applications	Linear for CO_2	Does not apply	Linear	Dependent on temp. norm. exponential	N.A.
NO, CO_2, H_2O	CO_2 > 25% SO_2 > 50 ppm NO_2 > 50 ppm Acids > 50 ppm	Other combustible gases	H_2O interferes 1 part in 2000 with CO	One complete analysis, others interfere	Requires 3 hours for temperature stability	Needs H_2O absorbers, known reference gas	Any reducing gas	Any gas condensible in low temperature operating range	Any unexpected component could interfere
± 0.5% F.S.	± 0.5 % F.S.	± 25 ppm	Needs a stable reference gas	± 2% F.S. over 30-day period	Change in N_2-O_2 ratio changes calibration	Extremely stable	1% F.S. temp. dependent 4% per 1°F	± 0.2°C	Temp. dependent, surface contaminant dependent
No problem	No problem	No problem	Detectors are a problem	No problem	No shock problem	Shock problem	0.3 g's at 5 cps 3-10 g's at 14-2000 cps	No problem	No problem
10 lb	5-3/4 lb	17-1/4 lb	75 lb	Minimum data not available	Minimum data not available	Minimum data not available	20 oz	2.5 lb	40 lb
[illegible]	[illegible]	[illegible]	162 cu in.	8 cu in. for electronics	Minimum data not available	Minimum data not available	26 cu in.	48 cu in.	800 cu in.
50 watts	30 watts no pump 100 watts with pump	Pump needed	High power requirement	100 watts plus pumps	Minimum data not available	Minimum data not available	29 watts plus pumps	40 watts	32 watts
Could be electrical, usually deflected light beam	Voltage	Voltage	Voltage	Voltage from a bridge	Photocell voltage output	Independent	55 mv/decade change in CO_2	0-5 volts	Output of pulse height analyzer voltage
Critical (needs temp. control)	0° - 50°C	0° - 50°C	No problem	Thermostatic control	Must be temp. controlled	Independent	Temp. range 40°F - 150°F constant temp. only	Constant heat sink needed	No problem
Affected by inertial changes	Independent	Independent	Independent	Independent	Independent	Independent	Independent	Independent	Independent
200-1000 mm Hg device	200-1000 mm Hg device	760 mm Hg pressure device	Pressure dependent 760 mm Hg device	Must be controlled 760 mm Hg device	760 mm Hg high pressure device	Independent of pressure effects 760 mm Hg	5 psi - 20 psi operating range 760 mm Hg device	Independent	Vacuum conditions preferred
± 500 ppm	5000 ppm	± 20 ppm	400 ppm on CO	30 ppm CO_2 and O_2	No data available	Complete freedom from sensitivity	Partial pressure CO_2 is 1-20 mm Hg	2 ppm	0.1-10% sample dependent
No problem	Condensation of H_2O vapor must be prevented	Dry sample	No problem	Instrument must be water compensated	Water vapor must be removed	water vapor must be removed	15 - 70% relative humidity for operation	No effect	Water vapor can affect calibration
Indefinite	Recalibrate every two hours	Recharge Hopcalite every 8 hours	Indefinite	Indefinite	Indefinite	Indefinite	4 weeks when relative humidity is 75%	Indefinite	Life of X-ray tube and detector

P-1868

2

X-rays from the sample, the primary X-rays are detected and compared to a background spectrum taken at the same tube parameters but with no sample in the sample holder. The characteristic absorption curves for various materials are known from their atomic structure and hence an identification of the sample can be made according to the particular absorbing frequency patterns. Here again, since the normal analysis output is film, this method cannot be employed as a fast readout analyzer.

4.4 ANALYSIS OF SENSOR SYSTEMS

Sensor systems based on the techniques previously discussed have been carefully evaluated. The important characteristics of each have been compiled and included for convenience in Table 24 and Table 25; Table 24 is devoted to lunar atmosphere analyses, and Table 25 is devoted to lunar soil analyses.

The interpretation of the tabular entries is straightforward; however, the following notes will help in using the tables. The sensors are grouped into vertical columns according to the particular component for which that sensor's use is dominant. Of course, the multigas sensors could well fit in several columns, but they appear only once. The specific sensors are listed under the gas to which they are sensitive.

The sensors operate according to the physical principles outlined in this subsection. It is well to keep this fact in mind particularly when considering the polarograph, pH sensor, and polarization sensor. Most of the sensor parameters (the extreme left-hand column) are well defined by common usage and no comment on their interpretation is required. However, the parameters which do need some elaboration are discussed in the next few paragraphs.

The term linearity means that the output signal is directly proportional to the input partial pressure of the constituent being measured. This parameter is most significant during calibration and preflight checkout.

The term interference is used to describe the phenomena that the same output signal will be produced by the sensor for two or more different inputs.

Susceptibility to shock, vibration, gravity, and humidity are reckoned in terms of human tolerance.

Table 25 - Summary of Characteristics of Possible Lunar Soil Sensors

Analyzer	Time of Flight Mass Spectrometer	Coincidence Mass Spectrometer	Magnetic Mass Spectrometer	Radio Frequency Mass Spectrometer	Omegatron Mass Spectrometer	Quadripole Mass Spectrometer	Emission Spectroscopy	X-Ray Analyzer
Sample Analyzed	Fe, Ni, Al, Mg, Ca, Si, O	Fe, Ni, Al, Mg, Ca, Si, O	Fe, Ni, Al, Mg, Ca, Si, O	Fe, Ni, Al, Mg, Ca, Si, O	Fe, Ni, Al, Mg, Ca, Si, O	Fe, Ni, Al, Mg, Ca, Si, O	Fe, Ni, Al, Mg, Ca, Si, O	Fe, Ni, Al, Mg, Ca, Si, O
Type of Analysis	Variable multi-component continuous + total mass range scan	Multi-component continuous	Fixed multi-component continuous	Variable single component continuous	Variable single component continuous	Variable single component	Single component continuous	Fixed multi-component cannot analyze unexpected sample
Sampling Rate	Depends on inlet system	Depends on inlet system	Depends on inlet system	Depends on inlet system	Depends on inlet system	Depends on inlet system	700 ml/min	Micro sample
Response Time	0.05 - 1 sec time constant of sample system	Sample system dependent	Sample system dependent	Sample system dependent	Sample system dependent	Sample system dependent	0.03 sec for 90% F.S.	3-30 min for analysis
Accuracy	0.5% F.S. sample dependent	N.A.	N.A.	N.A.	N.A.	N.A.	N.A.	1-10% F.S.
Linearity	Linear	Sample system dependent	Sample system dependent	Sample system dependent	Sample system dependent	Sample system dependent	+ to 10 vol. % - above 10 vol.% for N_2	
Interferences	Background gases	Background gases	Background gases	Background gases	Background gases	Background gases	Emission increases with H_2O concentration contaminants affect emission	Unexpected components can interfere
Stability	0.25% F.S.	N.A.	N.A.	N.A.	N.A.	N.A.	Pressure sensitive calibration changes with contaminants	Temperatures surface contaminants dependent
Susceptibility to Shock and Vibration	No problem	No problem	No problem	No problem	No problem	No problem	No problem if optical system is used	No problem
Weight	30 lbs with laser sample inlet system	N.A.	N.A.	N.A.	N.A.	N.A.	25 lb (nitrogen meter)	40 lb
Size	350 cu in.	N.A.	N.A.	N.A.	N.A.	N.A.	1200 cu in. (nitrogen meter)	800 cu in.
Power	250 watts	6 watts	3 watts	6 watts	≤10 watts	3 watts	200-300 watts plus pumps	32 watts
Form of Output	Electrometer 0-5 volts	Voltage	Electrometer voltage	Voltage	Voltage	Electrometer voltage	Voltage output from photocell	Output of pulse height analyzedd
Temperature Control	No problem	No problem	No problem	No problem	No problem	No problem	Discharge tube kept at temperature equilibrium	No problem
Gravity	Independent	Independent	Independent	Independent	Independent	Independent	Independent	Independent
Pressure	0.25-760 mm/Hg low or high pressure device	Low or high pressure device	Low or high pressure device	Low or high pressure device	Low or high pressure device	Low or high pressure device	1.4 to 3.4 mm/Hg low pressure device	Vacuum conditions preferred
Sensitivity	1 ppm 10^{-14} mm Hg $>10^6$ dynamic range	10^{-12} mm Hg 10^6 dynamic range	10^{-13} mm Hg 10^6 dynamic range	10^{-10} mm Hg 10^3 dynamic range	10^{-13} mm Hg	10^{-13} mm Hg 10^3 dynamic range	0.01 vol. %	0.1 - 10% sample dependent
Humidity	No problem	No problem	No problem	No problem	No problem	No problem	Calibration affected by water vapor concentration	Water vapor can affect calibration
Life of Analyzer	Indefinite	Indefinite	Indefinite	Indefinite	Indefinite	Indefinite	Discharge tube requires cleaning	Life of X-Ray tube

P-1868

The weights, sizes, and power requirements are the "best guesses" for these parameters as that which would result from a reasonably successful six-month development (miniaturization) program.

The form of output entries are, in almost all cases, listed as "voltage" even though a signal-to-voltage converter might be required. Those cases where the term "voltage" does not appear imply that it is not feasible to provide an airborne signal-to-voltage converter.

The temperature control and pressure parameters refer to the operating environment within the instrument and not necessarily to the temperatures and pressure of the environment in which the equipment is placed.

The sensitivity values listed are the maximum values which can be reasonably expected for an instrument resulting from an approximately 9-month development program.

Symbols L_1 to L_6 refer to the gases defined as the lunar atmosphere model.

These tables illustrate the primary characteristics of the available analysis devices capable of performing gas analyses.

4.4.1 Lunar Atmosphere

In order to effectively design an analyzer capable of performing a specific analysis it is necessary to; first, identify the nature of the anticipated samples; second, be aware of all available devices capable of performing analyses of a similar nature; third, on the basis of the anticipated samples and the possible analysis schemes, pick the most suitable and refine it to fit the specific analysis. Previous subsections have defined argon, carbon dioxide, sulphur dioxide, water vapor, xenon, and krypton as the lunar atmosphere model. The anticipated total pressure is in the 10^{-8} - 10^{-10} mm Hg range with possible components having partial pressures ranging from 10^{-8} to 10^{-14} mm Hg. An analyzer designed to have a dynamic range of 10^6 with the mid-range point changeable by a factor of 10^2 could analyze gases with partial pressures as high as 10^{-6} mm Hg and as low as 10^{-14} mm Hg.

The analysis has shown that the only sensors possessing characteristics suitable for measuring the low partial pressure atmosphere components anticipated at the lunar surface are the mass spectrometers. All of the mass spectrometers, except the Radio Frequency

Mass Spectrometer have the sensitivity required for even the 10^{-13} mm Hg pressure anticipated for argon (Herring and Licht Model). The physical parameters, size, weight, and power are suitable for the development of a lunar gas analyzer. All the other analysis devices do not provide an acceptable correspondence between the intended analysis requirements and the sensor characteristics.

By means of this analysis, Bendix believes that the proposed lunar atmosphere analyzer can be most easily developed from a basic Time-of-Flight Mass Spectrometer adapted to the particular needs of the lunar environment. The experience gained by the Research Laboratories Division in the successful development of both rocket-borne and satellite-borne miniature mass spectrometers will guide the design, development, and construction of the lunar gas analyzer. The lunar gas analyzer would be capable of measuring not only the anticipated lunar gases, argon, carbon dioxide, sulphur dioxide, water vapor, xenon, and krypton, but could scan the mass range from 1 amu to 500 amu to detect even the unexpected lunar atmosphere components. An analyzer designed specifically for lunar atmosphere analyses would have the characteristics shown in Table 26. A scanned mass spectrum from such an analyzer of the lunar atmosphere model appears in Figure 5.

Table 26 - Lunar Atmosphere Analyzer Characteristics

Analyzer Characteristics	Characteristic Values
Resolution	800 AMU
Mass Range	1-500 AMU (Scanned and fixed gates)
Response Time	0.05 sec
Accuracy	±2%
Linearity	±2%
Stability	±2%
Weight	25 lb
Size	250 cu in.
Power	40 W
Form of Output	Electrometer 0-5 V
Gravity	Independent
Input Pressure Range	10^{-8} - 10^{-14} mm Hg
Sensitivity	1 ppm, 10^{-6} dynamic range
Analyzer Life	Indefinite

P-2159

Figure 5 - Mass Spectrum of L

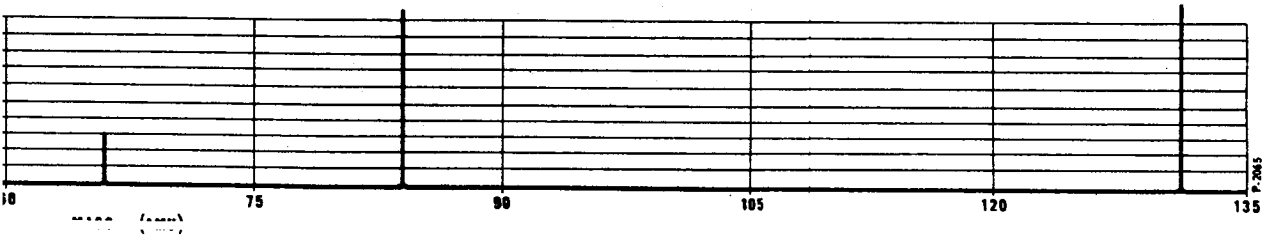

unar Atmosphere (Herring and Licht Model)

2

4.4.2 Lunar Soil

The information in Table 24 indicates that only one technique shows promise of being able to analyze solids directly as they are found in the lunar crust. This technique, called X-Ray Analysis, is included in the right-hand column. All of the other sensing techniques require some amount of sample gathering and processing prior to the analysis. Thus, the requirement that the analyzer be precisely positioned and the desirability of accomplishing some sample "batching" are major disadvantages of this type analyzer.

Each of the other techniques listed in Table 24 require a "vaporized" sample, and though several mechanisms for accomplishing this are discussed in later sections it is interesting to note here that only two methods appear feasible; the laser method and the high energy electron beam method. Bendix feels that the laser system is to be preferred since experience in the laboratory shows that large numbers of high energy electrons in the vicinity of a vaporized sample constitute one of the more effective ion noise generators yet devised. Readers interested in persuing this subject are referred to the extensive literature in the development of electron bombardment heated knudsen cell sample systems.

The general comments which appear immediately below, assume that a suitable vaporizing mechanism can be devised. An analysis of a single element sample is a relatively easy task; however, the analyses of multielement samples becomes progressively more difficult as the number of elements increases. The inclusion of compounds in the sample heightens the difficulty. Tables 27 and 28 show that the lunar soil model, indeed, contains several compounds.

To gain a general idea of the possible nature of a lunar soil spectrum consider that the elemental abundances of the lunar soil are as shown in Table 27. Then, several lunar compounds which could be formed from the above elements (they are normally found in some abundance on the earth) are listed in Table 28.

Consider that the dissociation and ionization probabilities for these compounds are such that the relative abundances of the fragments formed are in ratios of 10 to 1 for primary to secondary species as in the following example for Bayerite ($Al_2O_3 \cdot 3H_2O$):

Table 27 - Lunar Soil Model

Element	Percentage of Composition
Oxygen	60
Silicon	25
Aluminum	1
Iron	5
Magnesium	4
Calcium	2
Sodium, Potassium, Nickel, Cobalt, Sulphur, Carbon	3 (Total)

P-2159

Table 28 - Probable Lunar Soil Components

Compound	Symbol	Atomic Weight
Bayerite	$Al_2O_3 \cdot 3H_2O$	155.99
Aluminum Oxide	$Al_2O_3 \cdot$	101.94
Aluminum Sulphate	$Al_2(SO_4)_3$	342.14
Iron Carbonate	$FeCO_3$	115.86
Iron Carbonate	$FeCO_3 \cdot H_2O$	133.88
Iron Oxide	FeO	71.84
Iron Oxide (Hematite)	Fe_2O_3	159.70
Iron Metasilicate	$FeSiO_3$	131.91
Iron Sulphate	$FeSO_4$	169.31
Iron Sulfite	$FeSO_3 \cdot 3H_2O$	189.96
Silicon Dioxide	SiO_2	60.06
Magnesium Oxide	MgO	40.32
Magnesium Sulphate	$MgSO_4$	120.39
Magnesium Sulphate	$MgSO_4 \cdot H_2O$	138.49
Magnesium Sulphite	$MgSO_3 \cdot 6H_2O$	212.48
Calcium Magnesium Carbonate	$CACO_3 \cdot MgCO_3$	184.42
Calcium Magnesium Metasilicate	$CaMg(SiO_3)_2$	216.52
Calcium Magnesium Orthosilicate	$Ca_3Mg(SiO_4)_2$	328.68
Calcium Oxide	CaO	56.08
Calcium Peroxide	$CaO \cdot 8H_2O$	216.21
Calcium Di-orthosilicate	$2(CaSiO_2)$	172.22
Calcium Sulphate	$CaSO_4$	136.15
Gypsum	$CaSO_4 \cdot 2H_3O$	172.18
Sodium Aluminum Sulphate	$NaAl(SO_4)_2 \cdot 12H_2O$	458.29
Sodium Carbonate	Na_2CO_3	106.00
Sodium Carbonate	$Na_2CO_3 \cdot H_2O$	124.02
Magnesium Silicate	$MgSiO_3$	100.38
Magnesium Aluminate	$MgAl_2O_4$	142.26

P-2159

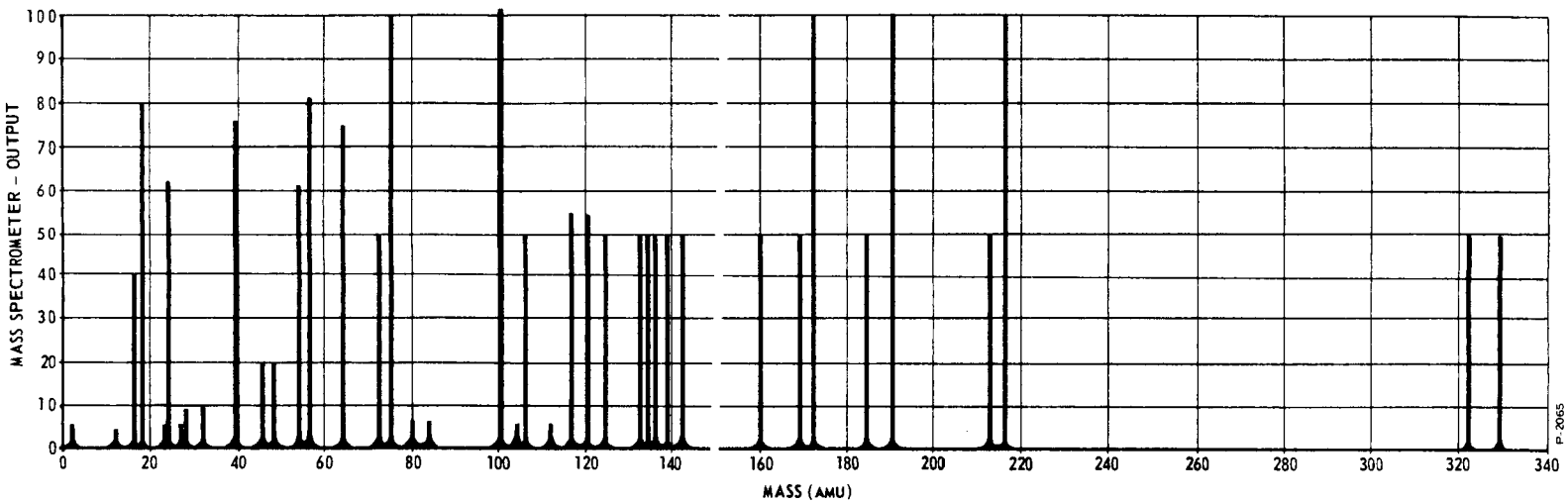

Figure 6 - Mass Spectrum of Lunar Soil Model

Mass Peak Contribution Due to:	Mass	Relative Abundance
$Al_2O_3 \cdot 3H_2O$	156	1
Al_2O_3	102	0.1
Al_2	54	0.01
O_3	48	0.01
$3H_2O$	18	0.1
O	16	0.01
H_2	2	0.01

A model soil spectrum based on the above compounds is shown in Figure 6. The relative abundance of the parent compounds is assumed to be unity instead of that dictated by the elemental abundance of the compound contituents. The reader should bear in mind that this model does not attempt to rigorously account for the concentration of individual constituents at the spectrometer ionization region.

The expected spectrum for a combination of the compounds listed in Table 28 can be estimated by a similar process.

The process results in a rather complex series of mass peaks whose amplitude varies as a function of mass position.

It is believed that a multi-channel analyzer should be used that simultaneously provides both fixed mass monitoring and scanning. In order to provide this capability, a Time-of-Flight Mass Spectrometer was selected.

4.5 COMPREHENSIVE DISCUSSION OF TIME-OF-FLIGHT MASS SPECTROMETRY

This subsection discusses each of the various parts of a Time-of-Flight instrument, such as the Inlet System, Ion Sources, Analyzer Section, Detector, and Output Systems in detail. Since the normal applications of the Time-of-Flight Mass Spectrometer are varied, more than one system is discussed in some cases. For instance, depending upon the inlet system employed, it is possible to analyze samples from either the solid, liquid, vapor, or plasma state. Each

of the possible inlet systems are discussed and the operating principles of each are explained.

The Time-of-Flight instrument can be utilized for the analysis of either neutral or ionic species. However, when energetic plasma ions are being analyzed a special inlet system is then employed. In order for the plasma ions to reach the spectrometer ion source region and be representative of actual plasma composition, the plasma inlet system which consists of differentially pumped-cones with holes at their points is used. This plasma probe is oriented to admit particles having their principal component of velocity at right angles to the mass spectrometer drift tube. Thus, the initial energies of the incoming particules do not affect the Time-of-Flight down the drift tube and maximum mass resolution can be preserved. For neutral analysis, of course some means of generating the ions is necessary. Generally an ionizing electron beam of approximately 70 ev is employed; however, there are other methods of ion generation. These methods are described.

Once the ions have been formed, the Time-of-Flight analyzer, by means of appropriate electric and magnetic fields, directs them toward the detector and multiplier. Several output systems; such as, the oscilloscope display, analog presentation by means of various electrometer circuits, or a digital presentation with a pulse counting technique are available for representing the analysis spectrum.

4.5.1 Inlet Systems

Regardless of the state of the sample plasma, gas, liquid, solid; it is the function of a spectrometer inlet system to provide the transfer mechanism from the state to the temperature and pressure conditions required by the ion source region of the mass spectrometer. This transfer should be effected so that the nature of the sample is changed as little as possible. The sample should not be contaminated by the inlet system nor have the relative concentrations of its constituents altered, appreciably. One inlet system cannot perform this rather formidable task for all sample conditions. Consequently, various inlet systems have been devised to accomplish particular sampling jobs. Most of the systems described in this subsection are presently employed routinely and are available as off-the-shelf items. However particular sampling requirements sometimes change the design of these inlet systems and consequently some development time might be necessary.

Table 29 - Availability of Inlet Systems for T.O.F. Mass Spectrometers

Inlet System	Presently Available?	Development Time
Right Angle (Plasma)	Yes	--
Laser	No	1 year
Knudsen Cell	Yes	--
Heated Filament	Yes	--
Sputtering	No	1 year
Electron Beam	No	1 year

P-1968

Table 29 shows the inlet systems that are presently available and the estimated time required to develop those that are not.

4.5.1.1 General

The most commonly used inlet system for a Time-of-Flight Mass Spectrometer is the one used for gas analysis. In fact, very special purpose Breathable Atmosphere Composition Analyzers are constructed which use this sample inlet system. The design of the system is not, however, restricted to just breathable gases nor to the pressure range (760 mm Hg - 190 mm Hg) normally associated with this analysis.

This sample inlet system ordinarily performs the function of reducing sample gas pressure from ambient level (usually atmospheric pressure) to the level at which the spectrometer operates (about 1×10^{-4} mm Hg), without altering sample composition. The sample system can also perform an additional function: it will operate on the incoming gas sample in such a way as to separate discrete gaseous components (CO and N_2) having the same mass. These constituents are otherwise indistinguishable in the mass spectrometer output. Separation of these gas sample constituents is accomplished by a chemical filter incorporated into the sample system. The following paragraphs present the factors which influence design of the sample system.

4.5.1.1.1 Sample Flow Theory

Design of the spectrometer sample system for gas analysis is based on the philosophy that if the sample out-flow mechanism of a given region is the same as the in-flow mechanism, the sample composition within that region cannot reflect any properties of the flow mechanism. In general, the sample transition from a high pressure region to the low operating pressure within the spectrometer vacuum housing will be characterized by a transition from viscous to molecular flow.

The viscous flow mechanism prevails in regions where the mean free path of the gas particles is much less than the dimensions of the enclosure. Diffusion rates are low, so it can be assumed that mass separation does not take place as the sample gas passes through a viscous flow region. Thus, the sample flow is mass independent, and true sample composition is preserved. Molecular flow prevails in regions where the mean free path of the gas particles is greater than the enclosure dimensions. Net flow rates in a molecular flow region are proportional to $1/\sqrt{M}$ where M is the mass of the particle. Thus it is evident that if, in a given region, the in-flow mechanism is viscous while the out-flow is molecular, the gas composition in that region will be weighted in favor of the heavier masses. But if the two flow mechanisms are the same, the gas composition will not be altered.

The mass spectrometer vacuum housing must be operated at pressures where molecular flow prevails; that is, at pressures such that the mean free path of gas particles is much greater than the enclosure dimensions. For this reason the spectrometer's high vacuum pumps operate in a molecular flow region; and, in order to preserve sample gas component ratios, the gas flow mechanism into the mass spectrometer must also be molecular. This is accomplished by leaking sample gas into the mass spectrometer ion source region through a small diameter orifice. On the inlet side of this orifice the sample gas pressure is reduced to a level at which the particle mean free path is greater than the dimensions of the orifice; e.g., for an orifice diameter of 0.002 inch, the sample system pressure would be about 1 mm Hg.

Since the gas flow mechanism into the sample inlet tube is viscous at or near atmospheric pressure, a viscous flow mechanism out of the sample system must be provided if true

sample component ratios are to be maintained. Since it has been established that the flow mechanism into the mass spectrometer must be molecular, it is evident that a second gas flow path out of the sample system must be provided. That portion of the sample gas which flows into the mass spectrometer through the molecular leak must be negligible relative to the viscous flow outlet from the sample system.

Viscous flow through the sample system is established by a rotary-type oil-wetted high vacuum pump. The atmospheric sample is pumped through a capillary tube into a chamber which is connected to the sample pump; one wall of the chamber includes the molecular leak into the mass spectrometer ionization region. The inside diameter of the capillary tube is selected to give the desired sample chamber pressure (usually about 1 mm Hg) for a given atmospheric pressure and sample flow rate. The sample flow rate is established by conductance-limiting the sample flow between the pump and sample chamber; i.e., by throttling the sample pump. Conductance-limiting the gas flow out of the sample chamber contributes to over-all stability of the atmospheric composition analyzer by reducing the dependence of sample chamber pressure on pump stability.

Optimum design of the sample system involves a compromise between several conflicting factors. To improve dimensional stability, it is desirable to increase the diameter of the molecular leak into the mass spectrometer. This, in turn, requires a lower sample chamber pressure to assure that the inter-molecular mean free path is greater than the dimensions of the leak. Conductance-limiting of the sample flow from sample chamber to pump is desirable for stability, but results in a pressure drop across the pump line. Thus, if gas flow in the pump line is to be conductance-limited, the ultimate pump pressure must be lower than the sample chamber pressure. Choice of sample flow rate represents a compromise between speed of response and sample consumption, as will be illustrated.

The ultimate pressure that can be attained by a given sample pump at a given sample gas flow is the basic limitation. With this parameter established, an optimum compromise is then made between sample chamber pressure and pump line conductance. The system design provides viscous flow throughout the sample system, and molecular flow into and out of the mass spectrometer.

In addition to preserving sample gas component ratios, the use of a sample system pump greatly increases speed of response to changes in gas composition. If the sample gas were leaked directly into the spectrometer from atmospheric pressure, changes in sample gas composition would be detected only as fast as the gas particles could diffuse through the inlet tube. The gas flow rate in the tube would be essentially zero, considering the very small number of particles leaked into the spectrometer. At high pressures, the mean free path of the particles is very short so that diffusion rates are low. Thus, the time of response to a change in sample composition would be very long. Using a sample system pump assures a fast sample flow through the inlet tube, while the small tube diameter keeps the consumption of sample gas at a low level. Hence, response to a change in composition does not depend on diffusion, but on the rate at which sample gas is being pumped through the sample system.

4.5.1.1.2 Chemical Filter System

A chemical filter can be incorporated into the sample system to eliminate ambiguity of output at mass 28; both molecular nitrogen and carbon monoxide fall at that mass number. The chemical filter system functions to separate these two sample gas components so that carbon dioxide can be measured independently without interference from the relatively high concentration of molecular nitrogen.

The system provides two sample flow paths in the viscous flow region; these paths are alternately selected by a solenoid-operated sample switch. One path does not alter the sample; the other path passes through the chemical filter region. The chemical filter first removes the carbon dioxide (mass 44) present in the sample, and then oxidizes carbon monoxide (mass 28) to carbon dioxide. Thus, the carbon dioxide measurement is made at mass 44 after removal of whatever carbon dioxide was present in the sample. Carbon dioxide and molecular nitrogen are measured through the unfiltered sample path; the normal concentration of molecular nitrogen in the controlled atmosphere is sufficiently high such that the carbon monoxide contribution to mass 28 from the sample or from fragmentation of carbon dioxide is negligible.

The chemical reaction involved in removal of carbon dioxide from the gas sample produces water. Thus,

a drying agent is inserted between those filter sections which remove carbon dioxide and those which oxidize carbon monoxide. This dryer removes water from the sample passing through the chemically filtered sample path.

Removing water from the sample gas in one sample path is advantageous. In a mass spectrometer system, water in the sample tends to condense on the inner walls of the vacuum housing, and re-evaporate at some subsequent time. This causes the system to have a long "memory" for water, which may mask short-term fluctuations in the partial pressure of water vapor. With the gas sample switched to the filtered channel, no water is present in the sample entering the mass spectrometer. Thus, the spectrometer measures the average level of the water background. When the sample is switched to the unfiltered path, the spectrometer measures water background plus water in the sample. Thus, the sample is "chopped" between the two levels, and an accurate measurement of water vapor present in the sample can be made despite average level variations in water vapor background.

Figure 7 shows a schematic diagram of a Time-of-Flight Mass Spectrometer incorporating a chemical filter and sample switch located at the low-pressure end of the sample inlet capillary tube at a pressure level of 5 mm Hg. The chemicals, deposited on porous suspension media, are packed into a tube in the proper sequence.

Two materials are commercially available for removal of carbon dioxide from a gas sample. Both employ sodium hyroxide as an active agent, and remove carbon dioxide in accordance with the following end reaction:

$$CO_2 + (NaOH)_2 \rightarrow Na_2 CO_3 + H_2O \ .$$

One of these materials, trademarked Ascarite, consists of sodium hyroxide deposited on silica gel. The other is Mikohbite, a proprietary reagent consisting of sodium hyroxide deposited on synthetic mica.

A number of effective drying agents for removing water vapor are available. One which has been successfully used in this application is anhydrous magnesium perchlorate. The reaction with water involves formation of a physical bond:

$$Mg(ClO_4)_2 + 2H_2O \rightarrow Mg(ClO_4)_2 \cdot 2H_2O \ .$$

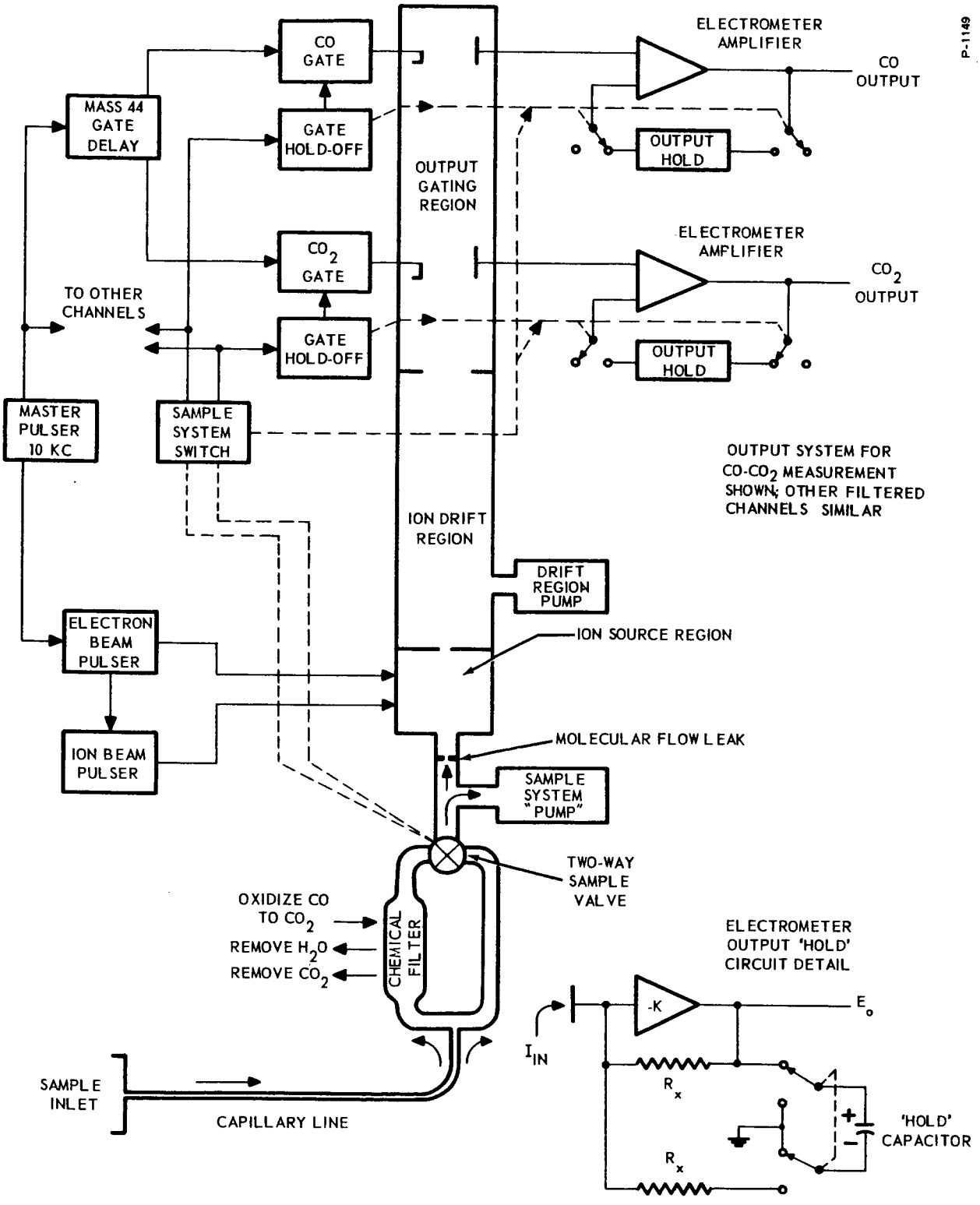

Figure 7 - Chemical Sample System -- Functional Diagram

Oxidation of carbon monoxide in the chemical filter sample system has been accomplished using iodine pentoxide in the following reaction:

$$I_2O_5 + 5CO \rightarrow 5CO_2 + I_2 \ .$$

The sample gas switch which selects either the filtered or unfiltered sample path will be programmed to provide 28 seconds of unfiltered sample flow, followed by a 2-second period during which the gas sample will flow through the filter section. The 28-second period will be sufficient to complete one scan of the mass spectrum of the trace gases. Sampling of the trace gases through the unfiltered channel only eliminates the possibility of erroneous measurements due to unexpected reactions between trace gases and filter elements. This sample programming will provide a carbon monoxide measurement every 28 seconds, with a 94 percent duty cycle for the remaining atmospheric constituents.

4.5.1.2 Plasma Inlet System

Analysis of ionized and neutral particles from a plasma at atmospheric pressure poses problems not ordinarily encountered in mass spectrometer applications. Operating pressures in the spectrometer source and vacuum housing must not exceed 10^{-4} mm Hg due to mean free path considerations and the possibility of arc-over of high potential elements. Therefore the plasma sample system must reduce sample pressure by a factor of at least 10^7. In order to assure that the plasma sample reaching the spectrometer ion source region is representative of actual plasma composition, the plasma sample probe must be designed to eliminate collisions of the incoming particles with the probe walls and with other particles. This is accomplished by dropping pressure very rapidly after the particles have passed through the first inlet orifice in the probe.

The plasma probe is oriented to admit particles having their principal component of velocity at right angles to the mass spectrometer drift tube. Thus, the initial energies of the incoming particles do not affect Time-of-Flight down the drift tube, and maximum mass resolution is preserved. In addition, compensation of the right-angle velocities of the particles by using deflection plates serves as a broad transverse energy filter, so that the energy distribution can be approximately determined.

Energetic particles introduced into the spectrometer ion source region gives rise to the possibility of displaced spectra, with resultant loss of resolution. Elimination of this problem requires special electronic circuitry to time and produce the source pulses, since the conventional spectrometer electronics system is primarily designed for a diffuse gas sample.

A very short sampling time is necessitated by the extreme heat generated by the plasma, plus the rapid spectrometer pressure rise due to sampling from atmospheric pressure. To obtain the best possible analysis during the short sampling period, the standard mass spectrometer electrometer circuits were modified to provide improved response. In addition, special circuitry was developed to synchronize the oscilloscope and the analog output system scanners with the plasma probe shutter.

The following subsections describe in some detail the operation of the right-angle inlet system, the electronics modifications, and the special circuitry developed for plasma analysis.

4.5.1.2.1 Right Angle Inlet System

Figure 8 shows a schematic diagram of the Time-of-Flight Mass Spectrometer as modified for plasma jet analyses. Plasma particles entering the probe are collimated by a series of orifices aligned at right angles to the spectrometer drift tube. Thus, particles entering the spectrometer ion source region have no significant components of velocity to affect their flight times.

The transverse velocities of the incoming plasma ions, vectorially added to the velocities imparted by the ion accelerating grids in the spectrometer source region, result in an ion flight path which is not parallel to the axis of the drift tube. If this trajectory is not corrected, the plasma ions will strike the drift tube walls before reaching the ion detector at the far end of the tube. The diagonal flight path is corrected by electrostatic deflection plates in the drift region. The potentials which must be applied to the deflection plates to achieve maximum output for plasma ions can be used to calculate the average energy of the incoming particles. In addition, the deflection plate potentials which produce maximum output of plasma ions will discriminate against non-energetic ions created in the spectrometer source region. This feature is particularly advantageous in

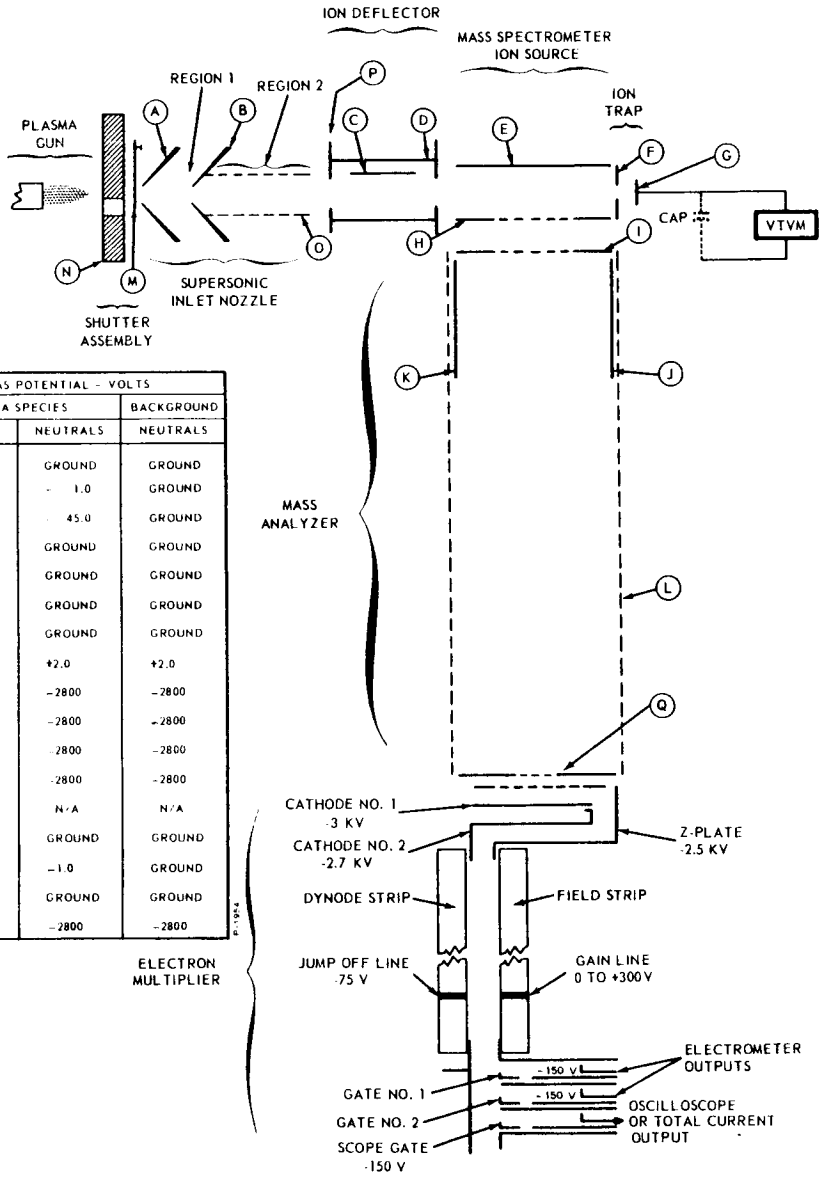

SYMBOL	ELECTRODE NAME	BIAS POTENTIAL - VOLTS		
		PLASMA SPECIES		BACKGROUND
		IONS	NEUTRALS	NEUTRALS
A	FIRST INLET CONE	GROUND	GROUND	GROUND
B	SECOND INLET CONE	- 1.0	- 1.0	GROUND
C	ION DEFLECTOR PLATE	- 45.0	- 45.0	GROUND
D	ION DEFLECTOR PLATE SHIELD	- 45.0	GROUND	GROUND
E	SOURCE BACKING PLATE	- 45.0	GROUND	GROUND
F	ION TRAP SHIELD	- 45.0	GROUND	GROUND
G	ION TRAP ANODE	- 45.0	GROUND	GROUND
H	ION FOCUS GRID	- 43.0	+2.0	+2.0
I	ION ENERGY GRID	-2800	-2800	-2800
J	RIGHT DEFLECTION PLATE	-2800	-2800	-2800
K	LEFT DEFLECTION PLATE	-2975	-2800	-2800
L	DRIFT TUBE LINER	-2800	-2800	-2800
M	FIRST INLET CONE ORIFICE SEAL	N/A	N/A	N/A
N	GRAPHITE SHUTTER	GROUND	GROUND	GROUND
O	PROBE LINER	-1.0	-1.0	GROUND
P	GAS BAFFLE	-45.0	GROUND	GROUND
Q	MULTIPLIER CATHODE SHIELD	-2800	-2800	-2800

Figure 8 - Plasma Mass Spectrometer Design

in the analysis of energetic neutral particles, since it provides a positive means of separating spectrometer background from the neutral particle beam.

The third collimating aperture in the right-angle inlet system is utilized as a gas baffle, which allows differential pumping between Region 2 and the Mass Spectrometer Ion Source. The conductance of the aperture is fixed at about 1 liter per second, with a 100 liter per second mercury diffusion pump on the spectrometer ion source region. Thus the pressure differential between Region 2 and Ion Source Region is approximately 100 to 1, resulting in low spectrometer background pressure.

The first inlet orifice is operated at ground potential. The second orifice is operated at a slight negative potential (about -1 volt), and all other elements in the right-angle inlet and spectrometer source regions are operated at a potential of about -45 volts to improve collimation and decrease the time required to replenish ions in the source region after each spectrum has been initiated. The ion focus grid is operated at a potential of +2 volts with respect to the source backing plate. This small positive potential nullifies fringe field effects from the high potential ion energy grid.

Five precision bias networks are constructed to determine correct biasing for the various inlet elements. Each of these networks is adjustable to produce a potential of ±50 volts across a 10-turn helical potentiometer. Polarity is selected with a switch. The helical potentiometers were equipped with 1000-division counting dials, with a resolution of 50 millivolts per division. Since the current flow to any of the inlet system elements is negligible (with the possible exception of the first inlet orifice, which is grounded), the bias voltages can be read directly from the dial, with an accuracy of 0.1 percent of maximum voltage.

Precision divider networks are provided for both horizontal deflection plates, since the horizontal deflection field compensates for the transverse velocities of the incoming plasma ions. Each horizontal deflection plate potential is adjustable over a range of 500 volts (+250 volts with respect to the ion energy grid and drift tube liner). Deflection potentials are adjustable over 100-volt increments with a 10-turn helical potentiometer. The direct reading dial resolution is 0.1 volt.

The ion deflector plate (C in Figure 8) prevents ions from entering the spectrometer source region after the ion focus pulse has been applied. A negative pulse is applied to the ion deflector plate at the same time that the focus pulse is applied to the ion focus grid (H). All ions not already in the spectrometer source region are prevented from entering this region during the period of the deflector plate pulse.

Potentials applied to all other elements in the inlet system are static, as shown in Figure 8, with the exception of the source backing plate. A negative square pulse is applied to the backing plate at some time subsequent to application of the focus pulse to the ion focus grid. The backing plate pulse reverses the field in the source region, effectively terminating the focus pulse.

At the far end of the source region an ion trap anode (G) is placed to collect those ions which traverse the source region between spectrometer cycles. Total ion current can be measured by connecting and electrometer-type vacuum tube voltmeter to this anode. To improve ion collection efficiency, the ion trap anode can be biased negative with respect to the remaining source elements. An ion trap shield (F) is included in the source structure to prevent source field distortion due to the potential on the trap anode.

4.5.1.2.2 Plasma Shutter

The extreme heat of the plasma would cause rapid erosion of the spectrometer probe tip if continuous exposure were permitted. The first inlet orifice is machined to a radius of 0.001 inch from inner to outer surface; since the angle between the inner and outer surfaces is only 6 degrees, the inlet probe tip region is very fragile. Exposure of the probe tip to the plasma is limited to a fraction of a second by a rotary graphite shutter driven by a variable speed motor. A fixed slot in the shutter exposes the probe tip to the plasma; time of exposure is governed by rpm adjustment of the variable speed motor which makes but one revolution.

The tip of the probe is normally closed by a light rubber-coated metal shutter which serves as a vacuum seal. A trip lever on the rotating graphite shutter flips the metal shutter out of the way just before the graphite shutter opens. After the graphite shutter slot has passed by, a second trip lever swings the metal shutter back to its initial position, sealing the probe tip.

Sealing of the probe tip between plasma analyses allows use of a vacuum ballast tank in the region between the first and second inlet orifices. The 300-liter ballast tank serves as a short-term infinite pump on this region during the period that the plasma probe tip is uncovered. When the tip is resealed, the ballast tank is pumped out by a 7 liter per second rotary forepump connected into the ballast tank. Approximately 15 minutes is required to reach an ultimate pressure of about 5 microns of mercury.

The graphite shutter's rest position is with the shutter slot oriented about 180 degrees away from the plasma probe tip. This allows sufficient time for the shutter drive motor to reach operating speed before the shutter slot uncovers the probe tip. The motor is started with a pushbutton switch which energizes a motor-starting relay. The relay latches ON through one of its own contacts. When the shutter has completed one revolution, it trips a microswitch in the relay latch circuit, dropping out the relay and stopping the motor. Shutter inertia is sufficient to coast past the motor stop microswitch, so that the shutter will recycle when the start pushbutton is again actuated.

During the time immediately preceding a plasma probe shutter cycle, the mass spectrometer is fully operative at background pressure. All circuits in the ion source and output system are being triggered at the normal repetition rate of 10,000 cycles per second. This poses a problem of synchronizing the oscilloscope display and the analog system scanners with the plasma probe shutter.

If the oscilloscope display is permitted to be ON prior to a run, the sweep will be triggered at the 10 Kc repetition rate of the spectrometer, producing a brilliant base-line which will fog scope camera film and obscure small signals present during the brief period of plasma analysis. There are two ways to eliminate this difficulty: one, the oscilloscope z-axis can be blanked except when the plasma shutter is open, or two, the sweep trigger to the oscilloscope can be interrupted except during the shutter-open period. The second method was used in these experiments, since it does not require modification of the oscilloscope. Unblanking of the oscilloscope would require tying into the d-c coupled z-axis modulation system, which is not available as a panel connection.

The analog system scanners also require synchronization with the plasma probe shutter. Since the probe exposure time is short, the scanning gates must be initially positioned very close to the mass peaks which will be scanned during the probe exposure time. Moreover, the scan rate must be fairly fast to ensure that the scanning gate actually sweeps over the mass peak during the probe exposure time. These factors combine to require precise synchronization of the scanners with the plasma probe shutter.

An obvious way out of this difficulty would seem to be to eliminate scanning, and to fix the gates on the desired mass peaks. This approach is impractical, however, because of a Time-of-Flight difference between the plasma particles and the non-energetic particles of the same mass; this difference is due to the difference in deflection plate potentials. Thus the gate locations for the non-energetic particle spectrum cannot be used with the plasma spectrum, and plasma exposure times are too short to allow positioning of the gates on the plasma spectrum itself. Any plasma mass peak output obtained with a fixed gate would be subject to uncertainty because of possible gate misalignment. The normal plasma sampling period of about 120 milliseconds makes it impossible to check gate alignment during this period. Longer sample periods are impractical because of the possibility of damaging the probe, and because of the rapid pressure rise in the spectrometer.

Synchronization of the oscilloscope and the analog system scanners with the plasma probe shutter is accomplished with an electronic gate circuit, triggered by a microswitch actuated by the rotating shutter. The microswitch is positioned so that it is actuated immediately prior to exposure of the plasma probe.

The microswitch triggers a monostable multivibrator which serves to produce a "clean" trigger waveform, since the microswitch opening and closing is characterized by multiple makes and breaks over a period of several milliseconds. The monostable multivibrator output triggers a phantastron, which produces a positive gate waveform of precise duration. The duration of the gate waveform is adjustable from 5 milliseconds to 5 seconds, in three ranges of one decade each.

The positive gate waveform is applied to one input of a dual input AND gate. The other AND gate input is the

spectrometer master pulse. When the phantastron gate waveform is present, master pulses are passed through the AND gate to trigger the oscilloscope. Absence of the phantastron waveform closes the AND gate so that master pulses are prevented from triggering the oscilloscope.

The positive gate waveform from the phantastron is also used to start the analog scanners. The scan control voltage for each scanner is generated by an operational integrator. When the phantastron is in the OFF state, the input to the integrator is zero, with consequent zero output. The positive gate waveform from the phantastron appears as a step function at the integrator input. The integral of the step function is a linear ramp voltage which serves to sweep the output system gates through their respective portions of the mass spectrum. The quiescent, or zero, output of the integrators can be adjusted to any desired level so that the output system gates are initially positioned adjacent to the mass peaks to be scanned.

4.5.1.3 Laser

The laser beam inlet system, as with other solid analysis inlet systems, provides the means necessary to change the solid sample to be analyzed into a gaseous form necessary for ionization and subsequent analysis. In operation, the laser beam, focused to obtain a high energy density, would be directed toward the surface of the material to be analyzed as shown in Figure 9. The energy carried by the laser beam would be partially absorbed by the material and increase its temperature. When the quantity of energy, E, absorbed by the sample is sufficient, the sample can be elevated to its vaporization temperature. An energy E is required to be absorbed from the laser beam to effect vaporization:

$$Q = \frac{E\ (\text{Joule})}{4.18\ \text{Joule/cal}} = \left\{ m \left[c_1 (T_\ell - T) + c_2 (T_g - T_\ell) + c_3 (T_f - T_g) \right] + \ell_1 + \ell_2 \right\} \quad (43)$$

where

$$Q = \frac{\text{Laser energy absorbed (Joules)}}{4.18} \left(\frac{\text{cal}}{\text{Joule}} \right)$$

m = Soil sample - gm

c_1 = Specific heat of solid phase - $\frac{\text{cal}}{\text{gm } ^\circ\text{K}}$

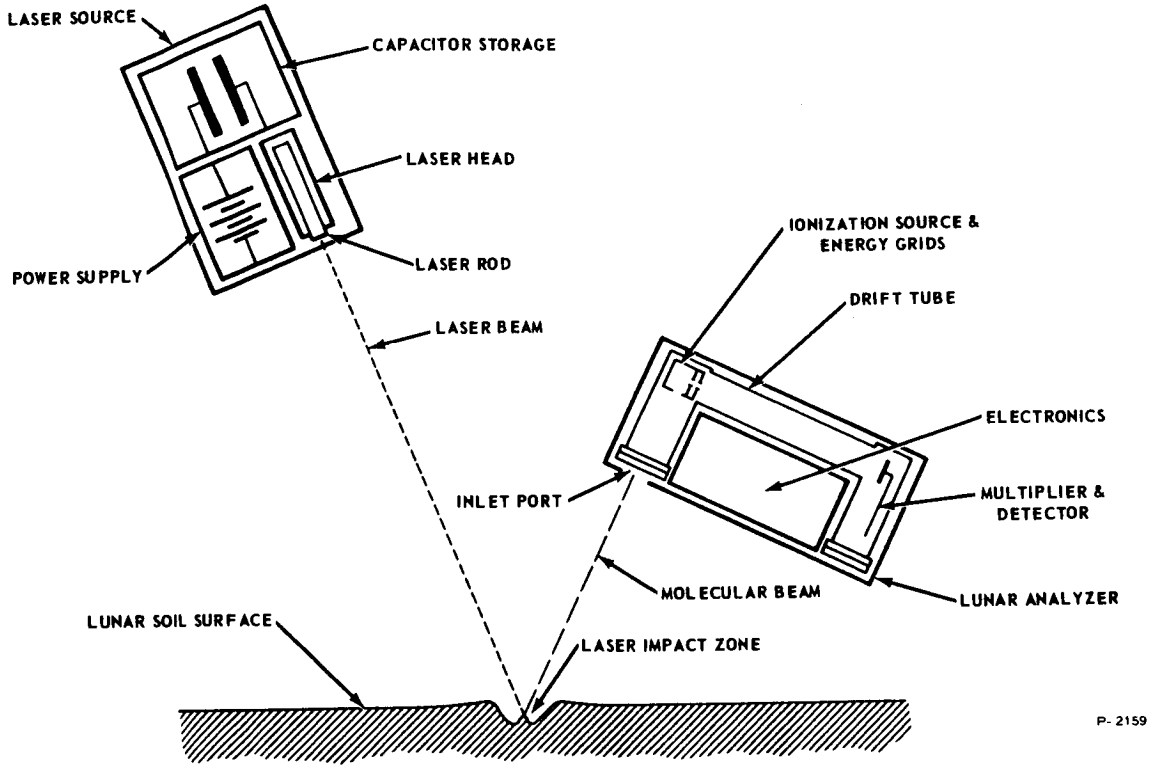

Figure 9 - Lunar Soil Analyzer

c_2 = Specific heat of liquid phase - $\frac{\text{cal}}{\text{gm } ^\circ\text{K}}$

c_3 = Specific heat of gas phase - $\frac{\text{cal}}{\text{gm } ^\circ\text{K}}$

ℓ_1 = Latent heat of fusion - $\frac{\text{cal}}{\text{gm}}$

ℓ_2 = Latent heat of vaporization - $\frac{\text{cal}}{\text{gm}}$

T_1 = Sample temperature

T_ℓ = Solid - liquid equilibrium temperature - °K

T_g = Liquid - gas equilibrium temperature - °K

T_f = Final temperature - °K

A laser beam emanating from a lasing rod and appropriately focused by means of a lens placed 10 cm away on an iron sample 40 cm from the lens can elevate the sample (as large as 1.2 milligrams) to the 3130°K required for vaporization, if it can transmit only 11 Joules of energy to the sample. The high temperature gas so formed can then effuse from the laser impact area. The effusing paticles will follow the cosine velocity distribution law of Maxwell-Boltzmann. The process can be likened to that of simple molecular flow from a gas at temperature T°K through a circular hole in a thin-walled chamber. The flow will follow this model if the background pressure is less than 10^{-6} - 10^{-8} mm Hg. This is necessary for free-molecular flow. If the background gases were higher than this limit the effusion processes would become a more complicated diffusion problem. If the molecular flow from the impact zone is sufficient to cause a large number N (molecules/sec) to enter the ionization region of the mass spectrometer, a mass analysis of the impact zone effusate can be carried out. The number of N molecules per second effusing from the impact area which have velocities so directed such that they lie within a solid angle $d\omega$ which intersects the mass spectrometer inlet port can written as:

$$N = \int_0^{\infty} \int_0^{\theta_1 = \tan^{-1}\left(\frac{r'}{r}\right)} \int_0^{2\pi} \frac{A}{4\pi} \, v \, dn_v \sin\theta \cos\theta \, d\theta \, d\phi \qquad (44)$$

where

$A_1 = \pi (r')^2$ inlet port area

r' = inlet port radius

r = distance from impact area to inlet port

v = velocity of effusing particles

θ = effusing angle measured from normal to surface

ϕ = effusing angle

$$dn_v = \frac{4M}{\pi \, 1/2} \left[\frac{m}{2kT}\right]^{3/2} v^2 e^{-\left(\frac{mv^2}{2kT}\right)} dv$$

Thus,

$$N = \eta A\left[\frac{2kT}{\pi m}\right]^{1/2}\left(\frac{r'^2}{r'^2 + r^2}\right) \text{ molecules/sec} \qquad (45)$$

For an iron sample assumed to have absorbed sufficient energy to reach it's vaporization temperature and some assumed system parameters:

$r' = 1$

$r = 40$ cm

$\eta = 3.54 \times 10^{18}$ molecules/cm^3

$A = 1.63 \times 10^{-4}$ cm^2

$T = 3130°K$

$k = 1.38 \times 10^{-16}$ erg/°K

$m = 9.32 \times 10^{-23}$ gm

$N = 1.9 \times 10^{16}$ molecules/sec

Simularly the average velocity can be determined for these iron particles:

$$\bar{v} = 3/8\left(\frac{2\pi k T}{m}\right)^{1/2} \text{ cm/sec} \qquad (46)$$

An expression for the average effusing particle density at the inlet of the mass spectrometer is

$$n_1 = \frac{N}{A \cdot \bar{v}} \frac{\text{particles}}{\text{cm}^3} . \qquad (47)$$

Again for iron and possible laser beam parameters

$$n_1 = 1 \times 10^{11} \text{ particles/cm}^3 . \qquad (48)$$

This density is more than adequate to obtain the minimal ion per seconds required at the stainless steel cathode to provide an observable output for a given mass peak. It remains to be verified whether the laser beam sampling technique can be accomplished in a representative manner. However, it is only necessary to perform experiments to provide the transfer functions between a given compound and its eventual mass

spectrogram. Such "nametags" logged for each of the anticipated samples would serve to identify these samples in a future analysis. Admittedly, such mass spectrograms can become exceedingly difficult if not impossible to analyze if complex samples are encountered.

4.5.1.4 Knudsen Cell

The Bendix Knudsen Cell Sample System has been designed for use with the Bendix Time-of-Flight Mass Spectrometer to both provide a method of quantitatively analyzing many materials which have negligible vapor pressure at room temperature, and provide the only reliable method of experimental investigation where thermodynamic equilibrium is required at elevated temperature.

The Bendix Knudsen Cell Sample System employs a combination of electron bombardment and radiation heating and can be operated at temperatures to about 2700°K. The complete equipment consists of the furnace assembly, molecular beam shutter assembly, a special replacement header, and a power supply.

The furnace assembly includes the Knudsen cell crucible, supporting tower, heat shields, filament assembly, heat sink, and vacuum housing. The molecular beam shutter provides a convenient method of interrupting the molecular beam effusing from the Knudsen cell. The replacement header provides an optical port for use in measuring the temperature of the Knudsen cell with a radiation pyrometer, including a second shutter which shields the inside surface of the optical port when temperature measurements are not being made, and a mounting for the molecular beam shutter actuating lever mechanical vacuum feedthrough. The power supply provides controllable operating potentials for the equipment.

A schematic diagram of the Bendix Knudsen Cell Sample System in place in the source region of a normal Bendix Time-of-Flight Mass Spectrometer is shown in Figure 10. The effusate from the Knudsen cell is collimated by the apertures in the heat sink and shield assemblies and the ion source hardware of the mass spectrometer. The resulting molecular beam upon entering the ionizing region of the mass spectrometer is analyzed 10,000 times a second. The molecular beam shutter provides a simple method of interrupting the effusing molecular beam; mass peaks whose amplitides are significantly reduced by interrupting the beam are verified as being components of the effusate.

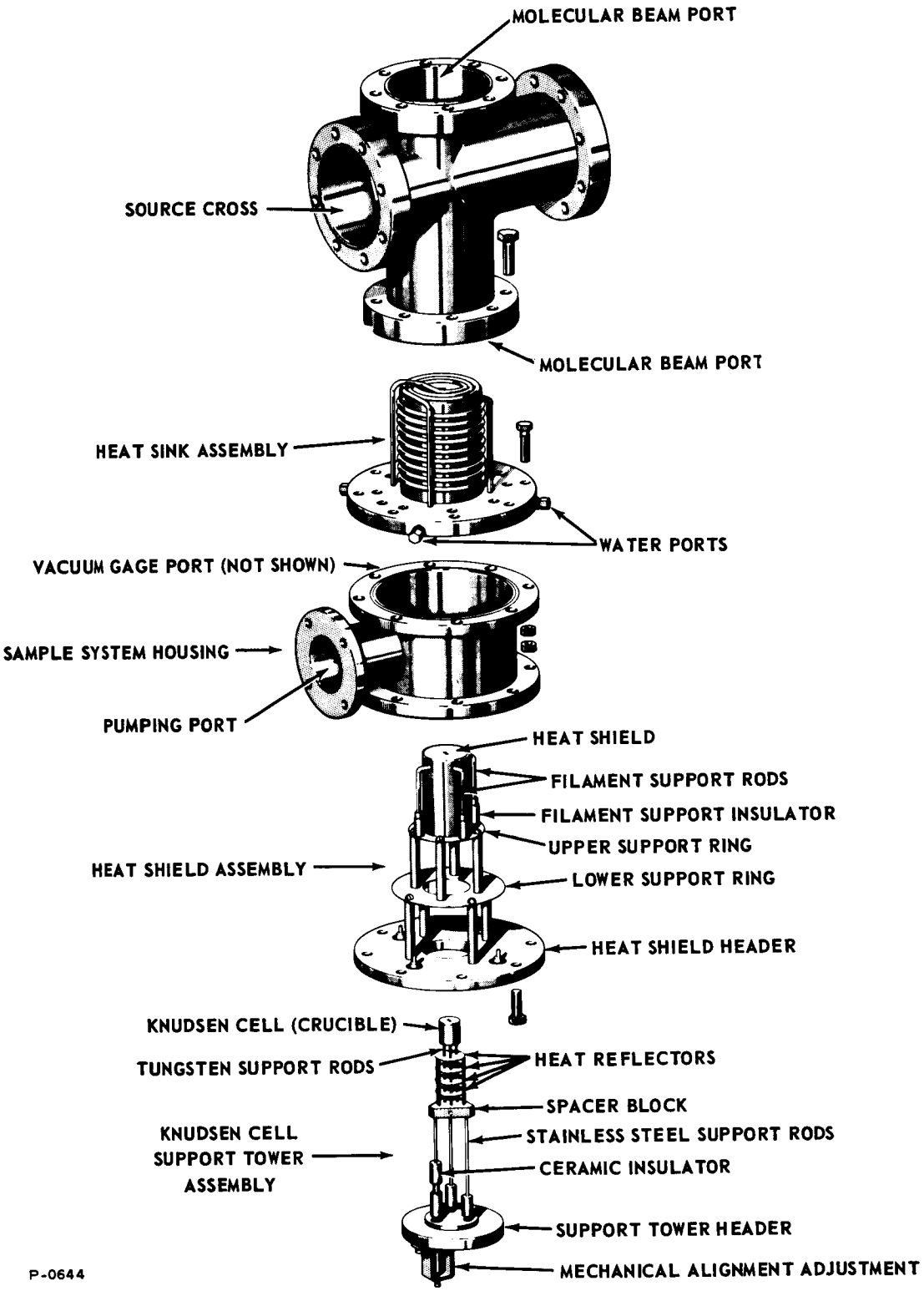

Figure 10 - Knudsen Cell Analyzer

The Bendix Knudsen Cell Sample System combines each of the characteristics of ease of operation, versatility of application, and simplified maintenance without sacrificing any of the operational capability the sample system or the mass spectrometer system.

4.5.1.5 Heated Filament Inlet System

The Hot Filament Sample Inlet System consists of a ball-valve vacuum lock, a sliding piston sample probe and an electrical driver unit. The sample probe is simply inserted into the mass spectrometer vacuum system through the vacuum lock. A tantalum ribbon filament which holds and heats the sample is held by two "quick change" supports which permit rapid change of the ribbon after each sample run. This filament can hold any liquid or solid sample to be evaporated for introduction into the spectrometer. The ribbon filament is mounted so that the sample is vaporized about 4 centimeters from the ionizing region of the mass spectrometer. The sample temperature is indicated to within ± 25°C by a calibrated meter which is mounted on the 5-1/4 inch front panel of the electrical driver unit.

The amount of sample required depends on the vapor pressure, length of time required for analysis, spectrum intensity desired, etc., but in most cases less than 10 milligrams will suffice.

Use of this sample system significantly reduces the residual sample in the mass spectrometer. Total vaporization sampling of many organic compounds produces severe instrument contamination; ten hours or more is sometimes required to remove 99 percent of the residue. The Hot Filament Sample Inlet System lowers this residue pump out time by a factor of ten to twenty.

The Hot Filament Sample Inlet System is constructed mostly of stainless steel. Teflon ball-valve seats and buna-n rubber "O" rings seals are used. The unit can be baked at temperatures up to 100°C. The Hot Filament Sample Inlet System can be constructed in a size compatible with any of the Bendix Time-of-Flight Mass Spectrometers or gas analyzers; however, a standard version is shown in Figure 11.

4.5.1.6 Sputtering

To analyze a solid material requires more complex analytical techniques than gaseous analysis. To obtain a sample

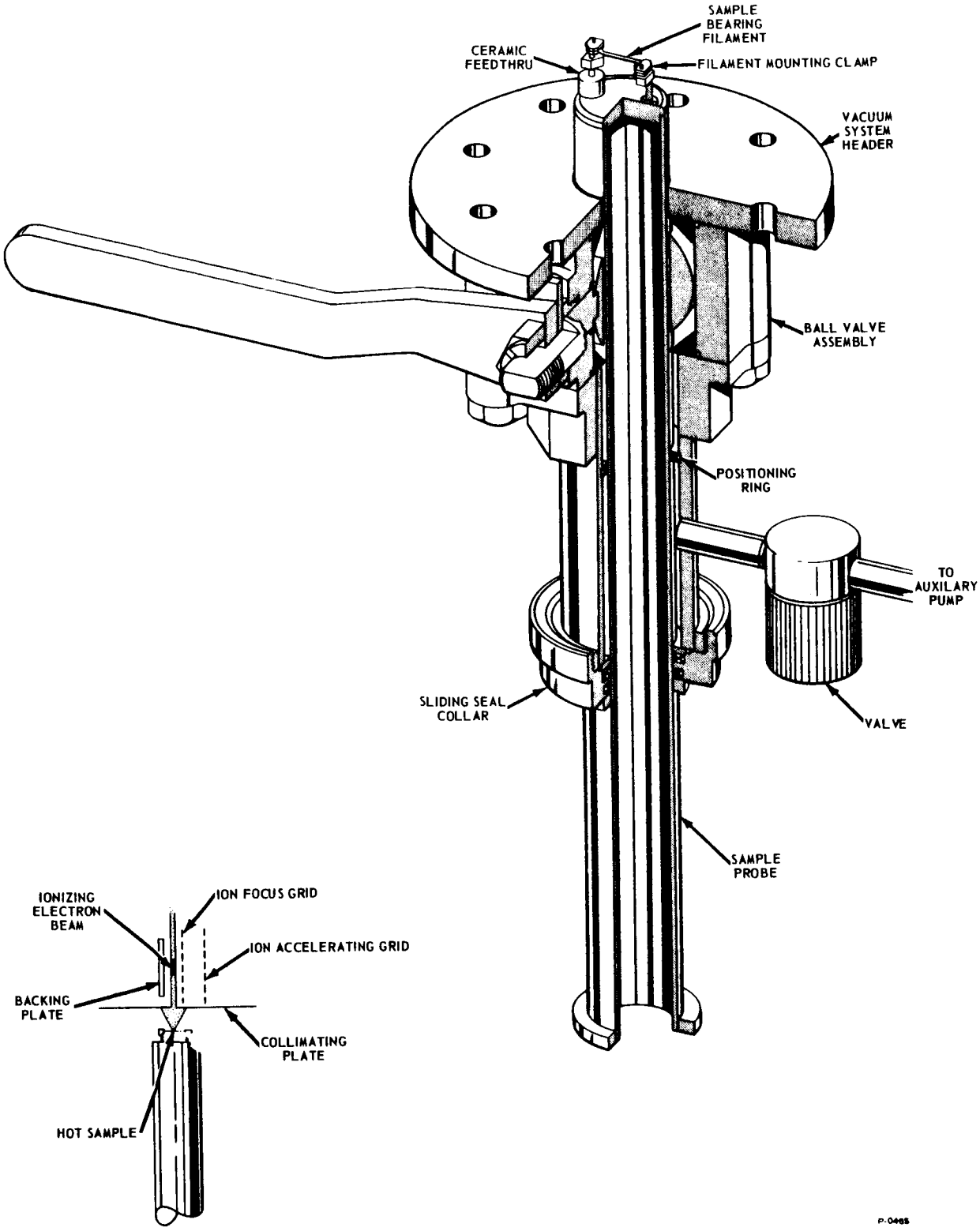

Figure 11 - The Bendix Hot Filament Sample Inlet System, Model B-106

of only the surface layer of a solid without contaminating the sample with the sampling system requires special care. One unusually effective way to perform such an analysis is to use the technique of "sputtering." It is possible for atoms of a surface to be bombarded by energetic gaseous ions and thereby vaporized or released from their surface bonds. This process is called "sputtering." After the vaporization of the surface atoms, it is a comparatively straightforward matter to inject these ions into a mass spectrometer where they can be analyzed according to their atomic mass. Analytical instruments based on the phenomenon of surface ionization coupled with an appropriate mass spectrometer have been developed.

The substance to be analyzed is mounted on a metallic target plate and introduced into a chamber which is subsequently evacuated to a pressure of about 10^{-6} mm Hg. A low voltage arc is then initiated in the ion source which is maintained in an atmosphere at about 0.01 millimeter of mercury of a noble gas. The arc is strongly constricted by an axial magnetic field so that a very dense plasma is created along the axis near the anode. Through a pinhole in the anode, typically 0.010 inch diameter, an intense beam of ions can be extracted and accelerated by a conically shaped electrode. In this manner, an ion beam of several milliamperes of small cross-sectional area can be obtained. The beam is deflected onto the target electrostatically and bombards it at an oblique angle of incidence; this causes a higher rate of sputtering than normal impact. Because the bombarding beam consists of ions from a chemically inert gas, such as argon, no chemical reaction occurs and the target is not contaminated. Once the ions have been formed they are introduced into the mass spectrometer where they are subsequently analyzed. The ion probe described in subsection 4.5.1.2 can be used to introduce the ions into the spectrometer for analysis. Such an instrument would be invaluable for measuring the surface dust layer anticipated on the surface of the moon.

Successful analysis of many samples has demonstrated the versatility of the instrument as an analytical tool for conducting as well as for insulating surface. (Emission of secondary surface electrons prevents build-up of a positive charge on the bombarded surface which thus essentially remains unchanged.)

In view of the high efficiency of ion production (approximately 1 sputtered atom per 300 ev Hg ion) non-destructive chemical analysis of film surfaces or bulk material requires as little as 10^{-14} grams of material sputtered.

4.5.1.7 Electron Beam Sputtering

An electron beam, much like that normally employed for "Electron Beam Welding," can be utilized to bombard the surface of a material to produce sputtering. The electrons are generated by a hot tungsten cathode and then accelerated electrostatically to high energies in a vacuum. These energetic electrons are then allowed to bombard the material to be analyzed. The resultant ions which are sputtered by the surface can then be introduced into a mass spectrometer to be analyzed. The technique is identical to that described in subsection 4.5.1.6 for sputtering. Again the process is advantageous since contamination of the sample by the sampling process is eliminated.

4.5.2 Ion Sources

Regardless of the condition of the sample prior to its arrival at the ion source region, solid, liquid, or gas, an appropriate inlet system must convert it to the gaseous form so that the sample can be transported. Once the neutral atoms or molecules reach the ion source region the components are ionized singly, doubly, or triply in relative proportions depending upon each atom's ionization probability and each molecule's characteristic cracking pattern.

In the case of sampling an ionic gas the need is no longer present for an ion source. However, special inlet systems are required for ion analysis. Care must be taken to insure representative sampling and to prevent the loss of too large a number of ions to the walls of the spectrometer.

4.5.2.1 Electron Beam Ion Source

The incoming sample gas is conducted directly into the enclosed ion source region via a teflon tube which butts against a stainless steel tube. The stainless tube is flattened where it is bolted to the interior source housing.

The sample gas is ionized by a pulsed electron beam that crosses through the ionization region between the source mounting base and ion focus grid. The electron beam is pulsed on at the spectrometer repetition rate (10 - 100 Kc); the pulse duration is approximately 0.25 microsecond. The electron gun structure is composed of a filament, control grid, electron energy grid, electron trap,

trap shield, and electron beam collimating magnet assembly. The energy grid, mounting pedestal, and trap shield are all at ground potential so that the electron energy and trap anode fields do not penetrate the ion source region. The ion focus grid is biased positive for optimum electron beam trajectory.

The ionizing electron energy is attained by biasing the filament and control grid negative with respect to the electron energy grid, and can be adjusted to any value between 0 and 100 volts. The control grid is biased to cut off the electron beam except during the ionizing pulse period. Collimating magnets and a slit in the electron energy grid serve to focus the ionizing electrons into a well-defined beam that passes through a slit in the trap shield upon leaving the ionizing region. The electrons are collected on the trap anode, which is biased at about +150 volts.

Immediately after the electron beam pulse, the positive ions which have been formed are drawn from the ion source region by a negative pulse on the ion focus grid. In the region between the ion focus grid and ion energy grid, the ions are accelerated to approximately 1200 volts energy. The ions then pass into the field-free flight region with velocities proportional to

$$\sqrt{\frac{e}{M}} \quad .$$

In transit down the flight tube the ions separate into sharply defined bunches according to their e/M ratios. These successive bunches are detected at the magnetic electron multiplier cathode (described in subsection 4.5.3).

A compensating magnet assembly clamped around the vacuum housing near the ion source region provides a magnetic field to correct ion trajectories, which are initially curved by the electron beam collimating magnets.

4.5.2.2 Electron Beam Ion Source Construction

The entire enclosed ion source structure is assembled on the source mount pedestal which bolts to the source header. The ion focus grid is mounted on four sapphire rods inserted into holes in the pedestal; the correct spacing between focus grid and pedestal is maintained by sapphire spacers slipped over the sapphire

rods. The ion energy grid is also supported by the sapphire rods, and is separated from the focus grid by sapphire spacers. Four metal caps are slipped over the sapphire rods where they project through the energy grid. A hold-down stack is fitted over the caps as a retainer. This plate is linked to two feedthrough connectors in the source header; tension is maintained by two coil springs. These springs also serve to conduct the ion energy potential (-1250 V) to the hold-down stack and energy grid.

The ion focus grid opening has a diameter of about 0.1 inch; it serves to constrict gas flow from the ion source region so that a differential pressure is maintained between the source region and the remainder of the mass spectrometer vacuum housing. This permits operation of the source at higher pressures than would be otherwise possible. The sample is introduced into an extremely small volume at a relatively high pressure, which minimizes the sampling time constant.

The electron beam filament and control grid are assembled on a block bolted to the source mounting pedestal. The electron trap anode and trap shield assembly are located inside the ion source housing and secured by two screws. Synthetic mica spacers insulate the anode and shield from each other and from the screws.

The electron beam collimating magnet assembly is clamped around the vacuum housing at the ion source. The magnetic circuit is shown in Figure 12.

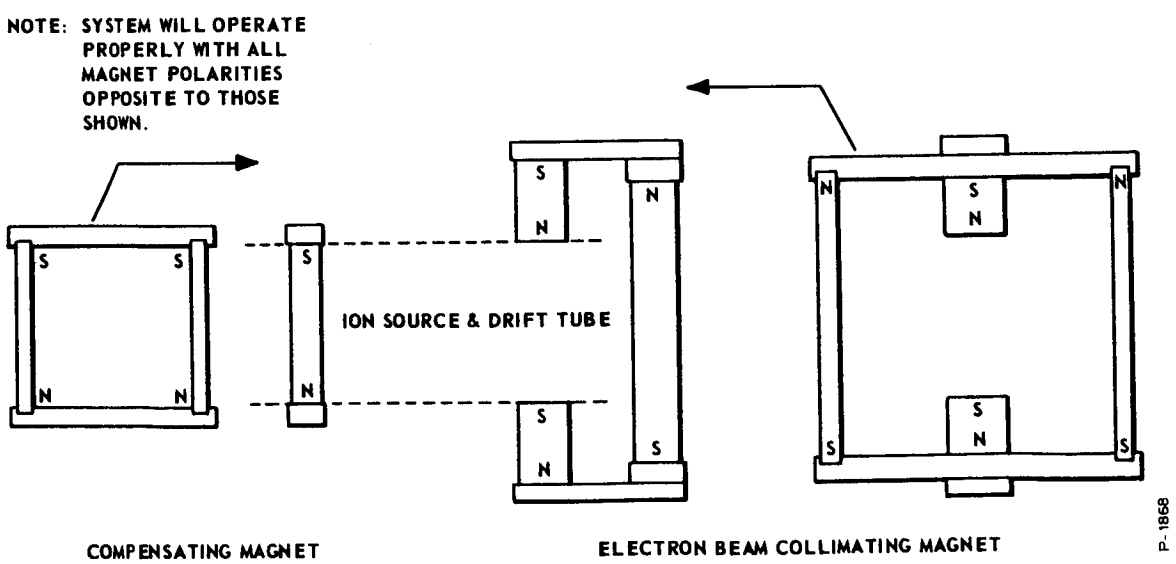

Figure 12 - Ion Source Magnet Orientation

4.5.2.3 Spark Ion Source

The sample to be analyzed with a Spark Source Spectrometer System is placed in a hole drilled axially into the grounded electrode. Vaporization of the sample material by the high intensity spark produces ions that migrate outward from the spark region. The energy distribution of these ions is a combination of thermal energies plus energies due to the intense electrical fields resulting from the high voltage applied to the spark electrodes. A segment of the ions produced in the spark region will have energies directed such that they pass through the two adjustable collimating slits, thus forming an ion beam. This ion path is essentially field-free from collimating slit No. 1 to the spectrometer source region between the backing plate and the ion focus grid. Ions traverse this path by virtue of the energies attained in the spark source region. Figure 13 shows a Spark Source System.

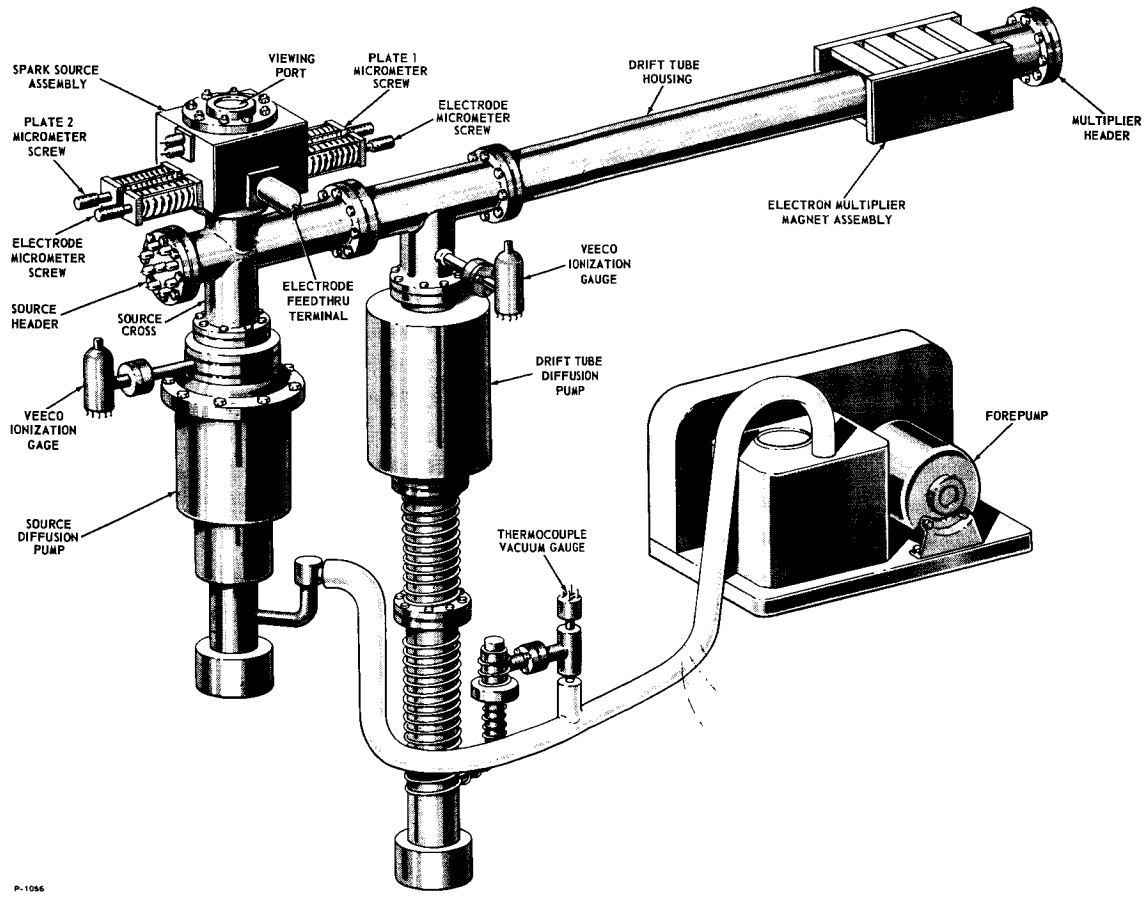

Figure 13 - Physical System of the Spark-Source Time-of-Flight Mass Spectrometer

To initiate each spectrum, ions are ejected from the spectrometer ion source region by a negative pulse on the ion focus grid. From the time of application of the ion focus pulse, the spark source spectrometer functions in the same manner as the conventional Time-of-Flight Mass Spectrometer, with the exception that the vertical deflection plates must be adjusted to compensate for the transverse energies of ions originating in the spark source.

A variable delay period must be inserted between the spark trigger pulse and the ion focus pulse to allow for ion transit time between the spark region and the spectrometer ion source region. The relationship between mass and energy of the ions created in the spark source is not completely known. If the energy is assumed to be mass independent, ions produced by the vacuum spark will arrive in the spectrometer source region in order of increasing mass. In effect, the system then becomes two Time-of-Flight Mass Spectrometers in series. A complete mass spectrum cannot be obtained for one setting of the operating parameters, since only those ions which are in the spectrometer source region when the ion focus pulse is applied will be detected.

4.5.2.3.1 Mass Spectrometer Analyzer

The mass spectrometer analyzer shown in Figure 14 is a Bendix Model 11 research-type Time-of-Flight instrument equipped, in addition to the oscilloscope output, with a two-channel gated output system. A gas baffle (see Figure 15) was inserted between the ion source region and the drift tube region, so that drift pressure was semi-independent of pressure in the spark source. The drift tube and multiplier regions of the vacuum housing were pumped by a CEC 200 liter per second mercury diffusion pump, backed by a Precision 150 forepump. Pressure at the CEC pump inlet was monitored by a Veeco ionization gage.

4.5.2.3.2 Mass Spectrometer Electronics

The electronic system includes the timing and pulse generation circuitry, to provide appropriately timed and shaped pulses for application to various elements of the mass spectrometer analyzer; an output system, to provide means for observing and recording the mass intensity information provided by the spectrometer; a high-voltage spark generator; and the power supplies

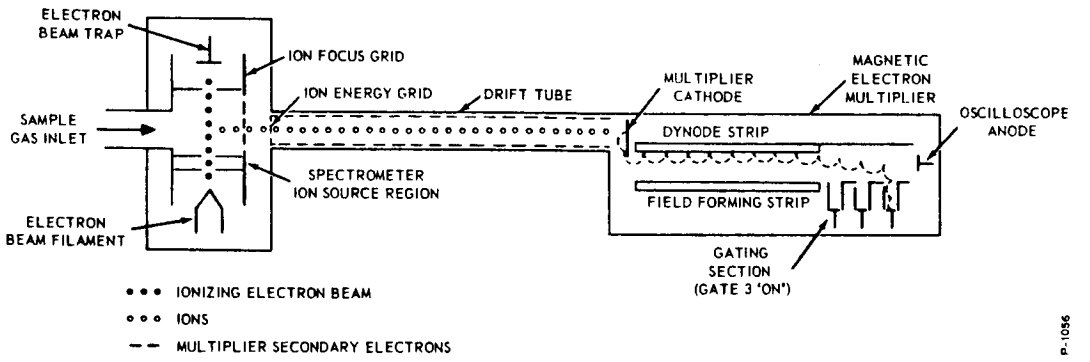

Figure 14 - Basic Time-of-Flight Mass Spectrometer Design

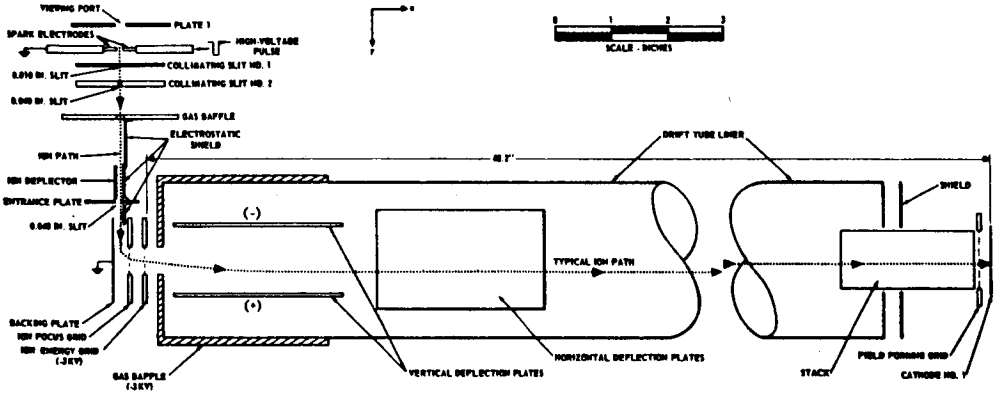

Figure 15 - Schematic Diagram of the Spark-Source Time-of-Flight Mass Spectrometer

necessary to provide the required operating potentials to the various electronic circuits.

A large portion of the electronic circuitry used with the Spark Source Spectrometer was developed especially for this application.

4.5.2.4 Arc Ion Source

An arc source has a potential of the order of 100 volts which pulls electrons out from a hot filament to an anode,

ionizing the gas in between. A perforated cathode placed in the discharge plasma so produced attracts positive ions, some of which pass through the hole and are available for acceleration. The operating pressure of a low-voltage arc is usually about 10^{-2} mm Hg, considerably lower than a glow-discharge, and the cathode potential is usually a few hundred volts. In view of this low cathode potential and the high ion density of the arc plasma (usually several orders of magnitude greater than the ion density of a glow discharge plasma), the cathode sheath, across which practically the entire cathode drop occurs, is generally very small (a fraction of a millimeter) -- much smaller than the mean free path of the electrons in the gas so that very few positive ions are produced in the sheath. Practically all the ions that pass through the hole in the cathode, therefore, have energies corresponding to the full cathode potential drop and so can be used to produce homogeneous ion beams of any desired energy. These types of low-voltage arc sources have been developed for the production of high ion currents.

4.5.2.4.1 Capillary Arc Source

The capillary arc provides a convenient source for the production of intense positive ion beams. One type of capillary arc, due to Tuve and others consists of a hole a few mm in diameter and a few cm long drilled in a metal block. At either end of the capillary, the hole is opened out to a few cm in diameter to accommodate a hot filament and an anode. Electrons drawn from the filament toward the anode ionize the gas in the capillary and an arc is struck, the ion density within the capillary being particularly high. The pressure in the capillary is of the order of 0.1 mm Hg. The arc body is usually allowed to float at some potential intermediate between that of the filament and the anode. Ions produced in the capillary are drawn out through the hole by a negative potential applied to electrode and then focused into a beam to an electrode.

4.5.2.5 Ultraviolet Ion Source

Ultraviolet light (2000-3800Å) falling upon a gas or vapor can cause some electrons to move to a higher energy level. If the energy of the incoming photons is the same, or very nearly the same, as the energy difference between two possible energy levels of the electron in the atom then the energy of the photon can be absorbed by the atom. The subsequent decay of this electron to a lower level or

its former level produces radiation of a particular frequency. This is normally called resonance radiation. For this effect to occur the incoming photon must have a frequency (energy) near that of the secondary emission decay frequency. If the photon's energy (frequency) is increased the resonance radiation ceases. This illustrates that the photon's energy-absorption characteristics are very particular. The photon must give up all or none of its energy.

If however, the incoming photon's energy is much greater than that required for resonance radiation and is sufficient to raise the internal electrons from the uppermost filled ("normal") level to the zero or escape level, then ionization occurs and the effect is called "photoelectric emission." Thus, it is possible to produce ions by means of ultraviolet radiation. Such a means can be employed as an ion source for spectrometric analysis.

4.5.3 Time-of-Flight Analyzer and Detector

Operating Principles of the Basic Time-of-Flight Mass Spectrometer

A brief exposition of the fundamental operating principles of the Time-of-Flight Mass Spectrometer is presented as background material to facilitate description of the special techniques developed for the Spark Source application.

A complete Time-of-Flight Mass Spectrometer installation is comprised of a sample system, a mass analyzer, and an output system. The function of the sample system is to introduce the sample into the spectrometer ion source region, in gaseous form, and at a pressure such that the mean free path of the particles is much greater than the dimensions of the analyzer region. The mass analyzer section operates on the gas sample to separate its constituent particles as a function of m/e ratio. The discrete bunches of ions thus formed are time-focused so that they impinge on a detector in order of increasing m/e ratio. The detector is a magnetic electron multiplier; the ion bunches impinging on the multiplier cathode produce secondary electrons in proportion to the number of ions. After multiplication, the resulting electron bunches pass into a selective gating system which permits measurement of the average electron current corresponding to selected m/e peaks, in addition to presentation on the scope anode of that portion of the mass spectrum not gated by preceding channels.

Ordinarily, a sample gas is admitted into the spectrometer ion source region by random diffusion of particles due to thermal energies. The particles are in neutral form and must be ionized before mass separation can take place. Figure 15 shows a schematic diagram of the fundamental Time-of-Flight Mass Spectrometer. The diffuse gas sample is ionized by a pulsed electron beam which traverses the ion source region. The resulting positive ions are ejected from the source region by a negative pulse applied to the ion focus grid. In the region between the ion focus grid and ion energy grid, the ions are accelerated to a common energy level. Thus, assuming that each particle is singly ionized, they emerge from the accelerating region with velocities proportional to $1/\sqrt{M}$. Beyond the ion energy grid is a field-free drift region at ion energy potential. In this region, the ions separate into bunches in accordance with m/e ratio, the separation increasing as the discrete bunches progress through the drift region.

At the far end of the drift region, the ion pulses impinge on the magnetic electron multiplier cathode. The group of ions of lowest m/e ratio arrives first, followed in succession by the heavier masses. As each group of ions strikes the cathode, a proportionate number of secondary electrons is emitted and multiplied through the continuous dynode-type magnetic electron multiplier.

The multiplier can be constructed with a multi-channel output gating assembly, which permits the multiplier output pulse corresponding to a selected mass peak to be gated onto a selected anode. All other mass peaks in the spectrum bypass this anode, but other mass peaks can be gated onto the anodes of other channels. Multiplier output gating is accomplished by timing a gate pulse to occur simultaneously with the arrival of the multiplier output pulse corresponding to the desired mass peak. The gate pulse is applied to a gating electrode in the selected channel, so that the multiplier output is deflected onto the associated anode only during the pulse period. Any spectral peaks not gated into one of the output channels will impinge on an ungated anode at the end of the multiplier gating region. If none of the spectral peaks are gated, then the entire mass spectrum appears as a succession of pulses on the last anode.

A complete spectrum appears in a period of a few microseconds and the entire cycle repeated at a high repetition rate, ordinarily 10,000 cycles per second. Thus, the real-time spectrum is generally displayed on an oscilloscope. However, the complete spectrum can be

displayed, using a scanning technique, on slow-response recorders. The gating pulse for one output channel is timed to occur slightly later in each successive spectrum. Thus the pulse can be made to sweep through the spectrum at a rate well within the response capability of the recorder. The entire spectrum appears at the sweeping gate anode, with a repetition frequency corresponding to the sweep rate.

Magnetic Electron Multiplier

The Magnetic Electron Multiplier, shown in Figure 16, is a combined ion detector and high gain, wide bandwidth, crossed field electron multiplier which incorporates an output gating feature. It is located in the large tube which extends at a right angle from the drift tube. The multiplier receives ions bunched in time according to mass. Upon impinging on the cathode of the multiplier these ions dislodge electrons which are then multiplied to a useful number. The multiplier has a gain of 10^5 to 10^7 and a gating feature at the output end wherein the current pulses due to any particular mass peak can be selected and deflected toward a signal anode.

The multiplier depends, throughout, upon the cycloidal motion characteristic of electrons in crossed electric and magnetic fields. This motion is the same as that of a point on the periphery of a rolling disc. This is illustrated in Figure 17(a). The solid line on the drawing indicates the path of an electron having zero initial velocity and moving under the influence of a magnetic field (directed into the page) and an electric field (directed as indicated). If the initial velocity of the electron is not zero, the path is modified to produce cusps that are not sharp, but rather are looped or rounded depending upon the direction of initial motion. Assuming zero initial velocity, the height of the cycloid is

$$h = \frac{2m}{e} \frac{E}{H^2} \tag{49}$$

and the length is πh. With E in volts per mil and H in gauss, the expression for electrons becomes:

$$h = 1.8 \cdot 10^6 \frac{E}{H^2} \text{ mils} \tag{50}$$

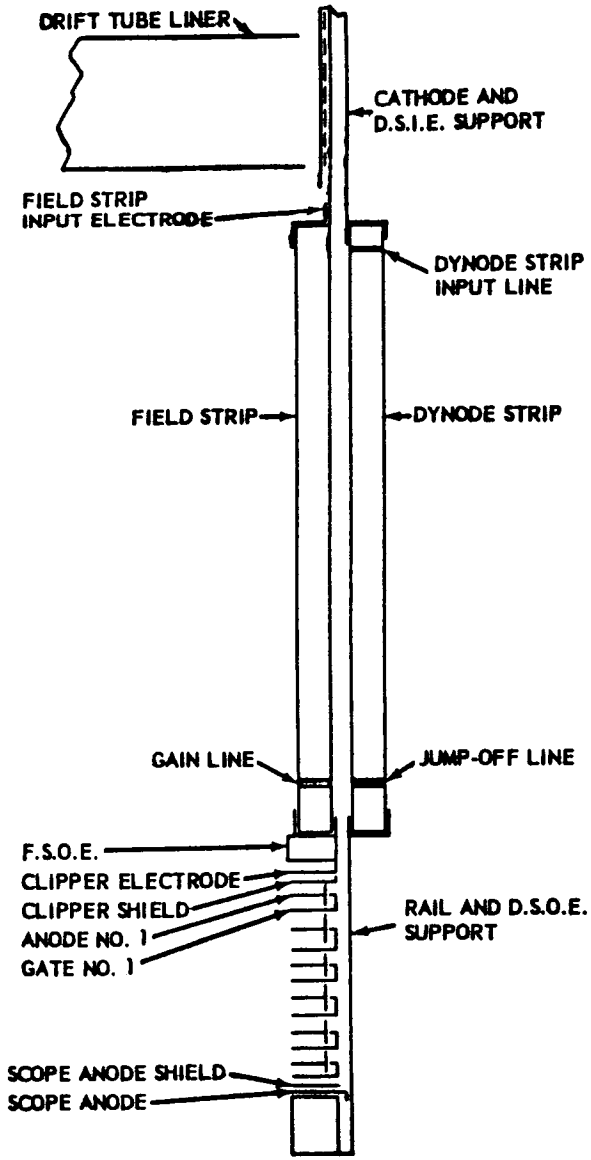

Figure 16 - Cross Section View of Electron Multiplier

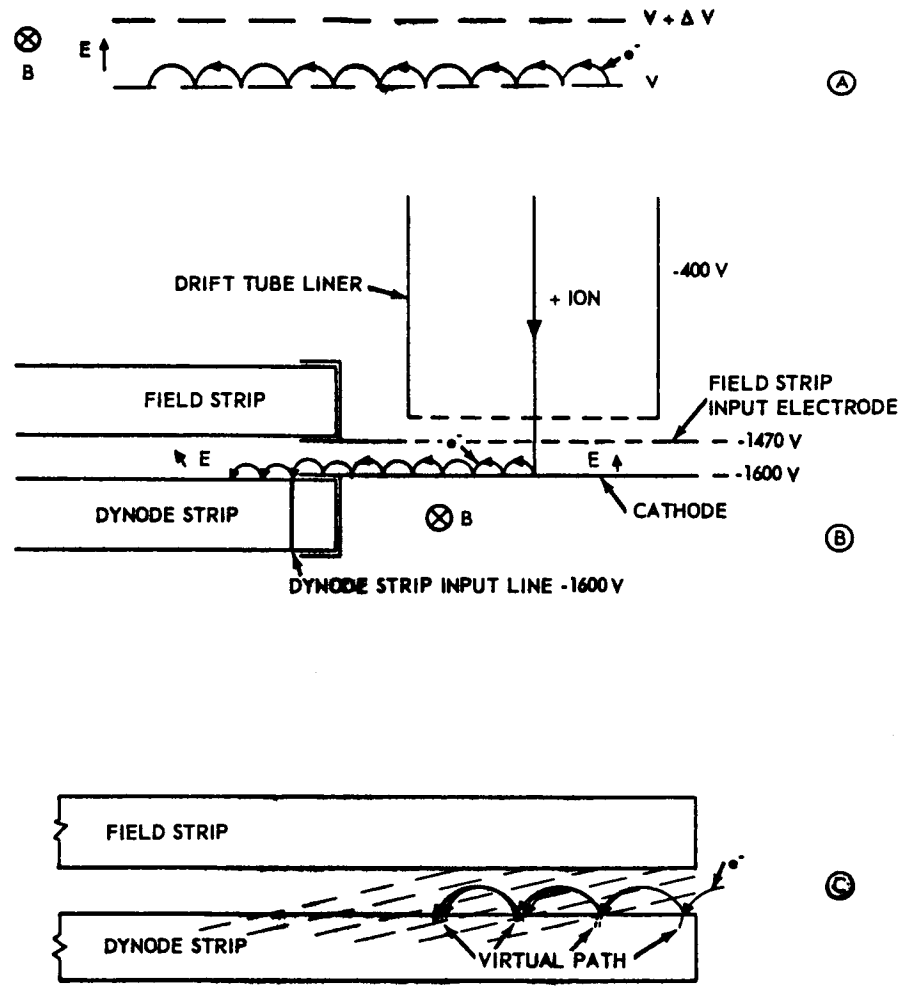

Figure 17 - Cycloidal Motion of Electrons and Multiplying Action of Multiplier

In the multiplier, therefore, where the fields are typically 120 volts per 120 mils and 240 gauss, respectively, the height of a cycloid is about 30 mils and the distance between cusps is about 100 mils.

The direction of progression of an electron under these conditions is perpendicular to both the electric field and magnetic field and the speed is given by $S = E/H$. For speed in inches per second with H in gauss and E in volts per mil, this becomes $S = E/H \cdot 10$ inches. Under the above stated field conditions, a progression speed of 4×10^8 inches per second is obtained. The reciprocal of this figure is actually more useful; namely, 2.4×10^{-9} seconds per inch.

In the mass spectrometer, electrons are dislodged by ions with energies of 1600 electron volts hitting the cathode. The electrons then move under the influence of the electric field between the cathode and field strip input electrode and a magnetic field normal to the electric field as indicated in Figure 17(b) (the ions are too heavy to be affected very much by the magnetic field). The electrons move along in cycloidal motion between the cathode and field strip electrode with the cusps of the cycloid returning to the surface of the cathode. Some of the electrons are lost but most continue on and reach the dynode strip.

As the electrons enter the region between the glass strips, they still attempt to return to their original voltage level but, because the potential gradient along the glass produces an electric field which is not perpendicular to the glass surface, the electrons collide with the glass dynode strip before reaching their original potential. The energy with which the electrons hit the surface is sufficient to dislodge secondary electrons on a somewhat greater than one-for-one basis. These new electrons then follow a similar path dislodging an even greater number of electrons as they collide again with the dynode strip (Figure 17(c)). In this way the few original electrons give rise to an electron current 10^5 to 10^7 times as great at the end of the dynode strip. Forty to sixty cycles of cycloidal motion are required to achieve this gain.

At the output end of the multiplier (Figure 18(a)) the potential gradient along the dynode strip is reversed. This is accomplished by a conductive line, called the jump-off line, painted across the dynode strip approximately 1/2 inch from the output end. The line is held at -45 volts by a Zener diode while the output end of the dynode strip is maintained at about -45 volts. This reversal of the

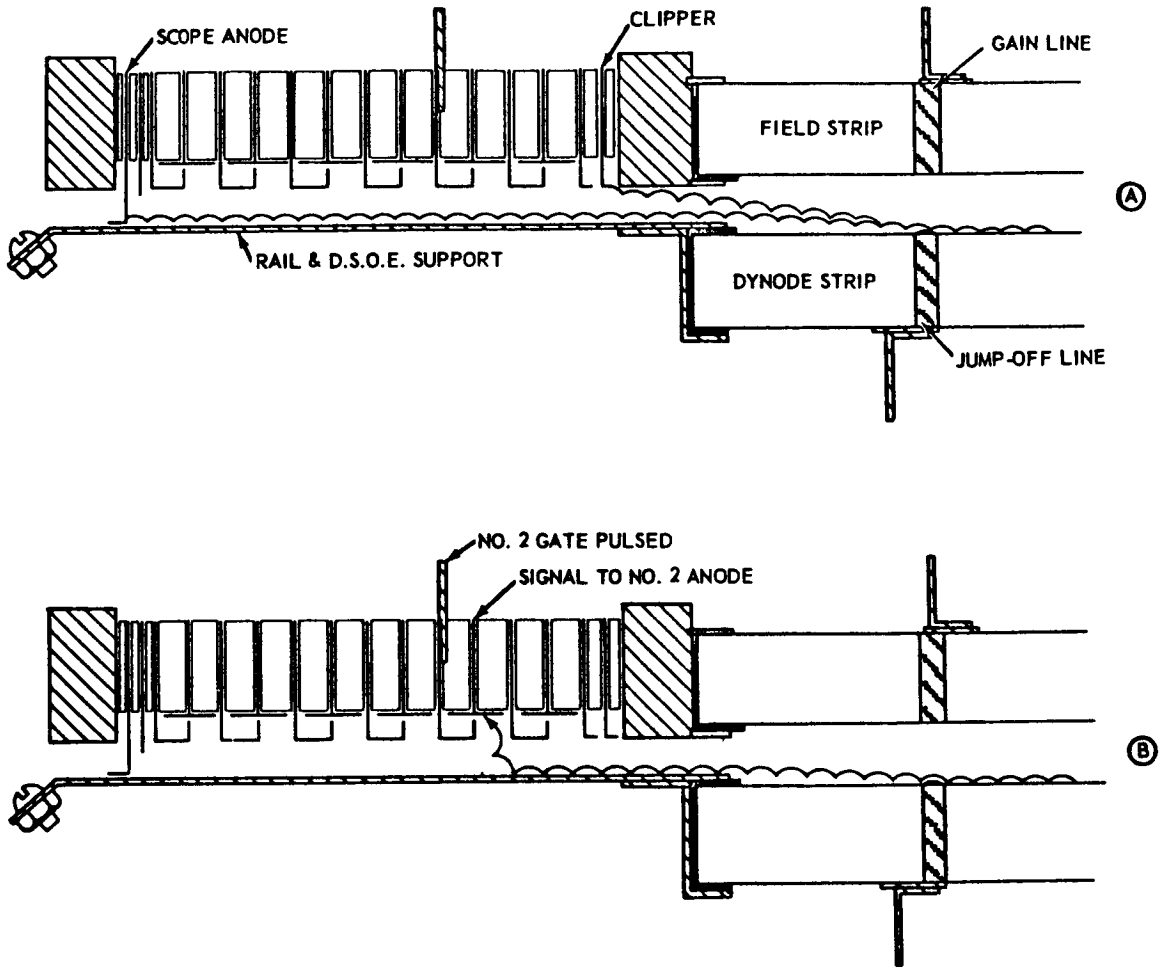

Figure 18 - Gating Action of Multiplier

potential gradient at the jump-off line causes the equipotential lines to be above the dynode glass and above the rail. Thus, the cycloiding electron sheet reaches the zero energy level (at the cycloid cusp) above the glass so that it cannot reach the surface of the strip. The potential of the jump-off line, (and therefore that of the electron sheet cusps) is maintained slightly above the rail in the region of the six output channels which are normally at 0 potential. When the potential level of the jump-off line reaches the end of the gating region it passes between the rail and the scope anode which is nominally at 0 potential. The electron sheet, in trying to follow this equipotential level under the scope anode, is collected with about 90 percent efficiency because of the close spacing between the scope anode and the rail.

However, if any of the 6 gates are pulsed to a voltage slightly more negative than the rail, (Figure 18(b)) the electron sheet will be deflected up into the channel and will attempt to pass between the negative gates and the collecting anode. Due to the close spacing however, the electrons cycloid into the anode and are collected. The anodes are recessed to avoid pickup of stray electrons. There is also a clipper electrode at the output end of the multiplier to collect errant electrons which are reaching an equipotential line too near 0 volts. This operates by acting as a partial gate; it is held at -30 volts. In order to reduce the capacitive feedthrough of the gating pulse from gate number 6 to the scope anode, a shielding electrode is inserted between the gate and the scope anode.

The gain of the multiplier is controlled by the potential applied to the gail line which is a conductive strip across the field strip near the output end. The gain is controlled by tapering the gradient between the dynode and field strip from the relatively large fixed value at the input end to a greater or lesser value near the output end. The gain increases as a function of increasing gradient at the output end up to a large value.

The gain of stray beam currents can become large enough to defocus the beam causing impairment of the rejection ratio between large and small peaks. This can be avoided by keeping the largest average current due to any mass peak well under 10^{-7} ampere. Optimum balance between gain and rejection ratio is obtained by experimentation.

Voltage and Magnetic Field Requirements - The voltage and magnetic field requirements are as follows:

1. The cathode and dynode strip input end are held at -1600V. The current to this point is determined by the resistances of the dynode strip and field strip and voltages across them.

2. The field strip input end support electrode is maintained at 1470 volts or about +130 volts with respect to the dynode strip input. The current to this point is determined by the field strip resistance.

3. The gain line voltage requirement is variable. Within the range of the control, making the gain

line more positive increases the gain. The control range is from 0 to +100 volts. The gain line is normally held at +100 volts.

4. The jump-off line is held at -45 volts ±2 volts.
5. The dynode strip output end and rail voltage is -50 ±2 volts.
6. The clipper electrode voltage is -30 ±1 volt.
7. The scope anode shield is grounded with a short lead.
8. Gating onto any channel is performed by pulsing the proper gate at about -60 volts.
9. The magnetic field is furnished by Cunife bar magnets which, with the pole pieces, form the mechanical framework for the multiplier. A magnetic field of approximately 250 gauss is obtained in this manner.

Mechanical Construction - The main body of the multiplier consists of 2 long magnetic pole pieces held apart by 38 Cunife bar magnets attached to the pole pieces (Figure 19). The multiplier assembly is supported at the header end by bolting it to the vacuum housing header. It is supported at the inward end by an attached ring which seats into a recess in the end of the multiplier housing. This ring is cut away to allow it to slide past the end of the drift tube. The drift tube opens into the hole in the field strip input electrode when the multiplier is installed.

The field is maintained between the field strip input electrode by a piece of 75 percent transmission etched nickel mesh sandwiched between the two pieces of the electrode.

The dynode strip input end support, field strip input end support, cathode, rail, and dynode strip output end support are suspended on sapphire rods and centered by screws with sapphire rod inserts. The field strip and dynode strip input ends are centered and placed in opposition to each other by sighting through the input end of the multiplier. The rail and dynode strip output end support is placed so that the rail side plates are spaced an equal distance from the gates on either side. The centering screws are retained with lock nuts which also hold the sapphire mounting rods in place.

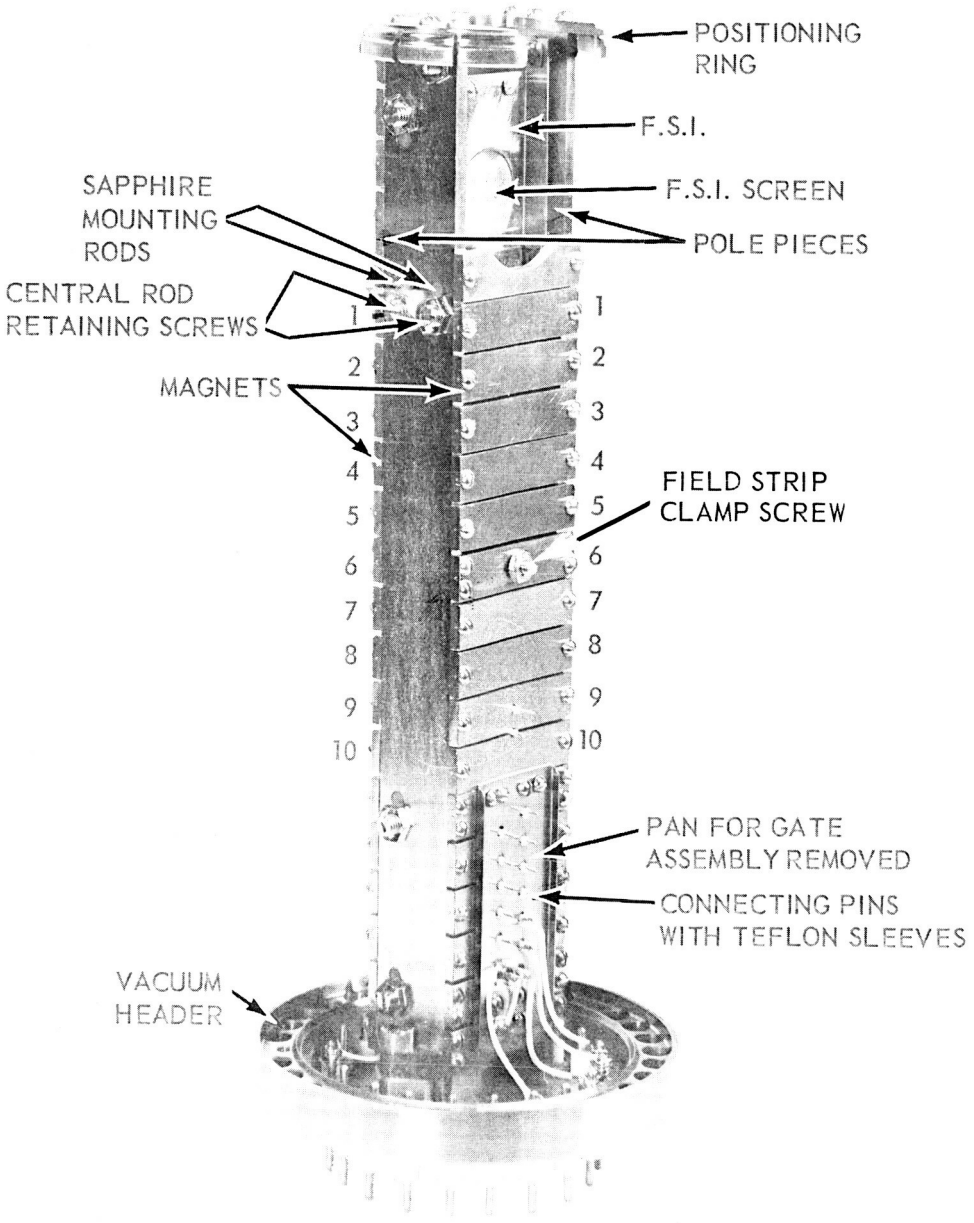

Figure 19 - Magnetic Electron Multiplier

The gate and anode structure pieces are sandwiched between ceramic spacers and the whole stack is compressed between metal blocks and supported by sapphire rods. The support blocks are held on the bar magnets with screws. The metal pan on the outside of the magnet assembly next to the gate structure is a support span between the two magnets which hold the support blocks. It holds the assembly together when it is removed from the pole pieces

Small stainless steel pins (0.025" diameter) are welded to the electrodes to which electrical connection are made through the magents. Teflon sleeves insulate these pins from the magnets. The electrodes in the gate and anode assembly are made of 5 to 10 mil stainless steel so care must be taken not to exert too much force on these pins.

The resistive glass strips have a coating on the inner surfaces. The resistivity is over 3 megohms per square. Contact is made to the ends of glass through the support members which contact brass pieces cemented to the glass with A-6 epoxy resin. Contact is established between the brass pieces and the resistive coating by silver paint. Contact to the dynode strip input end line, jump-off line, and gain line is made through pins welded to stainless steel plates which in turn are cemented to the glass and over which the silver lines are painted.

The glass strips are held against the support electrodes by screws through tapped holes in magnets on either side of the multiplier. The screws are kept from loosening by locknuts.

Maintenance - Aside from mechanical breakage, there are two difficulties which can arise in conjunction with the operation of the multiplier. The first, and most common, is "dirtying" of the glass. This phenomenon is caused by hydrocarbons being plastered into the glass by the electron beam and forming an insulating layer. Its effects are reduced gain and usually, but not always, unstable operation with cyclically varying gain. The only positive method of detection is visual. This is accomplished by removing the multiplier and observing the output end of the dynode strip, just before the jump-off line. A colored deposit will be found, with the darkest area near the center of the strip. In extreme cases this deposit will be a browish color. It usually extends back from the jump-off line one-half to one inch. This deposit can be removed by carefully rubbing the area with

a pink "Ruby" type pencil eraser. It is necessary to avoid excessive rubbing on the silver lines as they are easily damaged.

The second difficulty which can arise during the operation of the multiplier is "burn-out" of the glass strips. This is indicated by low gain or an unusual voltage arrangement to obtain normal gain. The gain decrease may occur over a short or long period of time, hours or days, depending on whether the glass "burn-out" is rapid or slow. The "burn-out" is caused by exceeding 0.1 watt per square inch heat dissipation for each strip of glass when the environment is near 25°C. In some cases of "burn-out," usually the more rapid cases, the cold resistance of the strips will change; but, where "burn-out" takes place slowly the only method of detection is a visual inspection of the coating on the glass. This is done by removing the glass, holding it up to light, and observing whether there are minute areas of irregular shape which appear to be more translucent than the immediately surrounding coating. If "burn-out" is encountered, the glass must be replaced.

To remove the glass it is necessary to remove 10 magnets on each side of the multiplier. Figure 19 shows the magnets, numbered 1 through 10, which must be removed on each side. Then the input end structure must be removed to allow the glass to slide free. Care should be exercised to prevent scratching the surface of the glass. Scratches can open the resistive coating or form nuclei for "burn-out." It is essential that good high-vacuum technique be observed whenever the multiplier or source are removed and worked on.

4.5.4 Time-of-Flight Output Systems

The three major types of output systems for Time-of-Flight Mass Spectrometers are described and their applications discussed. An oscilloscope output system is used to obtain quick answers with accuracy being limited to the accuracy of the oscilloscope employed. For very small mass peaks, accuracy degenerates to zero. An analog output system is considered to be the most useful and versatile output system. It uses a selective gated input to measure simultaneously the areas under several mass peaks. Using this type of output, spectral patterns which are normally generated in several microseconds can be recorded with a response of 100 cps or less. When the average number of ions per mass peak per mass spectrum is considerably less than one, a counter circuit (digital output system) can be used to totalize the ions which occur in specific mass peaks. Several mass peaks can be counted simultaneously.

Oscilloscope Output System

The most straightforward output system for these instruments is an oscilloscope. The horizontal sweep of the oscilloscope is synchronized with the ion ejection pulse from the ion source, while the vertical plates are connected to the output of the multipliers. The output signal then appears on the oscilloscope as a fixed pattern looking very similar to conventionally recorded mass spectra. The horizontal sweep can be varied in speed and delayed in time so that as little or as much of the spectrum as desired can be viewed.

While not necessary in most applications, there are some types of research which require analyses to be performed in only a few microseconds. Among these are shock wave work, some explosion phenomena, and flash photochemical reactions; such as has been pursued at Harvard University by G. B. Kistiakowski and his colleagues. In such situations, where analyses are made every few microseconds, the oscilloscope output system can be very useful when fitted with a camera that records each individual spectrum. It should be noted that even though a spectrum can take 20 or more microseconds to be detected, the ions in that spectrum were all formed during a single time interval which can be as short as a small fraction of a microsecond so that a single spectrum is representative of the average gas composition over a very short period. Thus, one obtains almost instantaneous analyses repeated at the repetition rate of the instrument. A drum camera provides a very simple photographic system to use for single spectrum photographs. The camera used at Harvard is of this type and utilizes a film strip positioned on the inside of a rotating drum. The drum rotates at about 100 cps, the centrifugal force being sufficient to keep the film firmly in place. This drum is approximately 8 inches in diameter, resulting in a film speed of about 1 cm per 100 microseconds. The repetition rate of the mass spectra was variable but usually set at 20 Kc. An F2.8 lens, linograph pan film, and a P11 phosphor on the cathode ray tube resulted in excellent photographs.

Any output system utilizing an oscilloscope is, of course, limited in accuracy by the oscilloscope itself. Although special techniques, such as the use of calibrated attenuators, can increase accuracy, it has been found that the average operator obtains an analytical accuracy of only a few percent at best. However, when the spectrometer is used for qualitative work, such as the identification of chromatograph peaks, the oscilloscope output system can be quite satisfactory.

Another limitation in the use of the oscilloscope is a restriction of dynamic range to a figure much less than the inherent capabilities of the instrument. This is not due to the limited size of the screen since this limitation can be obviated (although with some inconvenience) by gain changing techniques; but rather because the low-noise characteristics of the electron multiplier allow one to utilize very small ion currents. For instance, when gated properly, the electrical noise in magnetic electron multipliers can be made equivalent to an ion current of less than 10^{-21} ampere. With a repetition rate of 10 Kc for the mass spectrometer, this is equivalent to about one ion every million spectra. When the average number of ions of a particular mass is as low as 3 or 4 per spectrum, the trace on the oscilloscope will no longer be a well-shaped peak but will degenerate into a fuzzy picture somewhat resembling "grass." This is because a peak due to a single ion is short compared to the spread in ion flight times so that the few ions present cannot effectively add up to a single peak. Since on an oscilloscope one is looking at many spectra at once, this condition persists even after the number of ions per spectrum for a particular mass peak is well below one. Of course, the oscilloscope is almost useless for quantitative analysis in this range since there is no longer a change in peak height with ion abundance, but only a change in screen brightness.

Analog Output Systems

In order to use a Time-of-Flight Mass Spectrometer in a quantitative manner over a large range of peak heights it is necessary to integrate the current from individual mass peaks over a relatively large number of mass spectra, and to present the integrated signal in analog or digital form. By using a multiplier of the type previously described, it is possible to selectively gate a particular mass peak from each spectrum and cause it to be collected by one of the several anodes in the multiplier. The number of mass peaks that can be handled simultaneously in this manner is limited only by the number of anodes in the multiplier. The current reaching each of the anodes can then be measured by an electrometer circuit. An analog system works equally well on large or small peaks. The accuracy is not dependent on ion current level except as statistical fluctuations in the ion numbers for a particular mass peak cause corresponding fluctuations in the output signal. This factor can, of course, be controlled in the output system by a variable time constant control. It should be

noted that an analog system of this type actually measures peak areas rather than peak heights. A gate width comparable to the peak width is advantageous as far as stability is concerned, since the peak area is much less responsive to slight changes in focus than is the peak height. The wide gate is a disadvantage, however, when maximum resolution is desired. Since the cross interference in area of two adjacent mass peaks is much greater than the cross interference in the peak height, increased resolution can be attained, accompanied by some loss in stability, by narrowing the gate width.

By slowly increasing the delay of a particular gate pulse at a rate small in comparison with the repetition rate of the instrument, a slow scan of the spectrum can be produced so that the spectral pattern normally viewed with a several-microsecond scan on the oscilloscope can be reconstituted on a much longer time scale -- of the order of many seconds or minutes. Such a system allows the spectrum to be recorded and displayed on recorders having responses of 100 cps or less. Feedback type electrometer circuits used in conjunction with the scanning gate provide good frequency response with a high degree of stability. Thus the electrometer output can be coupled into two recorder channels set a decade apart in sensitivity, giving an accurate record covering more than a 100 to 1 range. Wide-band electrometers permit rapid scanning for fast sample analysis.

For some analyses, it is advantageous to gang several multiplier gates to one scanning device, with offsets between the several gates so that different regions of the mass spectrum are scanned simultaneously. Of course, this requires a multi-channel recorder.

It is also possible to directly measure and record the ratio of two mass peaks in the sample. This can be done by automatically varying the multiplier gain to maintain the output from one multiplier anode at a constant reference level. Because mass peak ratios are insensitive, at least in the first approximation, to changes in the electron beam intensity and to sample flow rates, ratio measurements are normally much more stable and subject to less long-term drift than direct peak measurements themselves.

In order to provide an analog output system which includes the particular performance features required in a specific application, but excludes those features which add complexity without a corresponding increase in useful versatility, it is convenient to have the analog output

system available in three basic units. The first unit contains the circuitry which would be necessary to perform only the basic functions of manually selecting a mass peak, gating that peak onto a particular anode, and monitoring the current with an electrometer amplifier. The second unit, the scanner unit, performs the functions of the monitor unit and also includes the circuitry necessary to provide a slow scan of the mass spectrum. It has been found useful to provide circuitry and controls to allow the automatic scan to start from a manually controlled position and to proceed in either direction. A variable scan rate control permits adjustment of the rate from about 0.01 microsecond to 150 microseconds of spectrum time per minute of real time. The third unit, the controller unit, also includes the basic circuitry of the monitor unit but, in addition, is able to control the gain of the multiplier so as to maintain the output of its electrometer circuit at a fixed level. This unit is required when one wishes to make direct ration measurements.

As previously indicated, each unit contains one gating circuit and can measure only one particular portion of the mass spectrum at a time. Simultaneous measurement of several mass peaks requires a corresponding number of analog units, which can be chosen to include the features required in the specific problem. For instance, the combination of a scanner and controller is particularly useful in obtaining a true spectral pattern when the sample under study might be varying in pressure. Such a case would be encountered when the spectrometer is used in conjunction with a gas chromatograph to identify the components emerging from the column. Ideally, the monitor units are all that would be required in an installation requiring the continuous monitoring of several mass peaks such as might occur in the continuous analysis of a particular chemical process. Practically, however, one can usually do better by including one controller unit which, by varying the gain of the multiplier, will keep one mass peak at a constant level so that the advantages of ratio recording can be realized. One can obtain complete versatility in a 2-channel system by including one scanner and one controller unit. If additional channels are desired, monitor units would normally be satisfactory. Simple electronic circuitry permits slaving the monitor gates to a scanner, if desired, so that different portions of the spectrum can be scanned simultaneously.

Digital Output System

As previously discussed, a Time-of-Flight Mass Spectrometer can operate in an accurate, quantitative manner when the average number of ions per mass peak per mass spectrum is considerably less than one. Under these conditions, of course, semi-quantitative measurements with an oscilloscope are difficult, if not impossible. The analog output system can operate in this range, but due to practical limitations on the maximum output current of the electron multiplier, the analog system reaches its lower limit at current levels considerably above those currents which are still quantitatively useful. It is possible, however, to accurately measure these very small ion currents by counting the multiplier output pulses corresponding to single ions. For instance, by utilizing gating techniques, one can select a particular portion of the mass spectrum, usually one mass peak, and determine the presence or absence of a single ion during this interval. A counter circuit can then total the counts which have occurred during this gating interval over any selected period. With this technique the gating can be accomplished through electronic circuitry exterior to the multiplier.

Inputs to a 2-channel system are a master pulse, coincident with the beginning of each mass spectrum in the mass spectrometer, and a spectrum input which is normally the output of an electron multiplier. The spectrum gating pulses are synchronized with the master pulse through independently adjustable trigger delay circuits. The trigger delay range in each channel should permit gating mass peaks from 1 amu to the heaviest mass peak which is of interest. An output is obtained from the spectrum gate circuit when a mass peak appears in that portion of the spectrum which coincides with the gating pulse. This output will register as one count in the associated decade counter chain if the counter gate through which the output must pass is open at the time. Resolution can be controlled by varying the effective gate width over a range of approximately 25 to 100 millimicroseconds.

The counting period can be set to terminate at a selected time or it can be terminated when a selected power of 10 counts has accumulated in one channel. The latter method is used when it is desired to obtain the ratio of 2 peaks. Whichever mode of operation is chosen, the display timer circuit is triggered at the end of the counting period, closing both counter gates. The accumulated count

in each channel is displayed for a period which should be adjustable from a fraction of a second to infinity for maximum operating convenience. At the end of the display period, the counters are reset, and the counter gates are opened. The counts-per-cycle meter provides a continuous indication of the count rate in either channel, so that it can be used to aid in aligning a gate with a mass peak. The gate display provides means for indicating the position of the gate relative to the spectrum on an oscilloscope display of the mass spectrum.

If the count representing a particular mass peak is allowed to accumulate until the total count is a power of 10, the total counts accumulated simultaneously on other channels can be read directly as a ratio to the first peak. Automatic decimal points can easily be incorporated to facilitate direct reading of the display. Ratio measurements taken in this manner have the same advantages as they have when taken with the analog output system. Timed mode of operation, in which all channels count independently for a preselected time interval, can also be provided. Useful counting periods normally vary from 10 milliseconds to about 100 seconds.

As previously mentioned, the count rate meter can be used to indicate the count rate being received in either channel. This is very useful because reliable data cannot be obtained easily from the pulse counter if the count rate is above approximately 0.1 count per cycle. This arises from the fact that the pulse counter is not responsive to pulse amplitude, since it detects only the presence or absence of a pulse. Therefore, a pulse which is the result of two or more ions arriving at the multiplier simultaneously still will register as only one count. It can be shown that if a given mass peak occurs an average of once every ten spectrometer cycles, about 5 percent of these peaks will contain two ions. Thus, the pulse counter readout in this case would be about 5 percent too low.

A digital output system of this type, when used to measure extremely small ion currents, does possess the very appealing feature of being able to gather all the information made available by the mass spectrometer itself. The only inherent error when using this system is that arising from the statistical variation in counting a randomly occurring signal over a fixed time. This error is an unavoidable consequence of the statistical nature of the ionization process, and it can be reduced only by using larger total counts. Additional inaccuracies will result, however, if the circuit parameters and the gain of

the multiplier cannot be adjusted so that all voltage pulses representing single ions are actually counted by the circuitry. In most Time-of-Flight Mass Spectrometers equipped with electron multipliers, peak heights of single ion pulses vary over a considerable range. The cause of this variation is not only the statistical process of secondary electron emission following ion impingement on the ion cathode, but also the statistics of the secondary emission process in the first few stages of the multiplier, or until the number of electrons has increased to the point where statistical fluctuations are unimportant. In practice, therefore, there can be a considerable difference in multiplier pulse heights for a single ion input and it is not always possible to adjust the multiplier parameters and circuit characteristics so that all of these pulses can be efficiently counted. If the discriminator circuits, which determine the minimum pulse height which can be counted, are set so that the discrimination level falls at a point of large slope on a plot of peak height versus occurrence probability, a very severe requirement is placed upon the stability of the discriminator level.

Of the many ways in which this type of output system can be used, three aspects of its use are particularly interesting. The first is the obvious one that the gating interval need not be one mass unit wide but can contain as many adjacent peaks as is desirable. Another aspect is that the system is naturally thought of as being useful for very small peaks; however, it can be used equally well to obtain a digital presentation of mass peaks which would normally contain many ions per peak, by the simple expedient of reducing the ionizing electron beam intensity. The third aspect concerns the integrating nature of this output system. Consider, for instance, an analysis problem involving the evaporation of a solid, where the rate of evaporation of the different solid constituents can vary considerably and cause complications in the analysis procedure. With an ion pulse counter having sufficient channels to monitor all the mass peaks of interest, all channels can be started prior to heating the small sample. Then when the sample is completely evaporated, or at least all substances which can evaporate are removed, the pulse counters can be stopped and their indications will be independent of the variations in evaporation rates for the various substances.

4.5.5 Summary

The preceding text describes in some detail the general characteristics of a Time-of-Flight Spectrometer and an inlet system sample evaporator using a laser beam for soil analysis.

Table 30 lists the over-all expected performance and physical parameters of this system.

A comparison of the characteristics of the soil analyzer and atmosphere analyzer are such that the former includes the latter. As a matter of fact, the equipment will be capable of performing both soil to atmosphere analysis by turning off the laser beam and increasing the gain of the magnetic electron multiplier.

The mass spectrometer proper can be produced by a straightforward engineering adaptation of available aerospace models paying close attention to both the radiation effects on the equipment and the outgassing effects of the spectrometer. The laser solids source requires somewhat more development.

It appears that a feasible solid sampling device based on laser techniques could be developed, as a result of the advancements in the state-of-the-art in this field. It is recommended that the necessary steps be taken to further evaluate this technology and to exploit its use in the lunar analysis area.

Table 30 - Characteristics of Lunar Soil Analyzer

Parameter	Value
Resolution	800 AMU
Mass Range	0-800 AMU
Response Time	0.05 sec
Accuracy	±2%
Linearity	±2%
Stability β	±5%
Weight	55 lbs
Size	700 $in.^3$
Power	290 W
Form of Output	Electrometer 0-5 V
Gravity	Independent
Sensitivity	1 ppm, 10^6 dynamic range
Life	Indefinite

P-2159

SECTION 5

SUMMARY OF EXPERIMENTAL ACTIVITY

This section summarizes the experimental activity undertaken on this program.

Experiments with the source analyzer assembly quickly showed that by operating the source at 10 kilovolts and employing drift tube length of 170 cm resulted in a basic instrument resolution of about 800 amu. In order to preserve this basic resolution in a system, adequately narrow multiplier gating pulses must be used. Though the required circuitry was developed on another concurrent program, the appropriate pulses can now be generated.

Figure 20 shows the relationship between Time-of-Flight (Curve A), adjacent mass separation (Curve B), and mass peak width at half

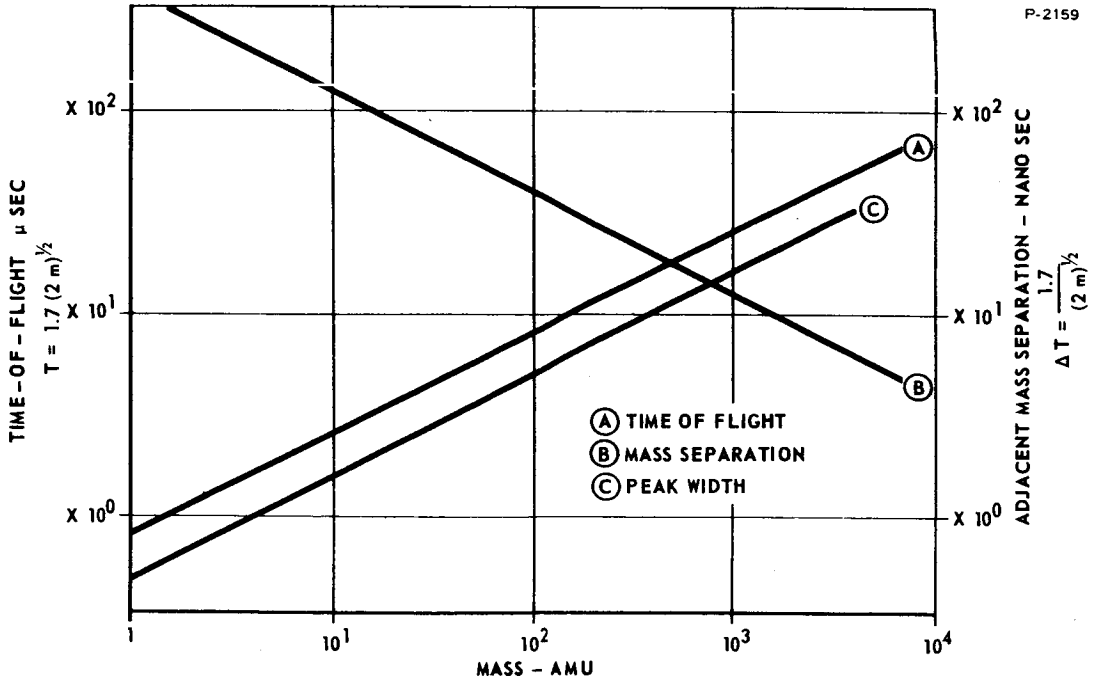

Figure 20 - Typical Resolution Characteristics for a Time-of-Flight Lunar Analyzer

amplitude (Curve C) for the Time-of-Flight lunar analyzer discussed in Section 4. It can be seen that the adjacent mass separation just equals the peak widths at 800 amu.

Experiments with currently used multiplier glass show that bake-out at temperatures in excess of about 200°C harms the active surface. However, a perusal of the effusion characteristics of molecularly-flowing gases, as discussed in Section 3, shows that the multiplier can be "baffled" from the analyzer so effectively that a pressure ratio of at least 10^4 will result. Since current systems are pumped below 10^{-9} mm Hg (occasionally), it should be readily feasible to keep the "background" of the analyzer, as contributed by the multiplier, below 10^{-13} mm Hg total pressure and the water vapor level to about X100 below this. Consequently, it is firmly believed that the multiplier can be operated without becoming contaminated by water vapor.

APPENDIX A

GENERAL CHARACTERISTICS AND MOTIONS OF THE MOON

The moon is an ellipsoid with its major axis pointed toward the earth and its shortest axis approximately normal to the plane of its orbit. It is roughly one quarter of the size of the earth and is the fifth largest satellite in the Solar System; however, its exact shape is not known and will not be until close-orbiting satellites are established around it. The moon's rotation about earth is elliptical with a slight eccentricity. Since its period of rotation and its period of revolution are equal, the same face is always seen from earth. Due to a "rocking" effect, it is possible, at one time or another, to see 59 percent of the moon; 41 percent is always visible and 41 percent is never visible, the remaining 18 percent is visible or invisible depending on the location and time of observation. Table 31 lists some important features of the moon.

Table 31 - Important Facts Concerning Luna

Density		$3.34\ g/cm^3$
Volume		$2.20 \times 10^{25}\ cm^3$
Gravitational acceleration		$2.38\ km/sec^2$
Mass		$7.35 \times 10^{25}\ g$
Diameter		2160 miles
Surface area	(Earth = 1)	0.074
Volume	(Earth = 1)	0.0203
Density	(Earth = 1)	0.604
	(Water = 1)	3.34
Mass	(Earth = 1)	0.0123
Gravity	(Earth = 1)	0.164
Oblateness		0
Escape velocity		1.48 miles/sec.
Albedo		0.07
Stellar magnitude		-12.6
Temperature of surface or of visible layers of opaque atmosphere		+270 to -240°F
Length of day (period of rotation)		655.72 hr.
Length of year (sidereal period of revolution)		27.298 solar days
Synodic period of revolution		29.54 solar days
Mean daily motion		13.2 deg.
Mean distance from Earth		238,857 miles
Perigee		231,463 miles
Apogee		252,710 miles
Mean orbital velocity		0.64 miles/sec
Direction of motion		Direct
Eccentricity of orbit		0.0549
Inclination of Equator to orbit		6° 41 min min
Inclination of orbit to ecliptic		5° 8.5 min

P-1868

APPENDIX B

TEMPERATURE MEASUREMENTS OF THE MOON

The moon's temperature, as observed with a pyrometer, drops 150°C within an hour during a total eclipse of the moon. Epstein[61] and Wesselink[62] showed how from this datum the thermal inertia can be derived. From the eclipse observations they derive an inertia of 0.001. The thermal inertia can be derived also from the temperature variation throughout a lunation just as the inertia of Mars was derived (average, 29 days, 12 hours, 44 minutes, 18 seconds). The variation throughout a lunation has not been adequately observed, but it is in fair agreement with the thermal inertia derived from the eclipse observations. From the theory and the inertia determined from the eclipse observations the temperature of lunar "midnight" should be (98°K). At the Lowell Observatory, G. P. Kuiper has obtained 424°K ±3°K for the point opposite the sun, which is in good agreement with 421°K ±5°K obtained by Pettit and Nicholson.[63]

Radio observations of the moon have been made over a range of wave lengths from 4.3 mm to 75 cm; the results are shown in the Table 32. Not all the observers have used the same assumptions about the lunar brightness distribution when reducing the data; this, together with differences in the methods of calibrating the antennae and receivers, probably accounts for much of the disagreement in the measured radio brightness temperatures.

Table 32 - Radio Observations of the Moon's Temperature

Wave-length (cm)	Apparent Black Body Temperature °K	Uncertainty	Observer
0.43	T_c = 170 to 290	25 percent	Coates (1959 a,b)
0.75	T_d = 125 to 175		Mitchell and Whitehurst (1958)
0.80	T_c = 197 - 32 cos (ωt - 40)	10 percent	Salomonovich (1958)
0.86	T_c = 150 (single observation)	40 percent	Hagen (1949)
0.86	T_c = 145 to 225		Gibson (1958)
1.25	T_d = 270 (single observation)		Dicke and Beringer (1946)
1.25	T_c = 249 - 52 cos (ωt - 45°)	5 percent	Piddington and Minnett (1949)
1.63	T_c = 224 - 36 cos (ωt - 40°)	±10 percent	Zelinskaya, Troitskii, and Fedoseev (1959)
2.20	T_c = 200 (constant to ±10°K)	5 percent	Grebenkemper (1958)
3.15	T_c = 195 - 12(±5) cos (ωt - 44 (±15°) ±25°K		Mayer, McCullough, and Sloanaker (unpub.)
3.20	T_d = 183 (constant to ±9°K)	±13°K	Zelinskaya and Troitskii (1956)
3.20	T_d = 170 (constant to ±12°)	±20 percent	Troitskii and Zelinskaya (1955)
3.20	T_d = 133 (constant to ±10°K)	±20°K	Kaidenovsky, Turusbekov, and Khaikin (1956)
10.0	T_d = 130 (single observation)	20 percent	Kaidenovsky, Turusbekov, and Khaikin (1956)
10.0	T_d = 315 (constant to ±50°K)	±50°K	Akabane (1955)
10.3	T_d = 207 (single observation)	±27°K	Sloanaker (unpub.)
21.0	T_c = 250 (constant to ±5°K)	12 percent	Mezger and Strassl (1959)
22.0	T_d = 270 (single observation)	±60°K	Westerhout (1958)
32.0	T_d = 246 (constant to ±5 percent)	±40°K	Ko (private communication)
33.0	T_d = 220 (constant to ±9°K) mean deviation	±33°K	Denisse and LeRou
75	T_d = 160 (single observation)		Seeger, Westerhout, and van de Hulst (1956)
75	T_d = 185 (constant to 10 percent)		Seeger, Westerhout, and van de Hulst (1957)

APPENDIX C

CALCULATION OF LIFETIMES OF VARIOUS LUNAR GASES

The following is a representative calculation of the lifetime, t_ℓ, of any gas. The factors have the meaning used in Section 3 and the values called out below.

$$M' = 7.35 \times 10^{22} \text{ kg}$$

$$G = 6.67 \times 10^{-11} \text{ Newtons} - \text{m}^2/\text{kg}^2$$

$$m = Mm_o = M \cdot 1.66 \times 10^{-27} \text{ kg} \cdot \text{amu}$$

$$k = 1.38 \times 10^{-16} \text{ ergs}/^\circ\text{K}$$

$$T_c = 400^\circ\text{K}$$

$$R_c = 1080 \text{ miles} = 1735 \text{ km}$$

$$Y = G M'm/k T_c R_c$$

$$Y = \frac{6.67 \times 10^{-11} \text{ Newtons} - \text{m}^2 \cdot 7.35 \times 10^{22} \text{ kg} \cdot 1.66 \times 10^{-27} \frac{\text{kg}}{\text{amu}}}{1.38 \times 10^{-16} \text{ erg } ^\circ\text{K}^{-1} \cdot \text{kg}^2 \cdot 400^\circ\text{K} \times 1735 \text{ km} \cdot 10^{-7} \frac{\text{Joule}}{\text{erg}}} \cdot M \text{ (amu)}$$

$$Y = 8.49 \times 10^{-1} M \text{ (dimensionless)}$$

$$C = \sqrt{\frac{3kT}{m}} = \sqrt{\frac{3kT\,8\pi}{m\,8\pi}} = \sqrt{\frac{3\pi}{8}} \cdot \sqrt{\frac{8kT}{\pi m}}$$

$$= \sqrt{\frac{3\pi}{8}} \cdot \bar{v} \text{ (average molecular velocity)}$$

$$C = 1.085\ \bar{v}(\text{avg}) = \sqrt{\frac{1}{M}} \cdot 3.15 \times 10^{5}\ \text{cm/sec}$$

and

$$\bar{v} = \sqrt{\frac{8kt}{\pi m}} = \sqrt{\frac{1}{M}} \cdot 2.90 \times 10^{5}\ \text{cm/sec}$$

Thus, since

$$t_1 = \frac{\sqrt{6\pi}}{3 g_\ell} \cdot \frac{Ce^{Y}}{Y} = \frac{4.34}{3 \cdot 1.62 \times 10^{2}} \cdot \frac{Ce^{Y}}{Y}$$

$$t_1 = 0.884 \times 10^{-2} \cdot \frac{Ce^{Y}}{Y}\ \text{second}$$

$$t_1 = 2.89 \times 10^{-10} \cdot \frac{Ce^{Y}}{Y}\ \text{year}$$

Or for computational purposes

$$t_1 = 2.89 \times 10^{-10} \times \text{antilog}\,(0.4349 \cdot Y) \cdot \frac{C}{Y}\ \text{year.}$$

APPENDIX D

PHYSICAL PROPERTIES OF MISCELLANEOUS GAS COMPONENTS

This table, Table 33, provides general background information about the properties of several miscellaneous gases which are expected to be associated with manned lunar landings.

Table 33 - Physical Properties of Several Atmospheric Gas Components

PROPERTY	NITROGEN N_2	OXYGEN O_2	CARBON MONOXIDE CO	NEON Ne	HELIUM He	HYDROGEN H_2	METHANE CH_4	NITROUS OXIDE N_2O	HYDROGEN SULFIDE H_2S	AMMONIA NH_3	NITRIC OXIDE NO	NITROGEN TRI OXIDE N_2O_3	OZONE O_3	ETHYLENE C_2H_4	ACETONE C_3H_6O	ACETYLENE C_2H_2
Atomic Number	7	16	N.A.	10	2	1	N.A.	N.A.	N.A.	N.A.	N.A.	N.A.	16	N.A.	N.A.	N.A.
Molecular Mass	28	32	28	20	4	2	16	44	34	17	30	7	48	28	58	26
Critical Pressure (Atms)	33.5	49.7	35.0	25.9	2.26	12.8	45.8	71.7	88.9	--	65	↑	54.6	50.9	47	62
Critical Temp. °C	-147.1	-118.8	-139	-228.7	-267.9	-239.9	-82.5	36.5	100.4	128	-94		-12.1	9.7	235	36
Critical Density g/cc	0.311	0.430	0.311	0.484	0.0693	0.0310	0.162	0.45	--	--	0.52		0.437	0.22	0.268	0.231
Density g/l 0°C 760 mm Hg	1.257	1.429	1.250	0.900	0.178	0.08988	0.7168	1.9778	1.539	0.7710	1.3402		2.144	1.2604	0.8113	1.173
Viscosity Micropoise	178.1	201.8	172	311.1	194.1	87.6	108.7	148.8	124.1	98.2	187.6		--	100.8	93.1	93.5
At Temp. °C	27.4	19.1	15	20	20	20.7	20	26.9	17	20	20		--	20	100	0
Specific Heat Cp Cal/g.	0.2477	0.2178	0.2478	--	1.25	3.389	0.5284	0.2004	0.2533	0.5232	0.2329		0.218	0.3592	1.45	0.3832
C_v Cal/g.	0.176	0.155	0.176	--	0.693	2.40	0.402	0.154	0.191	0.399	0.166		--	0.286	--	0.304
γ	1.400	1.401	1.404	1.64	1.660	1.410	1.31	1.303	1.32	1.310	1.400		--	1.255	--	1.26
°C	15	15	15	19	-180	15	15	15	15	15	15		100	15	26	15
Thermal Conductivity Kiloergs $(sec^{-1})(cm^{-1})°C^{-1}$	2.28 0°C	2.33 0°C	2.15	0.44	13.9	15.9 0°C	2.94 0°C	1.44 0°C	1.20 0°C	2.00 0°C	2.08 0°C		--	1.64 0°C	0.906 0°C	1.73 0°C
Velocity of Sound m/sec at 0°C, P = 1 atms	337.7	316.2	337.4	--	971	1261.7	430.5	260.5	289.3	414.8	325			317.0	208.4 58°C	327.5
Magnetic Volume Susceptibility emu x 10^{-10} at Temperature	-4.97 20°C	139.2 20°C	-4.80 20°C	-2.8 20°C	-0.78 20°C	-1.665 20°C	-5.08 20°C	--	--	--	612 20°C		--	-5.0 20°C	--	--
Dielectric Constant P = 760 mm Hg	1.000580 0°C	1.000523 0°C	1.00070 0°C	1.000127 0°C	1.00007 0°C	1.000264	1.000944	1.00113	1.00030	1.0072	--			1.00144	1.0159	1.00134
Index of Refraction	1.00297	1.000271	1.000340	--	1.000036	1.00132	1.000444	1.000516	1.00062	1.00037	1.00297			--	1.001079	--
Boiling Temperature °C, P = 1 atms	-195.8	-182.86	-190	-245.9	-268.9	-252.8	-161.5	-88.49	-61.80	-33.35	-151.8	↓	-111.9	-103.8	56.5	-83.6(subl.)
Melting Temperature °C, P = 1 atms	-209.86	-218.4	-207	-248.67	-272 26 atms	-259.17	-184	-102.4	-82.9	-77.7	-163.6	-102	-192.7	-169.4	-95	-81.8
Appearance Potential	N^+ 24.3 N_2^+ 15.55	O_2^+ 12.2	C^+ 22.8 CO^+ 14.1	Ne^+ 21.56 Ne^{++} 62.6	He^+ 24.58 He^{++} 79.0	H_2^+ 15.4 $H^+ + H$ 18.0	$CH_3^+ + H_2$ 14.3 CH_2 15.3 C^+ 26.2 H^+ 22.8	N^+ 21.4 N^+ 16.3	$S^+ + H_2$ 14.0 $HS^+ + H$ 15.2 H_2S^+ 10.47	NH_3^+ 10.52 NH_3^{++} 42.2	N^+ 21.7 O^+ 18.9 NO^+ 9.25			C_2H^+ 13.5 C^+ 24.7	$C_2H_4^+ + H_2O$ 11.4	$C_2H_2^+$ 11.41 C^+ 24.5

REFERENCES

1. Jaffe, L. D., "Sterilizing Unmanned Spacecraft," Astronautics and Aerospace Engineering, August 1963.

2. Lowe, H. N. Jr., et al., "Destruction of Microorganisms in Water, Sewage, and Sewage Sludge by Ionizing Radiations," Journal of American Water Works Association, Vol. 48, pp. 136-72, 1956.

3. Briggs, F. B., Wright, F. W., and Hodge, P. H., "Chemical Analysis of 643 Particles Collected by High Attitude Aircraft and Balloons," SAO-99, July 1962.

4. Waddington, C. J., "Composition of the Primary Cosmic Radiation," Progress in Nuclear Physics, Vol. 8, edited by O. R. Frisch, Pergamon Press 1960.

5. Kellogg, P. J., "Flow of Plasma Around the Earth," Journal of Geophysical Research, Vol. 67, No. 10, pp. 3805-11, September 1962.

6. Satellite Environment Handbook, edited by F. S. Johnson, Stanford University Press, 1961.

7. Bailey, D. K., "Time Variations of the Energy Spectrum of Solar Cosmic Rays in Relation to the Radiation Hazard in Space," Journal of Geophysical Research, Vol. 67, No. 9, p. 391, 1962.

8. Barton, J. A., "On Estimate of the Nuclear Radiation at the Lunar Surface," Advances in Astronautical Sciences, Vol. 6, pp. 794-804, The Macmillan Co., New York, 1961.

9. Jaffe, D. J., Rittenhouse, J. B., "Behavior of Materials in Space Environments," American Rocket Society Journal, March 1962.

10. Blair, R. R., "Surface Effects of Radiation on Transistors," Presented at the IEE Summer General Conference held in Toronto, Canada, June 1963.

11. Dollfus, A., C. R. Acad. Sci. 234, p. 2046, 1952.

12. Lipskij, J. N., Sternberg Astronom. Inst., Moscow 22,pp. 66-123, 1953.

13. Opik, E. J., Irish Astronom. pp. 137-143, 1955.

14. Elsmore, B., "Radio Observations of the Lunar Atmosphere," Philos. Mag., pp. 1040-1046, 1957.

15. Singer, S. F., "Atmosphere Near the Moon," Astronautica Acta 7, Nos. 2-3, 1961.

16. Jeans, J. H., The Dynamical Theory of Gases, (Dover publications, New York 1954), p. 344.

17. Spitzer, L., "The Terrestrial Atmosphere above 300 km," The Atmosphere of the Earth and Plants, edited by G. P. Kuiper, University Press, p. 241, Chicago 1962.

18. Milne, Trans. Cambridge Phil. Soc., 22, 484, 1923.

19. Jones, Trans. Cambridge Phil. Soc., 22, 535, 1923.

20. Vestine, E. H., The Rand Corporation, Res. Mem. RM-2106, January 29, 1958.

21. Lyot and Dollfus, C. R., 229, 1277-1280, 1949.

22. Herzberg, G., Po p. Astr., 54, 414, 1946.

23. Biermann, L., Zeits. Astro. Phys., 29, 274, 1951.

24. Clement, G. H., The Rand Corporation, Paper p. 833, Rev. May 7, 1959.

25. Krassovsky, Am. Roy. Soc., Washington Meeting, November 16, 1959.

26. Elsmore, B. and Whitfield, G. R., Nature 176 457, 1955.

27. Gold, T., J. Geophisic. Res. 64, 1798, 1959.

28. Herring, J. R., and Licht, A. L., "The Solar Wind, In," Proceedings of COSPAR Symposium, Nice, January 1960, Amsterdam, North Holland Publishing Co., 1960.

29. Pettit, and Nicholson, S. B. Ap. J. 71, 102, 1930.

30. Pettit, E., 1940, Radiation Measurements of the Eclipsed Moon: Astrophysical Journal, Vol. 91, pp. 408-420.

31. Jaeger, J. C., and Harper, A.F.A., 1950, Nature of the Surface of the Moon: Nature, Vol. 166, p. 1026.

32. Tyler, W. C., and Copeland, J., 1962, A Theoretical Model for the Lunar Surface: The Astronomical Journal, Vol. 67, p. 122.

33. Gibson, J. E., 1961, Lunar Surface Characteristics Indicated by the March 1960 Eclipse and other Observations: Astrophysical Journal, Vol. 133, p. 1072-1080.

34. Kislyakov, A. G., 1961, Results of an Experimental Study of Lunar Radio Emission at 4 mm: Soviet Astronomy - A. J., Vol. 5, p. 421-422.

35. Evans, J. V., 1962, Radio-Echo Observations of the Moon at 3.6-cm Wavelength: Technical Report No. 256, Lincoln Laboratory, Massachusetts Institute of Technology, p. 38.

36. Cudaback, D., 1963, Old Devil Moon: Newsweek, April 15 issue, p. 62.

37. Dollfus, A., 1962, The Polarization of Moonlight: in Physics and Astronomy of the Moon, edited by Z. Kopal, Academic Press, p. 154.

38. Fessenkov, V. G., 1962, Photometry of the Moon: in Physics and Astronomy of the Moon, edited by Z. Kopal, Academic Press, p. 126.

39. Sytinskaya, N. N., 1959, New data on the meteoric slag theory of the formation of the outer layer of the lunar surface: Soviet Astronomy - A. J., Vol. 3, pp. 310-314.

40. Moore, H. H., and Gault, D. E., 1962, Current tabulation of data from hypervelocity impact experiments: Astrogeologic Studies Semiannual Progress Report, February 26, 1961 to August 24, 1961, pp. 106-112.

41. Bjork, 1961, Analysis of the Formation of Meteor Crater, Arizona: A preliminary report: Journal of Geophysical Research, Vol. 66, pp. 3379-3387.

42. Whipple, F. L., 1961, The Dust Cloud about the Earth: Nature, Vol. 189, p. 127-128.

43. Gold, T., 1955, The Lunar Surface: Monthly Notices of the Royal Astronomical Society, Vol. 115, pp. 585-604.

44. Fairbairn, H. W., and Hurley, P., 1961, Radiation Damage in Zircon: Its relation to the ages of Paleozoic igneous rock: Transactions of the American Geophysical Union, Vol. 38, p. 99.

45. Wehner, G. K., 1961, Sputtering Effects on the Moon's Surface: American Rocket Society Journal, Vol. 31, p. 438.

46. Fisher, D. E., 1961, Space Erosion of the Grant Meteorite: Journal of Geophysical Research, Vol. 66, pp. 1509-1512.

47. Gilvarry, J. J., 1957, Nature of the Lunar Surface: Nature, Vol. 180, p. 911-912.

48. Green, J. 1961, The Geology of the Lunar Base: North American Aviation, Space and Information Systems Division, Report 61-358, p. 127.

49. Alter, D., 1962, in the Atmosphere of the Moon: Proceedings of the Lunar-Planetary Exploration Colloquium, Vol. 3, No. 1, p. 57.

50. Ryan, J. A., 1962, The case against thermal fracturing at the lunar surface: Journal of Geophysical Research, Vol. 67, pp. 2549-2558.

51. Gilvarry, J. J., 1960, Origin and Nature of Lunar Surface Materials: Nature, Vol. 180, pp. 886-890.

52. McGillem, C. D., and Miller, B. P., 1962, Lunar Surface Roughness from Crater Statistics: Journal of Geophysical Research, Vol. 67, pp. 4787-4794.

53. Dubin, M., and McCracken, C. W., 1962, Measurements of Distributions of Interplanetary Dust: The Astronomical Journal, Vol. 67, pp. 248-256.

54. Whipple, F. L., 1959, On the Lunar Dust Layer: Vistas in Astronautics, Vol. 2, pp. 267-272.

55. Gault, D. E., Shoemaker, E. M., and Moore, H. J., Spray Ejected from the Lunar Surface by Meteoroid Impact: NASA Technical Note D-1767, p. 39.

56. Grannis, P. D., 1961, Electrostatic Erosion Mechanisms on the Moon: Journal of Geophysical Research, Vol. 66, pp. 4293-4299.

57. Gold, T., 1962, Processes on the Lunar Surface: in Proceedings of the I.A.U., Pulkova Meeting, December, 1960.

58. Singer, S. F., and Walker, E. H., 1962, Electrostatic Dust Transport on the Lunar Surface: Icarus, Vol. 1, pp. 112-120.

59. Salisbury, J. W., Glaser, P. E., Stein, B.A., and Vonnegut, B., 1963 Adhesive Behavior of Silicate Powders in Ultrahigh Vacuum: Presented at the 44th Annual Meeting of the American Geophysical Union, April 17-20, Washington, D.C.

60. Hapke, B. W., 1962, Second Preliminary Report on Experiments Relating to the Lunar Surface: Center for Radiophysics and Space Research, Cornell University, Report 127, p.41.

61. Epstein, P. S., Phys. Rev. 33, 269, 1929.

62. A. J. Wesselink, Bull Astr. Inst. Netherlands 10, 1948, p. 351.